AN ABSTRACT OF THE THESIS OF

Mark Alexander Dexter Wilson (Name) for the Doctor of Philosophy (Degree)

in Physics (Major) presented on May 6, 1971 (Date)

Title: SPIN-FLIP PROBABILITY OF PROTONS INELASTICALLY SCATTERED FROM CARBON AND SULFUR

Abstract approved: Redacted for Privacy

Larry Schecter

The spin-flip probability of protons inelastically scattered to the first 2^+ excited states of ^{12}C and ^{32}S has been measured at proton energies of 15.93 MeV and 17.35 MeV for carbon and at 15.91 MeV and 17.57 MeV for sulfur. The $(p, p'\gamma)$ coincidence technique was employed, with the γ detector axis along the perpendicular to the reaction plane. The measured angular distribution of the fraction of protons undergoing spin-flip during inelastic scattering from carbon displays a prominent peak of about 0.30 in magnitude at a proton angle of about 130°, which is in good agreement with previous measurements in the same proton energy region. The measured inelastic proton spin-flip probability on sulfur is higher than that reported for any other nucleus, exceeding a peak value of 0.5 at $\phi_p = 145°$ at $E_p = 15.91$ MeV. A collective DWBA analysis of the spin-flip probability, employing the full Thomas spin-orbit interaction, was carried out.

The amplitude and position of the main experimental peak was reproduced in the case of protons on carbon, but the observed forward structure was not predicted. Attempts to fit the spin-flip probability of protons on sulfur at E_p = 17.57 MeV required an increase in the spin-orbit strength V_{SO} to 9.0 MeV, compared to the value of 6.2 MeV found by previous work to better fit the elastic polarization data. Efforts to fit the even larger value of the spin-flip probability observed at E_p = 15.91 MeV were even less successful since the DWBA analysis does not predict much variation with incident proton energy.

Spin-Flip Probability of Protons Inelastically Scattered From Carbon and Sulfur

by

Mark Alexander Dexter Wilson

A THESIS

submitted to

Oregon State University

in partial fulfillment of
the requirements for the
degree of

Doctor of Philosophy

June 1971

APPROVED:

Redacted for Privacy

Professor of Department of Physics

in charge of major

Redacted for Privacy

Acting Chairman of Department of Physics

Redacted for Privacy

Dean of Graduate School

Date thesis is presented May 6, 1971

Typed by Barbara Eby for Mark Alexander Dexter Wilson

ACKNOWLEDGEMENTS

The author is deeply indebted to Professor Larry Schecter for his continued support and encouragement which has spurred the satisfactory completion of this work and for his contributions to the understanding of the theoretical treatment.

The many helpful discussions with Dr. L. Wayne Swenson during the experimental measurements are gratefully acknowledged.

Special thanks go to Mr. Jack McKenzie, our cyclotron technician, for his unstinting efforts to maintain the steady accelerator performance essential for the successful outcome of the experiment.

The assistance of Dr. M. Norton Wise and Mr. Ira White during the long periods of data acquisition is greatly appreciated.

Thanks are extended to Dr. Helmy Sherif for the use of his computer code and for helpful correspondence.

Finally, gratitude is expressed to Mr. Terry Liittschwager of the University of Oregon Computer Center for his ready cooperation during the many calculations made with their facilities.

TABLE OF CONTENTS

LIST OF FIGURES

LIST OF TABLES

SPIN-FLIP PROBABILITY OF PROTONS INELASTICALLY SCATTERED FROM CARBON AND SULFUR

I. INTRODUCTION

All the properties of atomic nuclei should be calculable in principle from the nucleon-nucleon interaction, provided that it is a two-body interaction. In practice, this hope is not realized, so that the properties of nuclei are instead investigated by nucleon-nucleus scattering and reaction measurements, often using protons as projectiles. In the attempt to understand this latter interaction, since the many-body problem presents formidable obstacles, a phenomenological approach is often used. One of these is the optical model, in which the interaction is described by means of a complex potential with coulomb and spin-orbit terms, which reflect the dependence on the charge and spin characteristics of the interacting systems.

The spin-dependent contributions in the inelastic scattering of nucleons are not well understood. The angular distributions of scattered particles are not very sensitive to such terms, although they apparently play some part even in elastic scattering. On the other hand, polarizations, asymmetries and spin-flip probabilities are all sensitive to spin-dependent forces in various ways.

In the attempt to learn new information about the spin-dependent terms of the optical model, we have performed a measurement of the

spin-flip probability in the inelastic scattering of protons from ^{32}S and ^{12}C, leading in each case to the lowest 2^+ state. In contrast to the other two possibilities, this can be done without the necessity for polarized beams. The analysis involves a DWBA calculation using the full Thomas form of the deformed spin-dependent interaction.

Chapter II describes the method of measurement. In Chapter III we present some details of the theory employed. Chapter IV describes the apparatus and experimental techniques. The experimental results are presented in Chapter V, along with a description of the data collection and analysis. A comparison of the theory with the experimental findings and the resulting conclusions are given in Chapter VI.

II. METHOD OF SPIN-FLIP MEASUREMENT

The proton spin-flip probability is determined by measuring the angular correlation between the inelastically scattered protons and the de-excitation gamma-rays. The angles in the correlation function are defined in Figure 2-1. Since the z-axis is defined as normal to the reaction plane, $\theta_p = 90°$ and ϕ_p is the angle of the scattered protons with respect to the incident beam, directed along the positive x-axis. Spin-flip will refer to the case in which a scattered proton undergoes a reversal of the z-component of spin.

The technique employed here and in other recent work [1, 2, 3], to determine the spin-flip probability by measuring the correlation between the gamma-rays emitted along the z-axis and the protons scattered in the reaction plane is based upon a theorem by A. Bohr [4] . This theorem is expressed in the form of a simple rule which relates the polarizations and intrinsic parities in the initial and in the final states of two particles involved in a collision process which conserves parity and angular momentum. The rule:

$$P \exp(i\pi S_n) = P' \exp(i\pi S'_n) , \qquad (2\text{-}1)$$

where P and P' are the products of the intrinsic parities of the particles involved before and after the reaction and S_n and S'_n are the sums of the initial and final spin components along the axis $\hat{n}$ perpendicular to the reaction plane $\overline{K} \times \overline{K'}$. $\overline{K}$ and $\overline{K'}$ are the

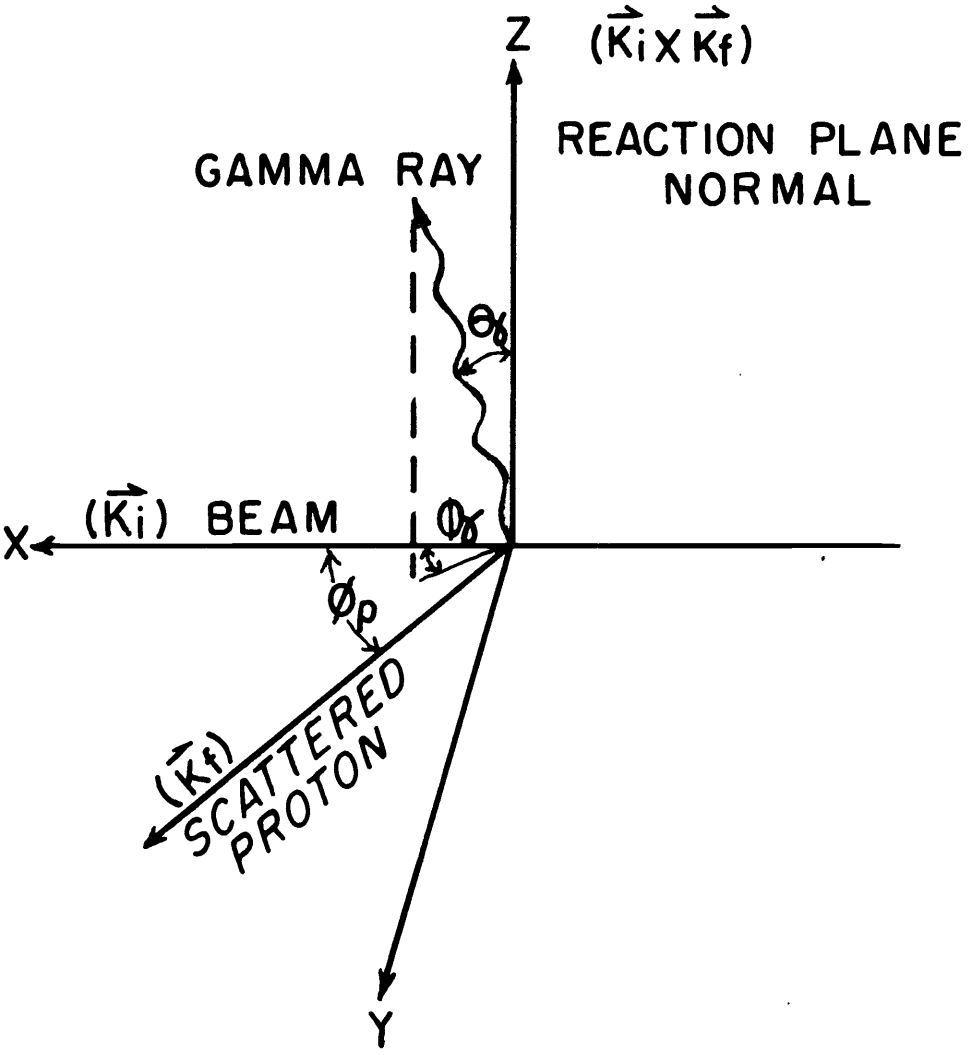

Figure 2-1. Coordinate system.

initial and final proton momenta.

A simple proof follows: Selecting the quantization axis along the direction $\hat{z} = \hat{n}$, the constants of motion are expressed in terms of eigenvalues $m_j = m_j'$ and $\underline{P} = \underline{P}'$, where m_j and m_j' are the components of the initial and final total angular momentum along $\hat{z}$ and $\underline{P}$ and $\underline{P}'$ are the initial and final total parities of the target-projectile system. Hence:

$$\underline{P} \exp(i\pi m_j) = \underline{P}' \exp(i\pi m_j') . \qquad (2\text{-}2)$$

For a projectile with spin s and intrinsic parity P_p incident on a target nucleus with total intrinsic angular momentum I and intrinsic parity P_t, $m_j = m_L + m_s + M_I$ and $\underline{P} = P_L P_p P_t$. Therefore

$$\underline{P} \exp(i\pi m_j) = P_L P_p P_t \exp[i\pi(m_L + m_s + M_I)] . \qquad (2\text{-}3)$$

Since L is the orbital angular momentum of the projectile relative to the target and P_L is the spatial parity of the target-projectile system, $P_L = (-1)^L$. Furthermore, $\exp(i\pi m_L) = (-1)^{m_L}$. Therefore

$$\underline{P} \exp(i\pi m_j) = (-1)^{L+m_L} P_p P_t \exp[i\pi(m_s + M_I)] . \qquad (2\text{-}4)$$

By selecting the z-axis perpendicular to the direction of propagation, the polar angle θ equals $\pi/2$, and in the partial wave representation of the scattering process, the orbital angular momentum

functions $Y_L^m(\pi/2, \phi)$ vanish for all odd values of $L + m_L$. Thus, for all the values of m_L which occur in a scattering process in which the quantization axis is perpendicular to the reaction plane, $L + m_L$ must be even; therefore, $(-1)^{L + m_L} = +1$. Therefore,

$$\underline{P} \exp(i\pi m_j) = P_p P_t \exp[i\pi(m_s + M_I)] , \qquad (2\text{-}5)$$

and the right hand side is also a constant of the motion.

Since $S_n = m_s + M_I$ and $P = P_p P_t$, we have, finally,

$$P \exp(i\pi S_n) = P' \exp(i\pi S'_n) \qquad \text{Q. E. D.}$$

This can be rewritten

$$P = P' \exp(i\pi \Delta S_n) , \qquad (2\text{-}6)$$

where $\Delta S_n = \Delta m_s + \Delta M_I = m'_s - m_s + M'_I - M_I$.

For nuclear transitions, 0^+ to 2^+, induced by inelastic proton scattering, the intrinsic parities remain unchanged and the Bohr theorem leads to the following conditions:

$$\text{for } \Delta M_I = M_2 = 0, \pm 2 , \ \Delta m_s = 0 , \text{ No Spin-Flip}$$

$$\text{for } \Delta M_I = M_2 = \pm 1 , \ \Delta m_s = \pm 1 , \quad \text{Spin-Flip} .$$

Therefore, since spin flip can occur only in the case that the $M = \pm 1$ substate is populated, the probability that the $M = \pm 1$ substate is excited during the inelastic scattering is the same as the

probability for proton spin-flip during the process.

Since, in the cases under consideration, the excited 2^+ state decays directly to the 0^+ ground state by way of gamma emission, it is possible to express the radiation intensity pattern simply in terms of the vector spherical harmonics: $I^M(\theta_\gamma, \phi_\gamma) \propto |X_2^M(\theta_\gamma, \phi_\gamma)|^2$. A look at the multipole field patterns for $L = 2$ in Figure 2-2 shows that a gamma detector placed along the z-axis will detect only gamma-rays emited from the $M = \pm 1$ substates of the excited 2^+ level. Since these M-states were populated only during proton spin-flip, a determination of the number of coincidences between the gamma-rays emitted along the z-axis and protons inelastically scattered to the 2^+ level through an angle ϕ_p determines the number of protons undergoing spin-flip during the scattering process. Since the gamma detector subtends a finite solid angle about the z-axis, some gammas resulting from de-excitation of the $M = 0, \pm 2$ states are also included. An estimate of the correction to the measured proton spin-flip probability due to the finite detector geometry is given in Chapter V.

It will be useful to develop an expression for the total intensity of the gamma radiation due to the de-excitation of all the M-substates populated by inelastic proton scattering from the 0^+ level to the 2^+ level. The transition amplitude for inelastic proton scattering is given by $T_{0\mu_0}^{M\mu}(\phi_p, E_p)$ [5, p. 7], where the subscripts are the initial

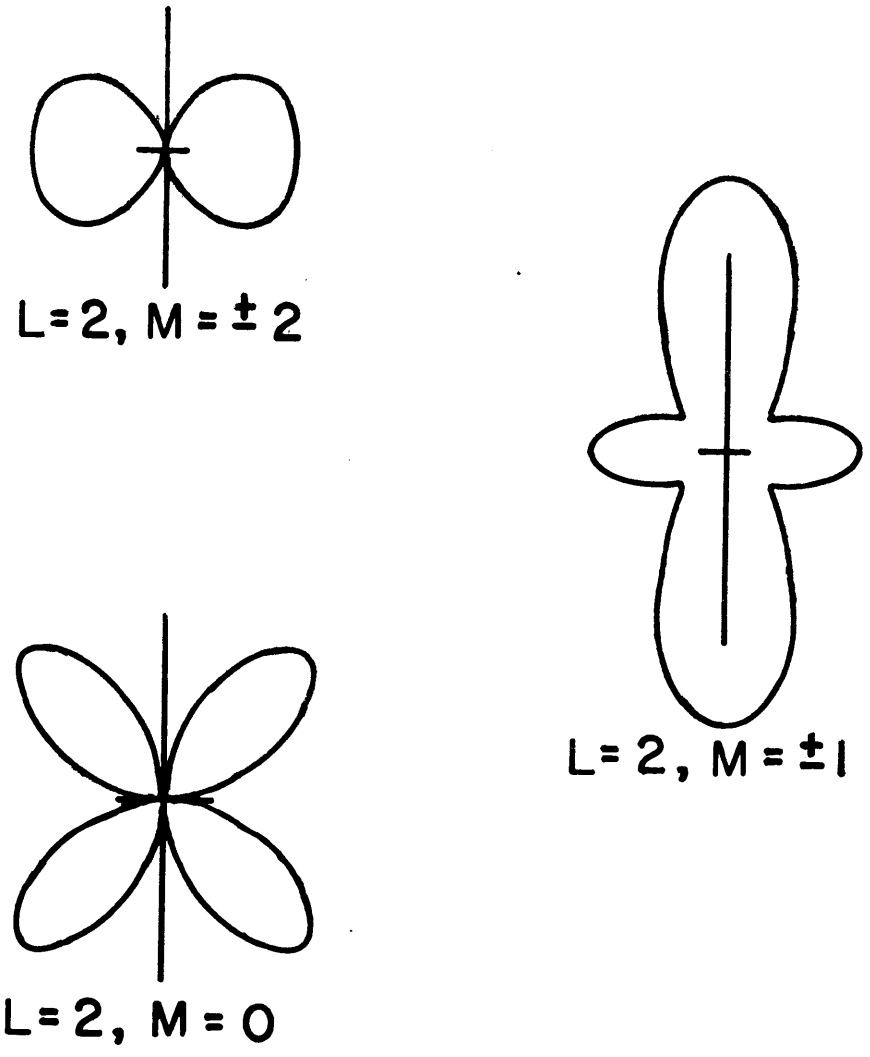

Figure 2-2. L=2 multipole radiation patterns.

and the superscripts are the final magnetic spin quantum numbers associated with the target and the projectile. The amplitude of the gamma radiation from the M^{th} substate is proportional to $T^{M\mu}_{0\mu_0}(\phi_p, E_p)X^M_2(\theta_\gamma,\phi_\gamma)$. The total intensity of de-excitation radiation in any given direction is given by a coherent sum over M-states:

$$I^{\mu}_{\mu_0}(\phi_p,E_p,\theta_\gamma,\phi_\gamma) = \sum_{MM'} T^{M\mu}_{0\mu_0} T^{*M'\mu}_{0\mu_0} X^M_2 \cdot X^{*M'}_2 . \quad (2\text{-}7)$$

For the present case, in which the incident beam is unpolarized and the proton detectors are insensitive to spin orientation, the sum is extended incoherently over the initial and final proton spin states as well:

$$I(\phi_p,E_p,\theta_\gamma,\phi_\gamma) = \sum_{MM'} \left(\sum_{\mu\mu_0} T^{M\mu}_{0\mu_0} T^{*M'\mu}_{0\mu_0} \right) X^M_2 \cdot X^{*M'}_2 . \quad (2\text{-}8)$$

The expression in parentheses is the density matrix [5, p. 7] describing the system consisting of the excited nucleus and the proton scattered through an angle ϕ_p.

Integration of I over the solid angle subtended by the gamma detector is next carried out. For a circular aperture which is symmetric about $\theta_\gamma = 0$, the integration over ϕ_γ is zero for $M \neq M'$. Thus, only terms with $M = M'$ remain in the summation over

M, M' and the intensity of de-excitation gamma-rays incident on a circular aperture of solid angle $\Delta\Omega$ along the z-axis can be written:

$$I(\phi_p,E_p) = S_0(\phi_p,E_p)\int_{\Delta\Omega}|X_2^0|^2 d\Omega + S_1(\phi_p,E_p)\int_{\Delta\Omega}|X_2^1|^2 d\Omega + S_2(\phi_p,E_p)\int_{\Delta\Omega}|X_2^2|^2 d\Omega \quad (2\text{-}9)$$

where S_0, S_1, S_2 are the diagonal elements of the density matrix, denoting the probability for leaving the nucleus in the $M = 0, \pm 1, \pm 2$ substates of the excited 2^+ level via inelastic proton scattering through an angle ϕ_p. As was demonstrated in the discussion of the Bohr theorem, $S_1(\phi_p,E_p)$ is also the probability that the proton undergoes spin-flip during the inelastic scattering process. Equation (2-9) will be used in Chapter V to determine the proton spin-flip probability from the experimental proton-gamma coincidence measurements.

III. THEORY

Collective surface excitations have been successful in describing, in a quantitative fashion, nuclear inelastic scattering in the intermediate projectile energy range (10 MeV to 100 MeV). It is therefore appropriate to consider the application of the extended optical model, in which the scattering is determined by an optical potential which is a function not only of the projectile coordinates, but also of the dynamical variables which describe surface excitations. It is convenient to relate the surface deformation to a radius parameter of the optical model in the following way: if the spherical optical potential has the form $U(r, R)$, where R is the radius parameter of the optical potential, and r is the projectile coordinate relative to the target center, then we choose the extended optical potential to be $U[r, R + \alpha(\hat{r})]$. Here $\alpha(\hat{r})$ is the deformation distance along the direction $\hat{r}$, and may be expanded in multipoles:

$$\alpha(\hat{r}) = \sum_{L, M} \xi_{L, M} Y^{*M}_{L}(\hat{r}) \qquad (3\text{-}1)$$

In application, it is desirable to expand $U(r, R + \alpha)$ in powers of $\alpha(\hat{r})$:

$$U(r, R+\alpha) = U(r, R) + \alpha \frac{\partial U(r, R)}{\partial R} + \alpha^2 \frac{\partial^2 U(r, R)}{\partial R^2} + \cdots \tag{3-2}$$

Since U is now a function of $\xi_{L, M}$, the dynamical coordinates describing the surface displacement, it will couple nuclear surface states. The Schroedinger equation and the boundary conditions of the projectile-target nucleus system yield a set of coupled differential equations in the projectile coordinates, infinite in number since the nuclear collective states in principle form a complete set. In one method of solution only a restricted set of states is considered, so that the ladder of coupled equations is terminated at some point.

A less arduous procedure results when the transition amplitude is calculated in Distorted Wave Born Approximation (DWBA); that is, the amplitude T_{fi} between initial nuclear state $|i\rangle$ and final nuclear state $|f\rangle$ is approximated by

$$T_{fi} \cong \langle f | \langle \chi^{(-)}(\bar{k}_f, \bar{r}) | \frac{\partial U(r, R)}{\partial R} \alpha(\hat{r}) | \chi^{(+)}(\bar{k}_i, \bar{r}) \rangle | i \rangle \tag{3-3}$$

where $\langle \chi^{(-)}|$ and $|\chi^{(+)}\rangle$ are exact solutions of the wave equation for the spherical potential $U(r, R)$, which satisfy appropriate boundary conditions. This is called Born Approximation because the coupled equations are now solved only to first order in U.

In the cases we will consider, the target is an even-even nucleus, in which case the nuclear matrix elements must have the form,

$$<f|\alpha(\hat{r})|i> \equiv <IM|\alpha(\hat{r})|00> = <IM|\xi_{IM}|00>Y_I^{*M}(\hat{r})$$

$$= C(I)Y_I^{*M}(\hat{r}) \qquad (3\text{-}4)$$

since the matrix element, from invariance arguments (Wigner-Eckart Theorem), must be just a number, $C_I = \beta_I/\sqrt{2I+1}$.

Provided that the interaction is assumed to be local, and that charge exchange effects can be neglected, the wave functions $<\chi^{(-)}|$ and $|\chi^{(+)}>$ are then expanded in partial waves, and the angular integrations then yield some Clebsch-Gordan coefficients and spherical harmonics which contribute to the dependence of the amplitude on scattering angle. There remains the final part of the calculation, the evaluation of the radial integrals of the form

$$\int_0^\infty f_{\ell'}(k_f, r)\frac{\partial U}{\partial R} f_\ell(k_i, r)dr$$

where $f_{\ell'}$ and f_ℓ are regular radial wave functions. The radial shape of the matrix element and consequently the shape of the angular distribution depends on the form of U .

It should be noted that the information to be extracted is limited by the properties of the χ's . The most important limitation is the localization of the region of interaction in calculating these χ's , since certain regions contribute more than others; a small change in position can result in a large change in momentum transfer.

Since we are dealing with spin $\frac{1}{2}$ charged projectiles, the optical potential used to generate the χ's is taken to have the form

$$U(r) = V_C(r) - V_0 f(r, R_0, a_0) - i(W - 4a_I W_D \frac{\partial}{\partial r}) f(r, R_I, a_I) + (\frac{\hbar}{m_\pi C})^2 (V_{SO} + iW_{SO}) \frac{1}{r} \frac{\partial}{\partial r} f(r, R_{SO}, a_{SO}) \bar{\sigma} \cdot \bar{\ell} \quad (3\text{-}6)$$

where $f(r, R_k, a_k) = [1 + e^{\frac{r-R_k}{a_k}}]^{-1}$, $R_k = r_k A^{1/3}$ with k representing the subscripts 0, I and SO for the spherical, imaginary and spin-orbit terms, respectively. V_C is the coulomb potential for a uniformly charged sphere of radius $R_C = r_C A^{1/3}$. The interaction which causes the event can now be written as:

$$\alpha \frac{\partial U}{\partial R} = \Delta U = \Delta U_C + \Delta U_0 + i\Delta U_I + \Delta U_{SO} \quad (3\text{-}7)$$

where

$$\Delta U_C = \frac{3ZZ'e^2}{R_C^2} \frac{C(I)}{2I+1} Y_I^{*M}(\hat{r}) \begin{cases} (r/R_C)^I & r < R_C \\ (R_C/r)^{I+1} & r > R_C \end{cases}$$

and

$$\Delta U_0 = -\alpha(\hat{r}) V_0 \frac{\partial}{\partial R_0} f(r, R_0, a_0)$$

and

$$\Delta U_I = -\alpha(\hat{r})[W - 4a_I W_D \frac{\partial}{\partial r}] \frac{\partial}{\partial R_I} f(r, R_I, a_I) .$$

Z and Z' refer to the atomic numbers of the projectile and the target, respectively. Following the prescription of Blair and Sherif

[6, 7], the Thomas form of spin-orbit potential

$$U_{SO} = \left(\frac{\hbar}{m_\pi c}\right)^2 (V_{SO} + iW_{SO})\,\overline{\sigma} \cdot \left[\,\overline{\nabla} f(r, R_{SO}, a_{SO}) \times \frac{1}{i}\,\overline{\nabla}\,\right] \qquad (3\text{-}8)$$

is expanded to first order in $\alpha_{SO}(\hat{r})$ to obtain for the deformed contribution:

$$\Delta U_{SO} = \left(\frac{\hbar}{m_\pi c}\right)^2 (V_{SO} + iW_{SO})\,\overline{\sigma} \cdot \left[\,\overline{\nabla}\left[\alpha(\hat{r})\left(\frac{\partial f}{\partial R_{SO}}\right)\right] \times \frac{1}{i}\,\overline{\nabla}\,\right] \qquad (3\text{-}9)$$

which can be written

$$\Delta U_{SO} = \Delta U_{SO}(1) + \Delta U_{SO}(2) \qquad (3\text{-}10)$$

where

$$\Delta U_{SO}(1) = \left(\frac{\hbar}{m_\pi c}\right)^2 (V_{SO} + iW_{SO})\,\alpha_{SO}(\hat{r})\,\frac{1}{r}\,\frac{\partial}{\partial r}\left(\frac{\partial f}{\partial R_{SO}}\right)\overline{\sigma} \cdot \overline{\ell} \qquad (3\text{-}11)$$

and

$$\Delta U_{SO}(2) = \left(\frac{\hbar}{m_\pi c}\right)^2 (V_{SO} + iW_{SO})\left(\frac{\partial f}{\partial R_{SO}}\right)\overline{\sigma} \cdot \left\{\overline{\nabla}[\alpha(\hat{r})] \times \frac{1}{i}\,\overline{\nabla}\right\} \qquad (3\text{-}12)$$

$\Delta U_{SO}(1)$ is the unsymmetrized version of the deformed potential used by the Oak Ridge Group [8] in their calculations. Some recent analyses, however, have shown that the full Thomas term results in somewhat improved fits for spin-flip probabilities [9, 10].

In the expressions above, the possibility that the α_k may differ has been explicitly included, and leads to parametrization of the

problem in terms of a set of β_k's.

In writing the transition amplitude, the spin dependence of $\chi^{(+)}$ and $\chi^{(-)}$ has been suppressed. However, the χ's are matrices in the particle spin space. For example,

$$\chi^{(+)}_{\mu_i}(\bar{k}_i\bar{r}) = \sum_{\mu_i'} |\tfrac{1}{2}\mu_i'> \chi^{(+)}_{\mu_i'\mu_i}(\bar{k}_i, \bar{r})$$

where μ_i is the spin projection of the incident particle and $|\frac{1}{2}\mu_i'>$ is the spin eigenfunction. The quantization axis is along the incident beam direction; terms with $\mu_i \neq \mu_i'$ allow the possibility of spin flip during the elastic scattering. The same holds for $\chi^{(-)}$, and in more explicit form the scattering amplitude is:

$$T_{fi} = \sum_{\mu_i'\mu_f'} <\chi_{\mu_f'\mu_f}(\bar{k}_f\bar{r})|<\tfrac{1}{2}\mu_f'|<IM|\Delta U|00>|\tfrac{1}{2}\mu_i'>|\chi^{(+)}_{\mu_i'\mu_i}(\bar{k}_i\bar{r})> \tag{3-13}$$

In terms of these scattering amplitudes $T(\mu_i;\mu_f M)$, if one takes advantage of their symmetry properties, the differential cross section is given by:

$$\frac{d\sigma}{d\Omega} = \frac{m^{*2}}{4\pi^2\hbar^4}\frac{k_f}{k_i}\sum_{\mu_f M}|T(\tfrac{1}{2};\mu_f M)|^2 \tag{3-14}$$

where m^* is the reduced mass.

The polarization is calculated to be:

$$P(\phi) = 2\mathrm{Im} \sum_{M} T(\tfrac{1}{2};-\tfrac{1}{2}M)T^{*}(\tfrac{1}{2};\tfrac{1}{2}M) \Big/ \sum_{\mu_f M} |T(\tfrac{1}{2};\mu_f M)|^2 \qquad (3\text{-}15)$$

and the probability for protons to excite a 2^+ state and undergo a spin-flip along an axis perpendicular to the scattering plane is:

$$S(\phi) = \tfrac{1}{2}\left[1 - \frac{\sum_{\mu_f M} (-1)^M T(\tfrac{1}{2};\mu_f M)T^{*}(\tfrac{1}{2};\mu_f -M)}{\sum_{\mu_f M} |T(\tfrac{1}{2};\mu_f M)|^2}\right] \qquad (3\text{-}16)$$

In these expressions, if all $\alpha_k = \alpha_o$, then the cross section for inelastic scattering contains a single deformation parameter, β_2. In such cases, the calculation of both $P(\phi_p)$ and $S(\phi)$ would be independent of β_2, since only ratios of $|T|^2$ are involved. Since we will be most interested in the spin-orbit contribution to ΔU in the calculation of $S(\phi_p)$, we set $\alpha_I = \alpha_o$ and then apply our theory in terms of the parameter $\Delta = (\beta_2)_{SO}/(\beta_2)_O = \beta_{SO}/\beta_O$.

It should be emphasized that there are two distinct contributions to the matrix element for spin flip. First, the spin-orbit term in the spherical optical potential can cause spin flip in either initial or final scattering states. Second, the transition operator leading to the final

inelastic state can cause spin flip.

The 2.240 MeV (2^+) state in ^{32}S is expected to exhibit the usual deformed, collective character of similar low-lying states in even-even nuclei. A variety of recent experiments has justified this expectation. While practically all even-even nuclei show either dynamic or intrinsic quadrupole distortion, the size of β_2 (the quadrupole deformation parameter) is not definitive as an indication of collective distortion, because it includes effects which vary with nuclear size, as predicted by single-particle estimates. One way to estimate the "collectiveness" of an excitation is to use $\beta_2/(\beta_2)_{SP}$, where $(\beta_2)_{SP}$ is for a single-particle configuration. A possibility suggested by Blair [11] as useful in comparing values of the deformation parameter obtained by different methods, is to examine the quantity $\delta_2 = \beta_2 R$. The results for the first 2^+ state in ^{32}S are:

Table 3-1. Experimental values for $\delta_2 = \beta_2 R$.

Nuclear Scattering	Analysis	δ_2
(α, α')	Sharp Cut-off Diffraction Model	1.17 [13]
(α, α')	Coupled Channels	1.1 [14]
(n, n')	DWBA	1.27 [15]
(p, p')	DWBA	1.41 [16]
Electromagnetic Processes		δ_2
(e, e')		0.95 [17]
Resonance Fluorescence		1.07 [18]
Projectile Coulomb Excitation		1.28 [19]

These values, derived from the application of collective models to both electromagnetic and nuclear processes, are generally consistent and infer $2.6 < \beta_2/(\beta_2)_{SP} < 3.7$, indicating the "collectiveness" of the state. It is therefore to some extent justified that the collective DWBA model be used for analyzing details of the spin-flip process in ^{32}S.

In the case of ^{12}C the deformation parameter β_2 extracted from inelastic scattering leading to the strongly excited 2^+ level is so large that the first order DWBA treatment is questionable. Nevertheless, some attempts have been made with reasonable success [3]; we shall try the same approach.

Austern [12] has observed that many of the features of the inelastic scattering of strongly absorbed particles can be understood within the DWBA framework as depending principally upon the angular momentum transfer and mode of excitation. However, in general the DWBA collective approach does not seem to provide simple expressions by which one can extrapolate experience; rather, each experiment requires a new computation. A more serious criticism is that the method does not in general contribute much physical insight into some of the more striking qualitative features of the interaction. It is also found that $(\beta_2)_{SO}$ is appreciably larger than $(\beta_2)_0$ in many cases [7, 20]. And, finally, there are structure and isotope effects which cannot be explained with the DWBA collective model.

All these difficulties might be resolved with a microscopic description of the interaction, which would take into account the detailed structure of the initial and the final states. Some calculations of this type have been done [2] in which the nuclear states are treated as accurately as possible, and the interaction between the projectile nucleon and the target nucleons are assumed to be closely related to the free nucleon-nucleon interaction. Depending on the configurations necessary, the form factors can then assume many different shapes, whereas in the collective model the form factor has the same shape for all one-phonon states in the same nucleus.

However, the attempts to carry out such a program have not yet produced results better than the collective model fits to $S(\phi)$. In general, very accurate wave functions are necessary, since core polarization effects are quite important. For this reason the microscopic model would be most effective for nuclei near closed shells, where the wave functions can be calculated with some degree of assurance. One calculation has been made [21] in which such deficiencies have been partially corrected by the inclusion of a collective model representation of a direct core-polarization term in an antisymmetrized Distorted Wave approximation. The exchange terms yield structure which is not observed, even though realistic interactions were used. It has been suggested that the lack of agreement may be due to the neglect of exchange core polarization effects.

Thus, despite its obvious defects, the DWBA collective model seems appropriate for the analysis of spin-flip inelastic scattering of protons from ^{32}S.

IV. APPARATUS AND EXPERIMENTAL TECHNIQUES

Particle Accelerator and Beam Handling System

The proton beam was obtained from the Oregon State University 39 inch cyclotron. The cyclotron pole tips were recently modified to produce an azimuthal variation and positive radial field gradient in the magnetic field, to provide for the acceleration of protons into the slightly relativistic region of 18 MeV to 20 MeV. In addition, a variable frequency capability was included in the R. F. system to increase the range of proton energies available at extraction radius.

At present, negative hydrogen ions are accelerated to simplify extraction. An aluminum foil, 0.0002 inches thick, 3/16 inches wide and 1/2 inches high, is placed near the maximum internal beam radius and strips essentially all of the incident H^- ions. The stripper azimuthal position is externally adjustable to steer the protons into the beam handling system. An extracted beam current of one microampere is usually obtained.

Figure 4-1 shows the arrangement of the cyclotron and beam handling system. Three feet downbeam from the stripper foil is the entrance to a 20 inch long double quadrupole magnetic focussing lens, with a 3 inch aperture. A pair of adjustable carbon slits are located 22 inches from the quadrupole exit, near the horizontal focal plane.

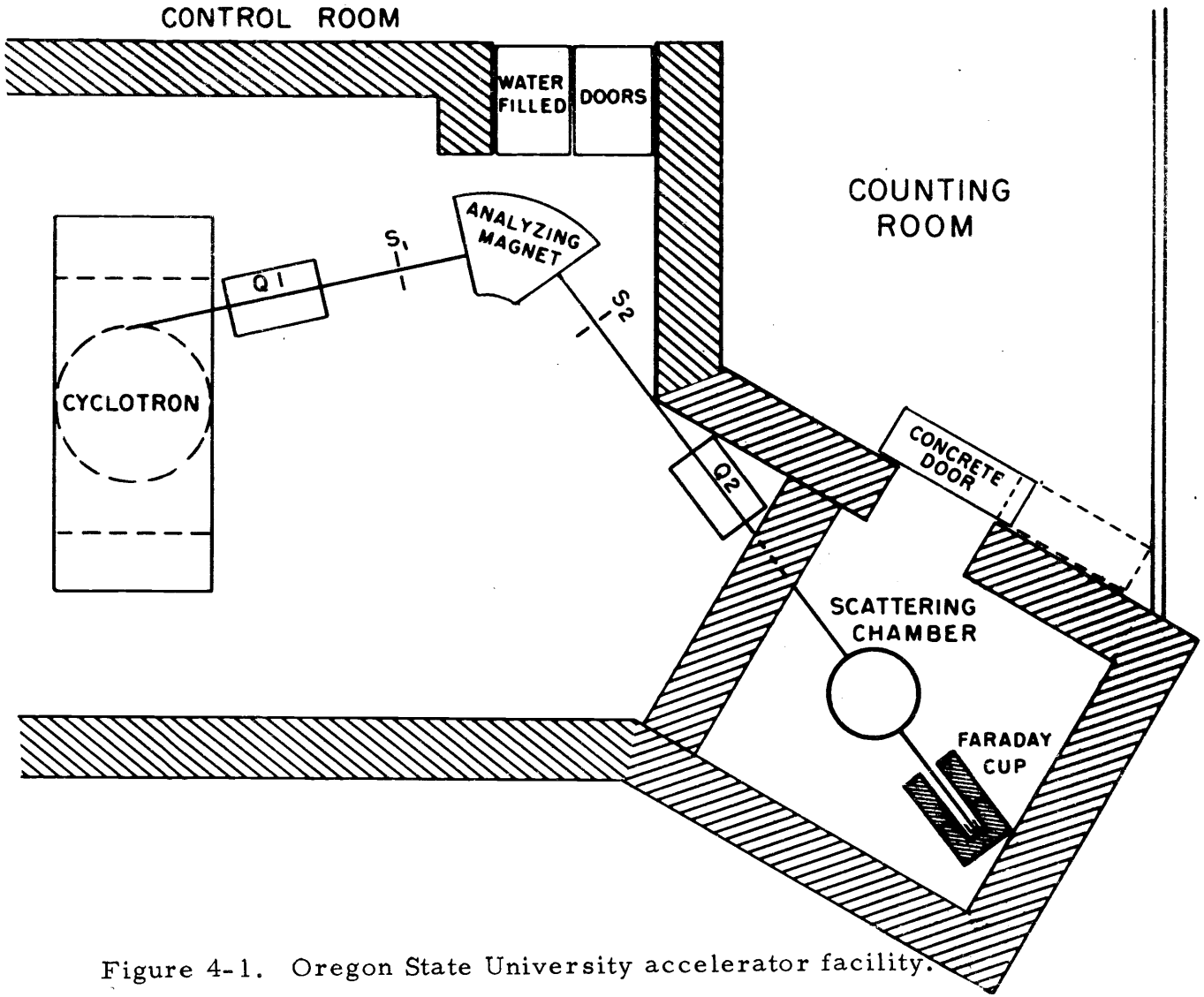

Figure 4-1. Oregon State University accelerator facility.

The entrance to the analyzing magnet is placed 21 inches from the carbon slits. The beam deflection by the magnet may be varied about 70° by $\pm$ 20°, thus providing for switching as well as momentum analysis. In the present experiment the deflection angle is 80°. The magnetic field is measured by an NMR probe with solid state electronics [22].

Beam analysis is completed by positioning a pair of tantulum slits 35 inches down beam from the magnet exit. The slits are mounted on vernier micrometers for optimum control of beam resolution.

Due to a lack of turn programming in the cyclotron, the analyzing system can be adjusted to select a beam from a continuous band of proton energies over a range of 2% to 3% of E_p, at a fixed cyclotron frequency, without loss of analyzed beam intensity.

A second pair of magnetic quadrupole lenses is positioned with the entrance 6.66 feet from the analyzing magnet exit slits. This lens serves to focus the object formed by the analyzing slits at the center of the scattering chamber, 10 feet further down beam from the last quadrupole.

A removable wall 2 feet thick, of high density concrete blocks has been constructed between the second quadrupole and the scattering chamber to reduce background radiation in the experimental area due to the cyclotron and the analysis slits.

The scattering chamber is a commercial design with an inside

diameter of 17 inches. Both the floor and the ceiling are rotatable in vacuum seals, with the angular positions read by a vernier scale to 0.1°. Electronic signal vacuum feed-through connectors are located near the hubs. These features provide for the accurate positioning of two sets of independently movable particle detectors, which may also be moved radially along slots in both the floor and the ceiling of the chamber.

For beam alignment and definition, two 3-position collimator turrets are located 12 inches and 29 inches, respectively, from the chamber center.

The beam passing through the chamber is stopped in a Faraday cup 7 feet behind the chamber. The tantalum cup and an electron suppressor ring are mounted inside the beam tube on feed-through insulators and are surrounded by 2 inches of lead and 4 inches of concrete to reduce radiation in the chamber area. During the present experiment the last 5 feet of the beam tube and the Faraday cup were connected together and insulated from ground in order to include small-angle scattered beam in the monitoring. In addition, the last 3 feet of the beam tube was surrounded by 4 inches of concrete.

Beam current is monitored by connecting the Faraday cup to a current indicator and integrator located in the cyclotron control console. Beam levels of 2 to 5 nanoamperes were used, depending on target thickness and proton energy. The beam current was limited by

consideration of pile-up, counting rate loss and accidental coincidence rate.

The energy of the proton beam was measured in the scattering chamber by the kinematic cross-over method of Bardin and Rickey [23], corrected for relativistic effects by the procedure of Smythe [24]. This technique is used to relate the incident proton energy to the scattering angle at which protons elastically scattered from hydrogen have the same energy as when inelastically scattered from the third state of ^{12}C at 9.629 MeV. The estimated uncertainty in our energy measurement is $\pm$ 100 keV.

The energy spread in the analyzed beam was determined from the pulse height distribution corresponding to protons elastically scattered from a thin gold foil. The measured FWHM of ΔE_p varied between 80 keV for analyzing slit spacing $\Delta S_{in} = \Delta S_{out} = 0.100$ inch, to 100 keV for $\Delta S_{in} = 0.200$ inch and $\Delta S_{out} = 0.100$ inch. The electronic contribution to the measured spread was estimated to be between 25 keV and 50 keV.

The spin-flip measurements were made at the following proton energies:

SULFUR

$E_p = 15.91 \pm 0.1$ MeV, $\Delta E_p = 100$ keV

$E_p = 17.57 \pm 0.1$ MeV, $\Delta E_p = 90$ keV

CARBON

$E_p = 15.93 \pm 0.1$ MeV, $\Delta E_p = 100$ keV

$E_p = 17.35 \pm 0.1$ MeV, $\Delta E_p = 80$ keV.

During the course of spin-flip measurements at each proton energy, the analyzing magnet field, and therefore the momentum selection, was maintained constant to 0.05% as determined by the NMR probe. Thus, the field drift contributed less than $\pm$ 15 keV to changes in the proton energy.

The beam was focussed and aligned to get maximum transmission through the collimators in front of the scattering chamber, and to center the beam. The collimators were then removed to reduce the background radiation in the detectors.

The beam spot at the target position was 1/8 inch to 1/16 inch in diameter as determined by viewing, via remote television camera, the scintillations in a quartz target placed in the beam. There was no apparent drift in the beam spot position when reviewed occasionally during a series of spin-flip measurements. Very little repositioning was ever needed from day to day, except after a change in proton energy.

An additional check of the beam alignment in the scattering chamber was obtained from the kinematic cross-over energy measurements. Differences in the cross-over angle as measured from the left and

right sides of the beam line could be construed as due to imperfect beam centering. The measured left-right differences in the cross-over angle were less than 1/4° at 50°. Since the proton detector was at the same radius for the spin-flip measurements, this discrepancy would be a good estimate of the angular uncertainty in the inelastic proton scattering. This uncertainty was negligible for the proton acceptance angles (several degrees) employed.

Targets

The carbon target was a polyethylene foil about 0.002 inch thick. Proton energy loss in the target was 50 keV to 75 keV for 17.3 MeV incident protons, determined in the following way: The full-width at half maximum of the elastic peak of protons scattered through a forward angle, 40°, was subtracted from the FWHM of the elastic peak at 160°. This difference was divided by two, reflecting the fact that protons scattering through 160° from the front of the target passed through material corresponding to twice the target thickness, while those scattering through 160° from the back surface of the target lost no energy in the target.

The same target was used for the carbon spin-flip measurements at both energies. The target withstood the proton bombardment quite well. A slight, heat-caused "wrinkling" was observed, and a brownish spot less than 1/16 inch in diameter gradually appeared.

The sulfur targets were self-supporting gold-plated foils of natural isotopic abundance (96%, ^{32}S). The target thickness, in terms of incident proton energy loss, ranged between 50 keV and 100 keV.

The targets were prepared in the following way:

1. A press mold was made. It consisted of a pair of 2 inch diameter, 1 inch thick, surface-hardened and polished chrome-steel discs, with three guide pins to prevent the two surfaces from sliding during pressing.
2. The mold was warmed to about 120° F.
3. Sulfur powder was then heated in a clean test tube near boiling, becoming a dark viscous liquid.
4. A small drop of sulfur was poured in the center of the lower half of the mold, the mold was then quickly closed and pressure was applied for 2 to 3 minutes by a hydraulic press. The applied pressure varied up to 20 tons, and depended on the mold temperature and desired thickness. Over-heating of the mold and/or too much pressure resulted in very thin targets. Mountable targets down to 20 keV thick were accidentally achieved.
5. The mold halves were carefully separated and the foil was lifted off while still flexible, using a very sharp, clean razor edge to separate, peel and lift the foil from the mold surface.

6. The foils were then trimmed and loosely sandwiched between aluminum target frames with 5/8 inch diameter target holes. The target frames were tightened only after the foils had crystalized in order to reduce stresses which might crack the foils.

7. A thin layer, 5 to 10 micrograms/cm^2, of gold was vacuum evaporated onto the target surfaces to retard subliming of the sulfur in the evacuated scattering chamber.

The sulfur targets became very fragile soon after they were pressed. Small shocks could produce cracking and flaking. The scattering chamber had to be let up to air slowly to avoid damaging the targets. The durability of the targets under proton bombardment in the vacuum chamber varied over a wide range, and seemed to depend both on the foil preparation and the nature of the evaporated gold film (a metallic lustre gave better results than a dull, black, powdery finish). One target was reduced to 30% original yield after only 6 hours bombardment. The most successful target withstood 4 days of proton bombardment for 12 hours per day, with only a 20% reduction in initial yield. The average target suffered a 50% yield loss in about 24 hours of running.

Detector Geometry

Figure 4-2 is a schematic of the top view of the scattering

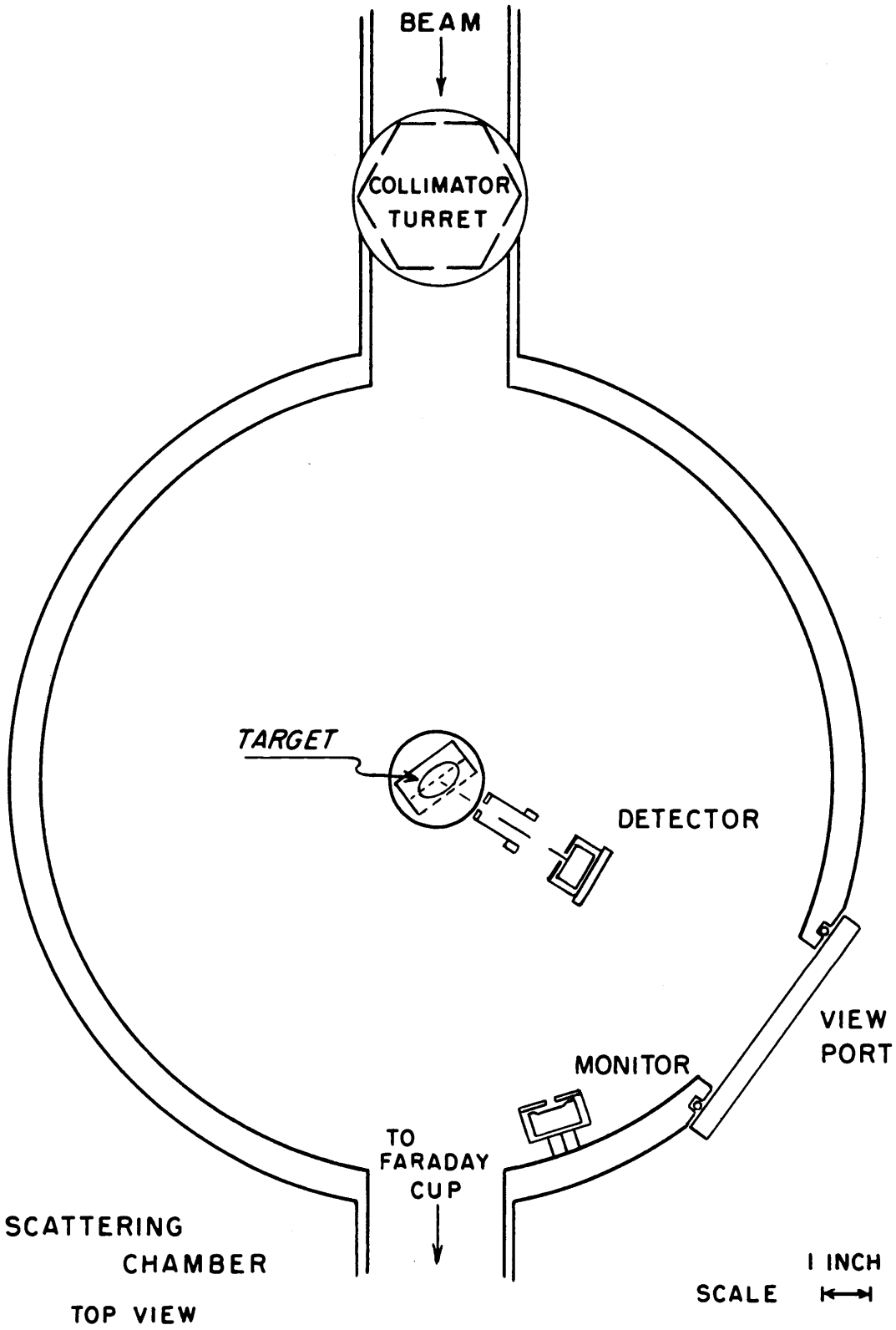

Figure 4-2. Scattering chamber (open), top view.

chamber with the lid removed.

The proton detectors used for the spin-flip measurements were commercially available lithium-drifted silicon diodes with a 3 mm depletion depth and a $\frac{1}{2}$ inch diameter active area. The detector resolution proved to be constant for bias voltages between 500 volts and 600 volts.

The proton detector geometry for the spin-flip measurements is indicated below:

Target	Energy	Radius	Aperture	Acceptance Angle, $\Delta\phi_p$
Carbon	17.35 MeV	3.0"	1/8"w x 7/16"h	3.5°
	15.91 MeV	3.5"	1/8"w x 7/16"h	3.0°
Sulfur	17.57 MeV	3.0"	1/4"w x 3/8"h	6.0°
	15.93 MeV	3.5"	1/4"w x 3/8"h	5.1°

A 3/16 inch diameter tantalum collimator placed between 3/4 inch and 7/8 inch from the target served to prevent stray protons scattered from the target frame from entering the detector.

In order to monitor the target condition, a detector was mounted on a vacuum feed-through connector on the chamber wall at 20° to count the elastically scattered protons. The detector aperture was 1/16 inch in diameter at a radius of $7\frac{1}{2}$ inches from the target. This solid angle provided a reasonable counting rate for the beam currents and targets used. The detector was a commercially available, 200 mm^2 area, surface barrier diode with a depletion depth of 850

microns at 290 volts. Resolution was improved, however, by raising the bias voltage to 315 volts. The protons were degraded by nickel foils placed in front of the detector in order to stop the protons within the active volume of the detector.

Figure 4-3 is a schematic vertical cross-section of the scattering chamber, showing the particle and gamma detectors and the target arrangement. Note that the top position on the target ladder was angled 15° from the vertical. This is the position used by the spin-flip targets, and prevents the de-excitation gamma-rays emerging near the vertical axis from being attenuated in the target frame.

The gamma detector is positioned along the vertical axis of the scattering chamber. The 3 x 3 NaI(Tl) scintillation crystal is located with the front surface of the light-tight covering 7-13/16 inches from the target center. The crystal is shielded from room background by a 1/8 inch brass cylinder surrounded by a 1-3/8 inch thick lead cylinder. The cylinders are sectioned for handling ease.

Covering the front surface of the crystal face is a 2 inch lead ring with a bevelled hole of 10.1° half-angle. As positioned along the vertical axis, the collimator aperture corresponds to a truncated, inverted 20.2° cone with the apex at the center of the target. The exit end of the collimator aperture exposes all but 1/8 inch of the diameter of the crystal face.

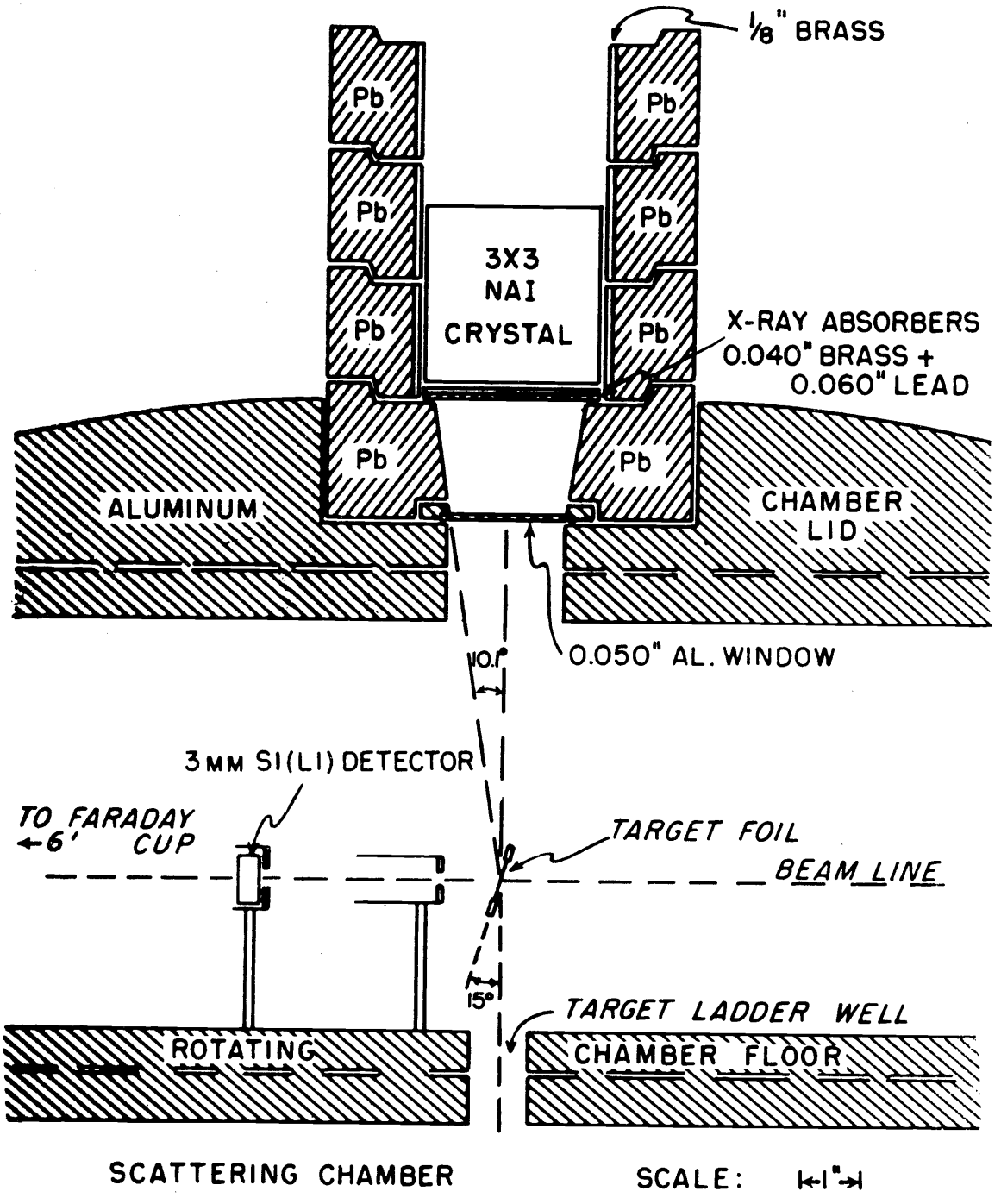

Figure 4-3. Scattering chamber (cut-away), side view.

In order to reduce the low-energy background radiation from the chamber, an absorber of 1/16 inch lead foil followed by a 1/32 inch brass sheet was inserted between the collimator and the crystal.

A 0.050 inch aluminum window sealed the vacuum chamber without attenuating the radiation from the target.

Electronics

Figure 4-4 is a block diagram of the electronic components employed in the spin-flip measurements.

Signals from the proton detector, after pre-amplification, are conducted via 25 feet of coaxial cable through a concrete wall 2 feet thick into the counting room, where the signals are amplified further and shaped by an amplifier with an RC clipping time constant of 0.25 microsecond. The short clipping time causes a slight loss of energy resolution, but improves the timing resolution, to be described later.

The prompt bipolar output signal from the amplifier enters a timing single-channel analyzer with the discriminator level and width set to accept signal amplitudes corresponding to protons inelastically scattered from the first excited 2^+ level of the target nucleus. The discriminator signal is used to gate the delayed proton signals entering the first ADC of the dual parameter analyzer. In addition, the discriminator output is used to trigger a scaler and thus count the number of inelastic protons from the 2^+ level scattered into the detector.

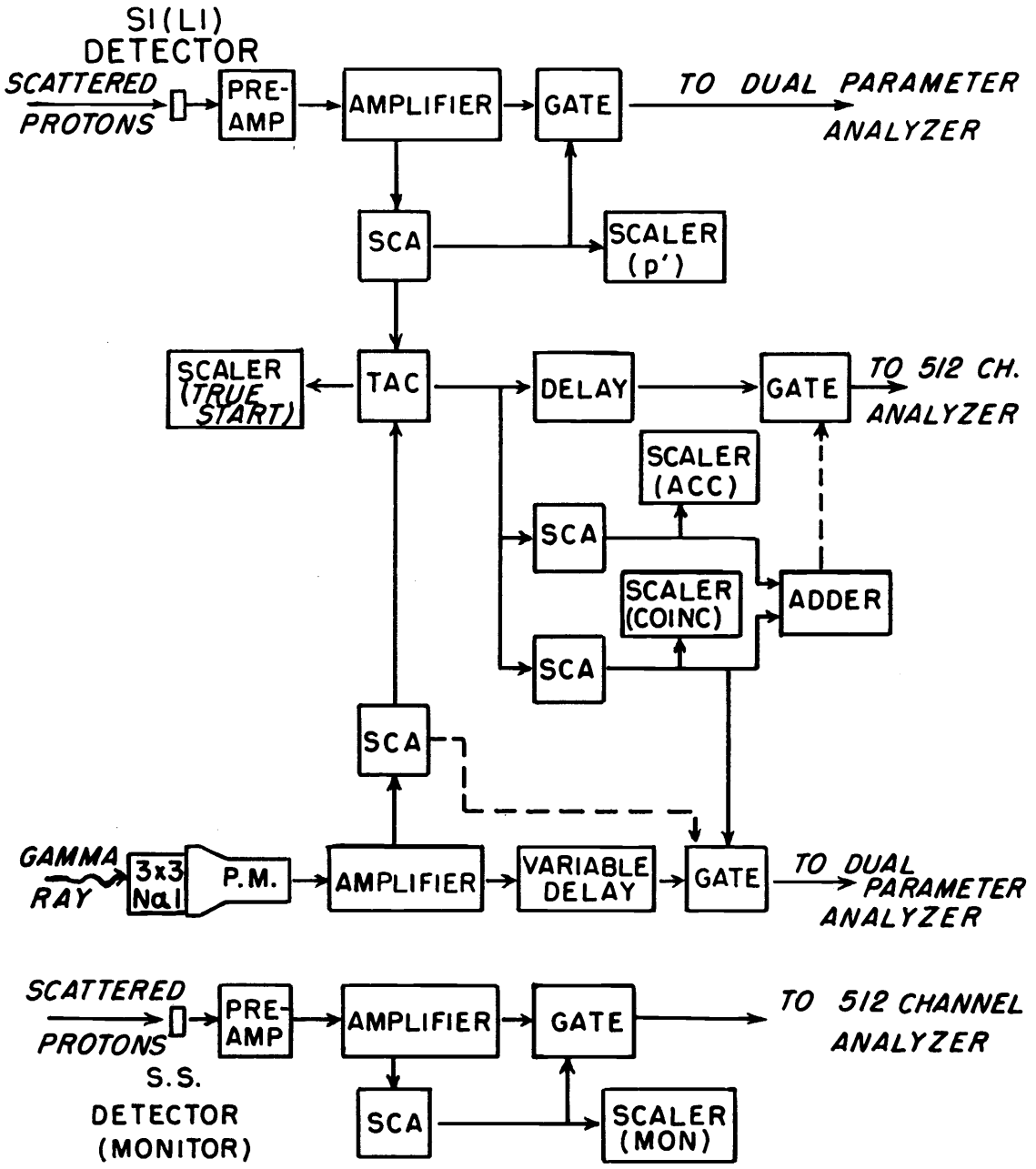

Figure 4-4. Block diagram of electronic circuit.

The gamma signals are taken directly from the photo-multiplier tube base to the counting room amplifier without pre-amplification. This provides a signal into the amplifier with a faster rise time, resulting in improved timing resolution. The photomultiplier was operated at 1150 volts. The output of the amplifier is a delay-line clipped, bipolar signal with a very fast zero cross-over.

This signal enters a timing single-channel analyzer, with the discriminator level and width set to include the range of scintillator signal amplitudes corresponding to the full energy peak of the de-excitation gamma rays and most of the signals from the Compton-scattered gamma rays. The lower level setting is governed by consideration of background levels, accidental rate and "timing walk". The discriminator signal could be used to gate the delayed gamma signals routed to the second ADC of the dual-parameter analyzer.

The timing single-channel analyzers in the proton and gamma signal circuitry also generate a negative 1 volt pulse, less than 5 nanoseconds wide, at the point of zero cross-over of the bipolar signals whose amplitudes are within the selected range of the discriminators. These timing signals operate a time-to-pulse-amplitude converter (TAC). The proton cross-over timing signal initiates a pulse in the TAC which increases in amplitude linearly with time, and the gamma cross-over timing signal stops this rise. Hence, the TAC output pulse amplitude is proportional to the time elapsed between the

proton and gamma signals.

If there are proton and gamma signals in true coincidence, such as in the electromagnetic decay of states excited by inelastic proton scattering, then there will be a predominance of TAC output signals of a given amplitude. Accidental coincidences will produce signals of a random amplitude.

In the timing single-channel analyzer (SCA), the cross-over pick-off may be adjusted for a given pulse shape from the amplifier in order to minimize "time walk" due to the finite spread of signal amplitudes accepted by the discriminators, especially the gamma signals. Fast cross-over of the bipolar signals, obtained by adjusting the amplifier shaping, also improves timing resolution.

Figure 4-5a displays the amplitude distribution of the TAC output for the reaction $C(p, p'\gamma)$. The large peak is due mainly to real proton-gamma coincidences, and is less than 10 nonoseconds, FWHM. The smaller peaks are accidentals, which are bunched due to the pulsed beam nature of the cyclotron. Note that the period of the peaks is 42 nanoseconds, which corresponds to the 23 MHz cyclotron frequency.

The TAC output also enters two single-channel analyzers. In one, the discriminator levels are set to encompass the coincidence peak; in the other, the discriminator levels bracket an accidental peak. Figure 4-5b depicts the results of gating the delayed TAC pulses

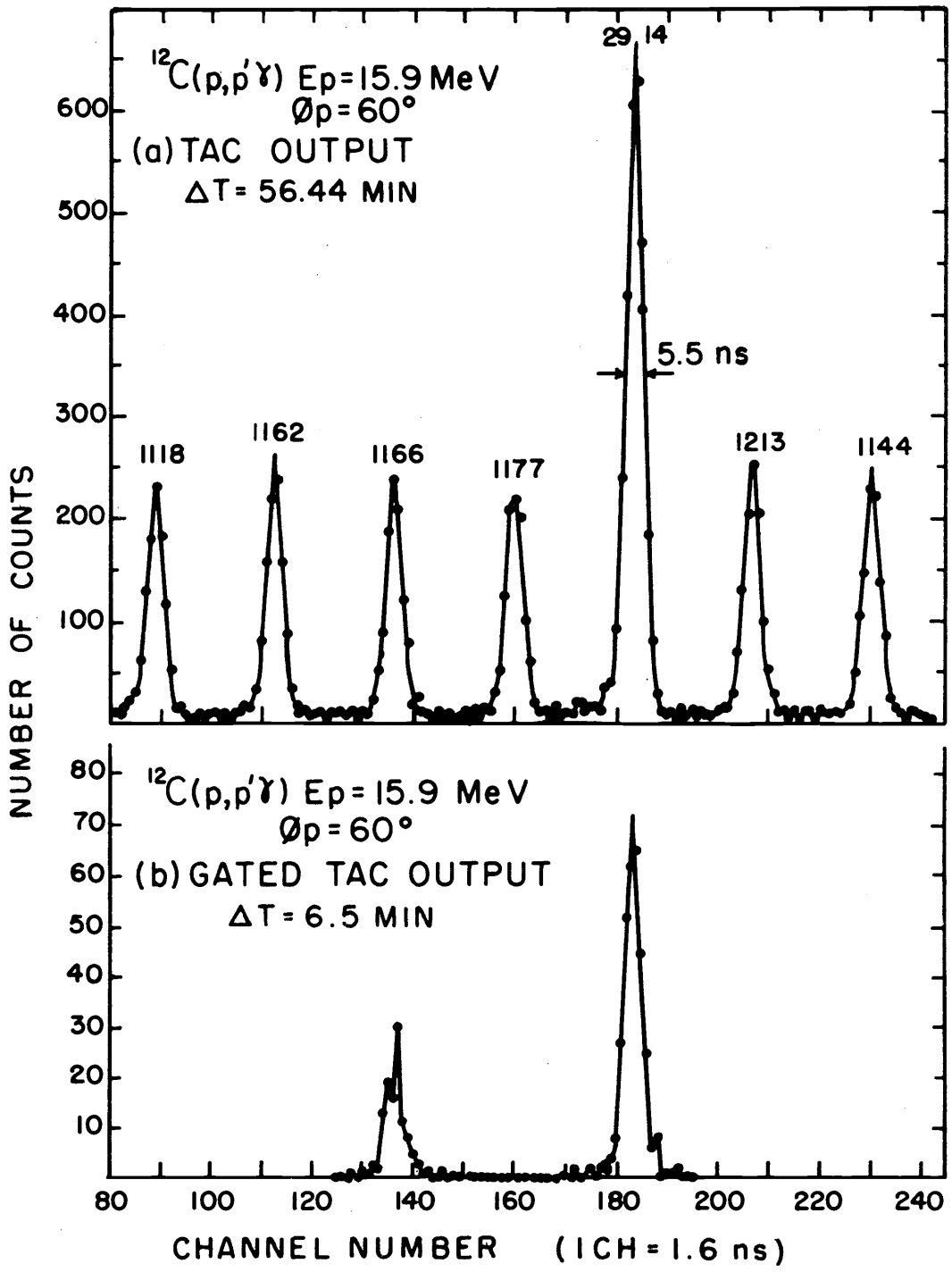

Figure 4-5. (a) Time-to-amplitude converter (TAC) output spectrum.
(b) TAC output spectrum, gated by the sum of the outputs from the two SCAs selecting the coincidence peak and one accidental peak.

routed into a 512-channel analyzer with the sum of the two SCA outputs. The output of the SCA set on the coincidence peak is also used to gate the delayed gamma signals prior to the second ADC of the dual-parameter analyzer, thus resulting in a gamma spectrum consisting mainly of the gammas in coincidence with the inelastically scattered protons.

In addition, the outputs of the two SCA's connected to the TAC output are used to trigger two more scalers. In this way the coincidence and accidental rates are monitored, as well as the inelastic protron signal rate. This was useful in calculating rough values for the proton spin-flip probability during the data taking.

V. DATA COLLECTION, ANALYSIS AND RESULTS

The time required for data collection varied from about 15 minutes per scattered proton angle at forward angles for $^{12}C(p, p'\gamma)$ to 2 to 3 hours at the angles of lowest yield of protons inelastically scattered from ^{32}S. The collection time was dictated by the need to accumulate sufficient counts in the coincidence and accidental monitors to reduce the effects of statisical fluctuations.

Data were usually taken at 5 degree intervals in the experiment on carbon and at 10 degree intervals on sulfur.

Coincidence Spectra

The coincidence and accidental spectra generated by the TAC and recorded in the 512 channel analyzer were typed out after each run (see Figure 4-5). The number of events under each peak was then determined. To further minimize the effects of statistical fluctuations, the accidental counts were averaged over four peaks, two on the either side of the coincidence peak.

The number, N_t, of true proton-gamma coincidences was then obtained by subtracting the averaged accidentals from the total coincidences. Statistical uncertainties in these results varied from less than 4% at back angles to more than 10% at forward angles, and formed the major contribution to uncertainties in the spin-flip measurement at most angles.

Proton Spectra

Samples of the energy distribution of protons scattered from carbon and sulfur are shown in Figures 5-1a to 5-1d. Results are displayed for both forward and backward scattering angles to indicate the rather low background levels encountered and the effects of target thickness on the width of the peaks. The window set by the SCA to encompass the protons from the lowest 2^+ level is indicated in each figure.

By comparing the relative position and shape of the ungated proton spectrum to that of the gated spectrum taken at the same angle but for the duration of the coincidence collection time, the stability of the proton detection system is demonstrated. In Figure 5-1d, a gain shift of less than 1 channel out of 250 is observed during the nearly two hours spent at 160° on sulfur.

Background subtraction was carried out in the following way: the background level under the 2^+ peak was extrapolated in a short, ungated run. The total number, B, of events in the window of the long, gated run was counted, along with the total number, A, and background number, C, in the same channels in the ungated spectrum. The background in the long, gated run is then $C \times B/A$. The net counts during the long runs is $B(1-C/A)$ and is the number of protons inelastically scattered into the detector from the 2^+ level during the

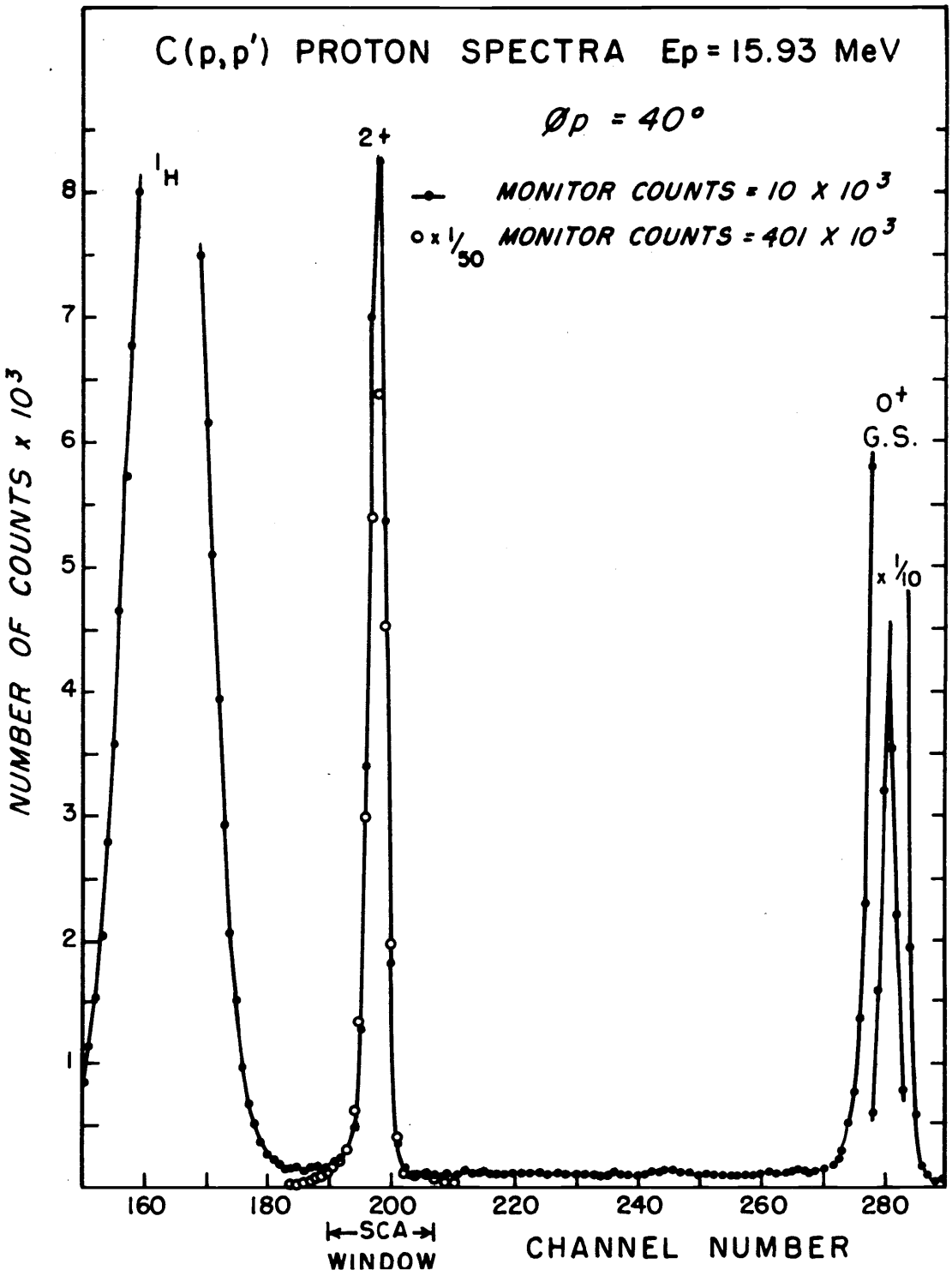

Figure 5-1a. Energy spectrum of 15.93 MeV protons scattered from carbon through 40° (lab).

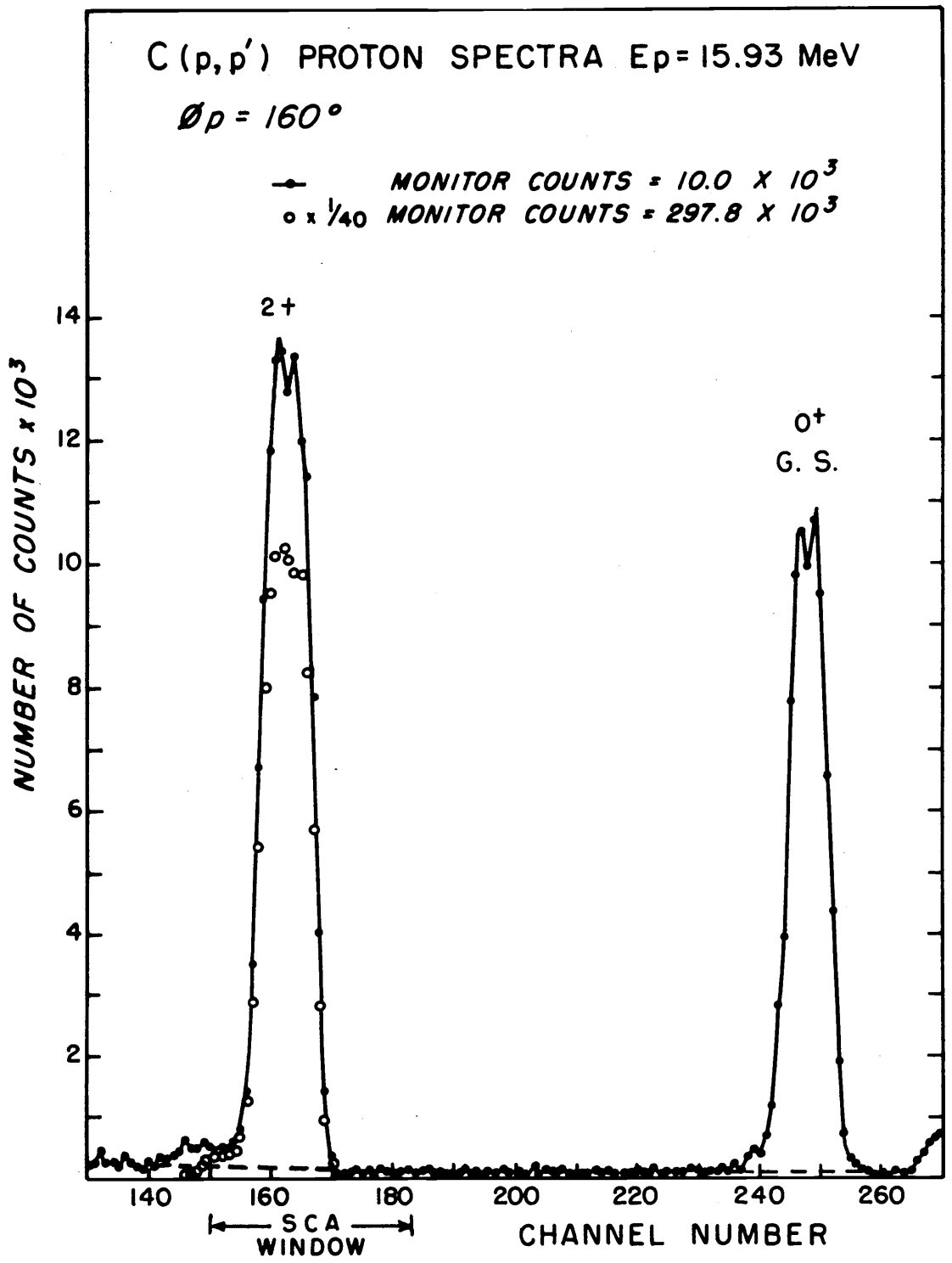

Figure 5-1b. Energy spectrum of 15.93 MeV protons scattered from carbon through 160° (lab).

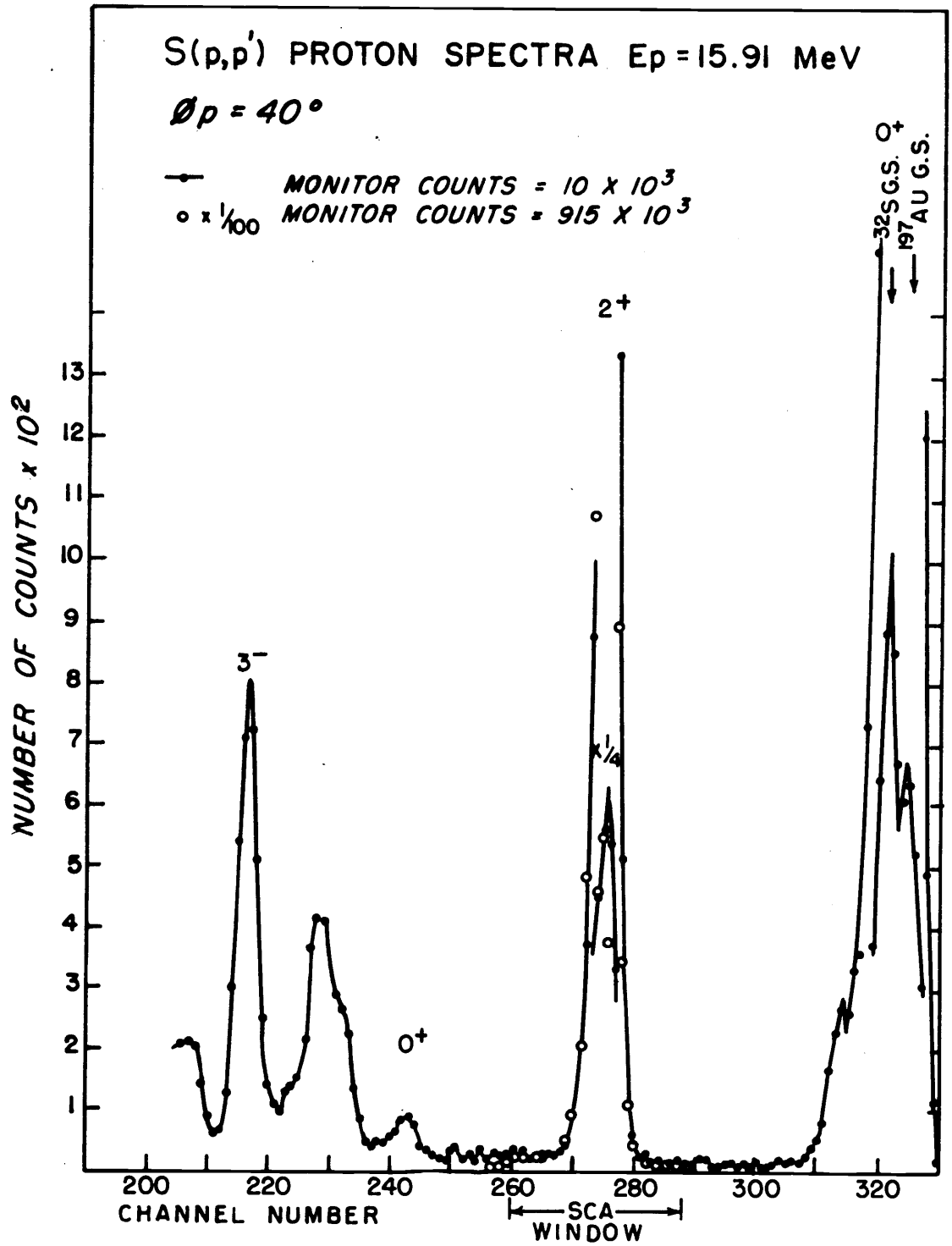

Figure 5-1c. Energy spectrum of 15.91 MeV protons scattered from sulfur through 40° (lab).

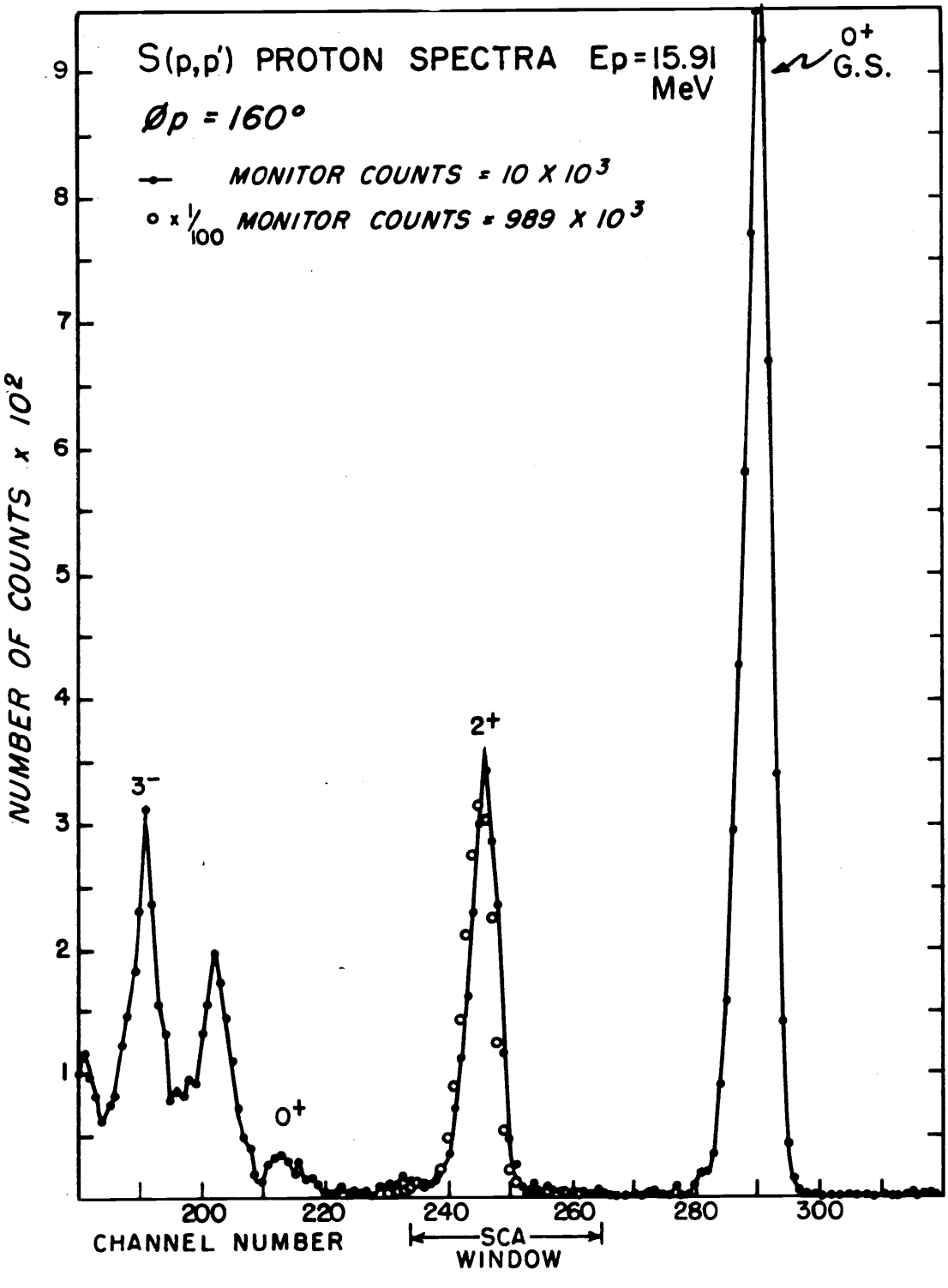

Figure 5-1d. Energy spectrum of 15.91 MeV protons scattered from sulfur through 160° (lab).

time that N_t true coincident proton-gamma events were recorded. The amount of background subtracted was never more than a few percent of the net protons except at the most forward angles. In addition, little evidence of target contamination which could affect the number of counts in the 2^+ peak was observed any angle. The uncertainties in the background estimation were negligible relative to the statistical uncertainties in the number of true coincidences.

Two types of information were used to estimate analyzer dead-time losses of inelastic proton counts. 1) Since the elastic peak accounted for more than half the analyzing time in the ungated spectrum, the analyzer dead time should be reduced significantly for the gated spectrum. When the total number of counts under the 2^+ peak was compared for gated and ungated spectra taken for the same number of monitor counts, the two totals agreed to within the statistical uncertainty of the numbers involved (about 1%), except at $\phi_p = 30°$. This indicated that at most angles dead-time losses were negligible. 2) During the coincidence measurements, half the dual-parameter analyzer monitored the coincidence gammas, which were accumulated at a very low rate. The other half stored the gated proton spectrum. Comparison of the live times of the two halves during any given run revealed dead-time losses for proton analysis of less than 1% at all angles.

Gamma Spectra

Figures 5-2a and 5-2b display the ungated and proton-gamma coincidence gated gamma spectra resulting from 15.9 MeV protons on carbon. Figures 5-3a and 5-3b display the same information for the case of a sulfur target. Even in the ungated spectra, it is clear that radiation from the first 2^+ level in each target constitutes the main source of gamma-rays incident on the detector. In the gated spectra, the contrast above background has been considerably enhanced. This is most noticable by comparing the relative contributions of the background annihilation peak at 0.51 MeV in the gated and ungated spectra for $S(p, p'\gamma)$. From these spectra, it becomes quite evident that the recorded proton-gamma coincidences result from proton excitation and subsequent radiative de-excitation of the first 2^+ levels in carbon and sulfur.

In order to determine the absolute proton spin-flip probability it is necessary to determine the absolute efficiency of the gamma detection system. Three contributions to the efficiency will be considered: 1) system dead-time losses due to high counting rate, 2) loss of signals with amplitude below the setting of the lower-level discriminator, 3) acceptance solid angle and intrinsic efficiency of the NaI crystal detector.

Losses due to high counting rate were observed only for the

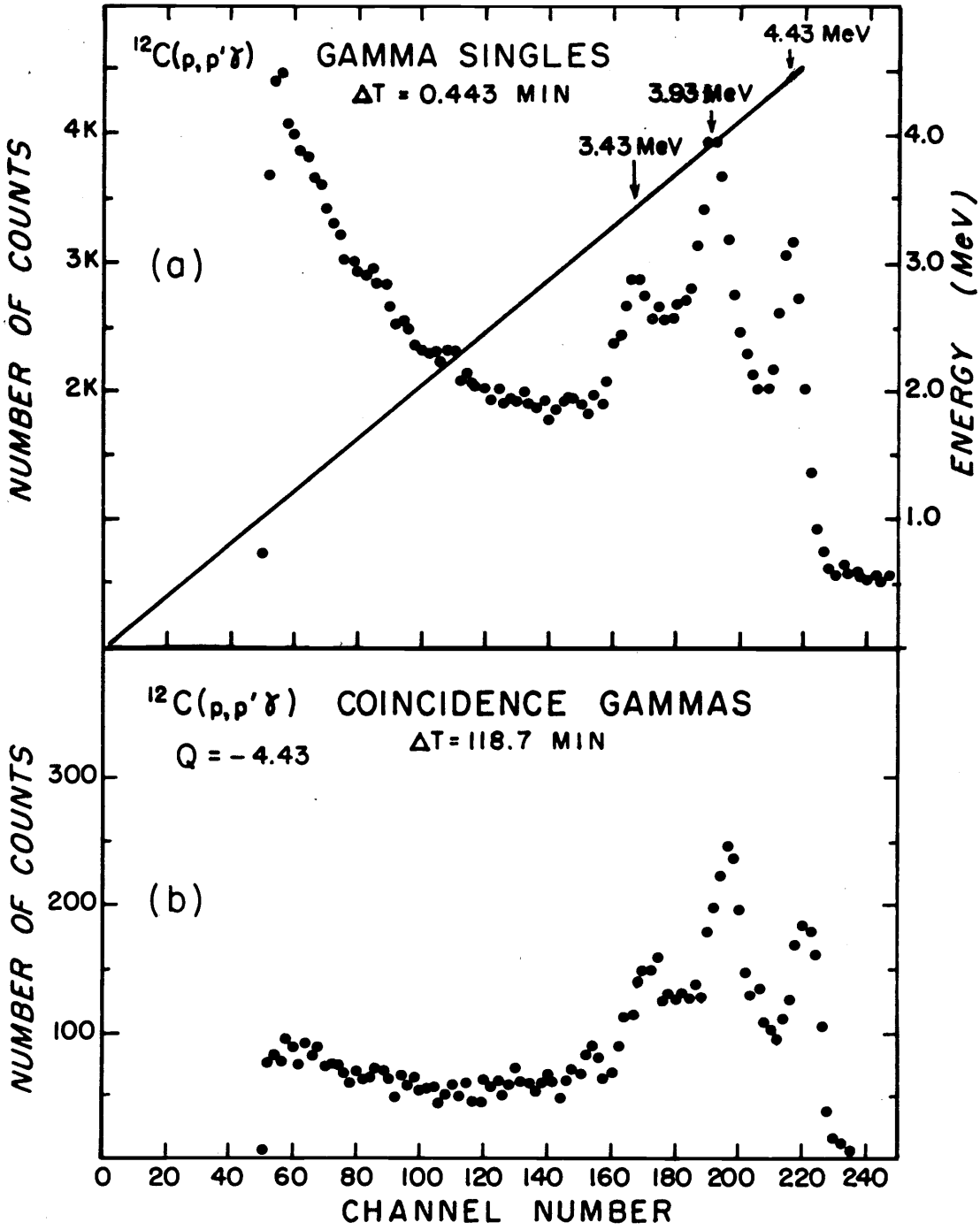

Figure 5-2. (a) Gamma-ray spectrum resulting from 15.93 MeV protons on carbon.
(b) Spectrum of gamma-rays in coincidence with protons inelastically scattered from the 4.43 MeV level in ^{12}C.

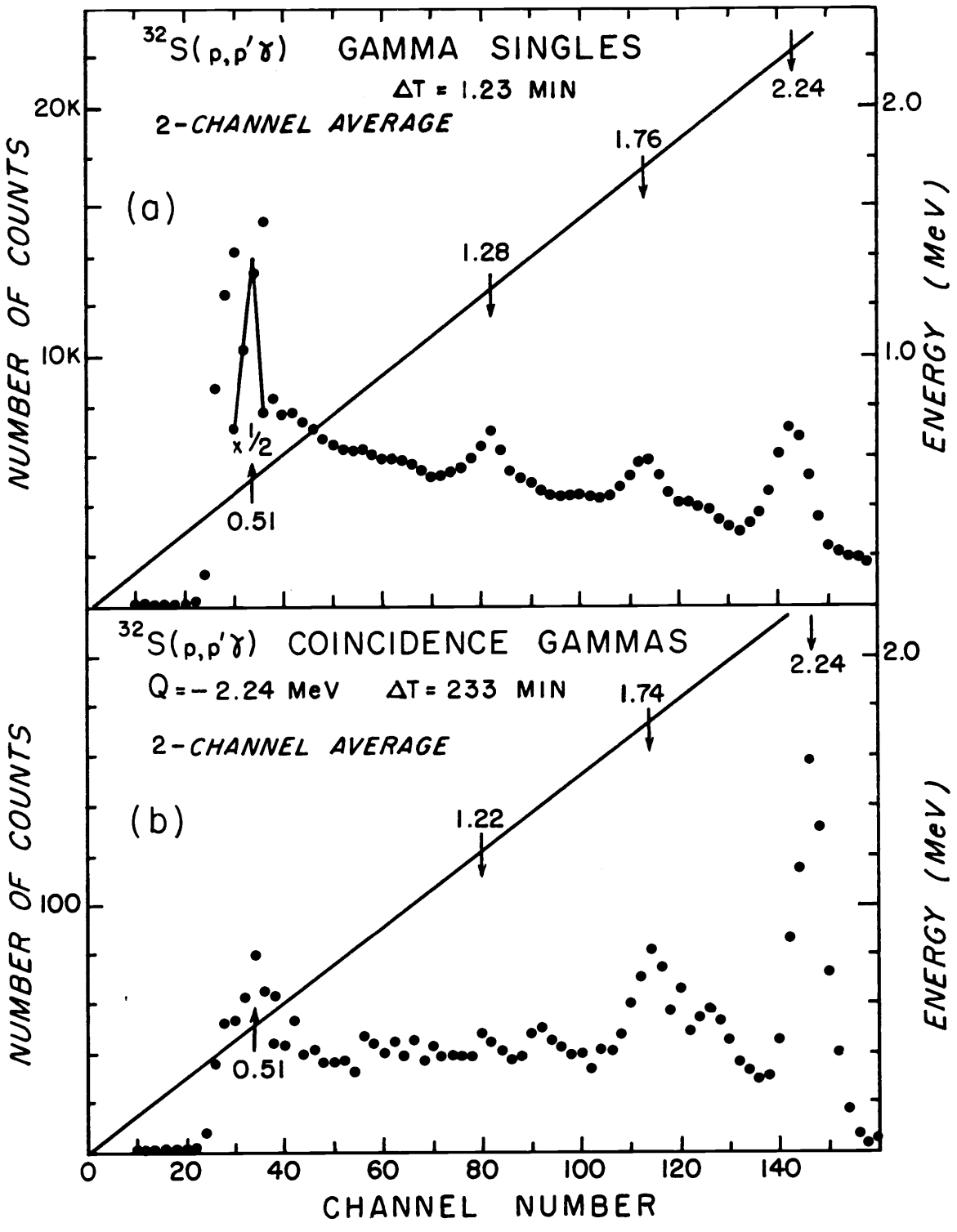

Figure 5-3. (a) Gamma-ray spectrum resulting from 15.91 MeV protons on sulfur.
(b) Spectrum of gamma-rays in coincidence with protons inelastically scattered from the 2.24 MeV level in ^{32}C.

reaction $S(p, p'\gamma)$ at the higher incident proton energy. Figure 5-4 demonstrates how this effect is measured. The ratio of true coincidences to inelastically scattered protons, N_t/N_p, at the high-yield angle $\phi_p = 140°$, is plotted as a function of the product of target thickness times beam current. The target thickness is expressed in terms of yield into the monitor counter per microcoulomb of protons collected in the Faraday cup. A yield of about 50×10^3 per microcoulomb corresponds to a target about 50 keV thick. For a target of this thickness, it is apparent that N_t/N_p is nearly constant with beam current, for currents below four nanoamperes. Hence, below this level, the measured spin-flip probability will not be affected by the counting rate. In practice the beam current was held to such a level that, for a given target yield, only corrections of two to six percent were required to adjust for counting rate losses.

Figures 5-5a and 5-5b show the effect of the setting of the lower level gamma-signal discriminator on N_t/N_p. The value of N_t/N_p is plotted as a function of $(C_p - C_{LL})/C_p$, where C_p is the channel position of the full-energy peak of the detected gamma-ray, and C_{LL} is the position of the lower level discriminator. From Figures 5-2b and 5-3b, it is seen that the discriminator was usually set well into the region of detected compton-scattered electrons. Assuming the distribution of compton electrons remains approximately flat to zero energy (a reasonable assumption based upon published [25] curves of

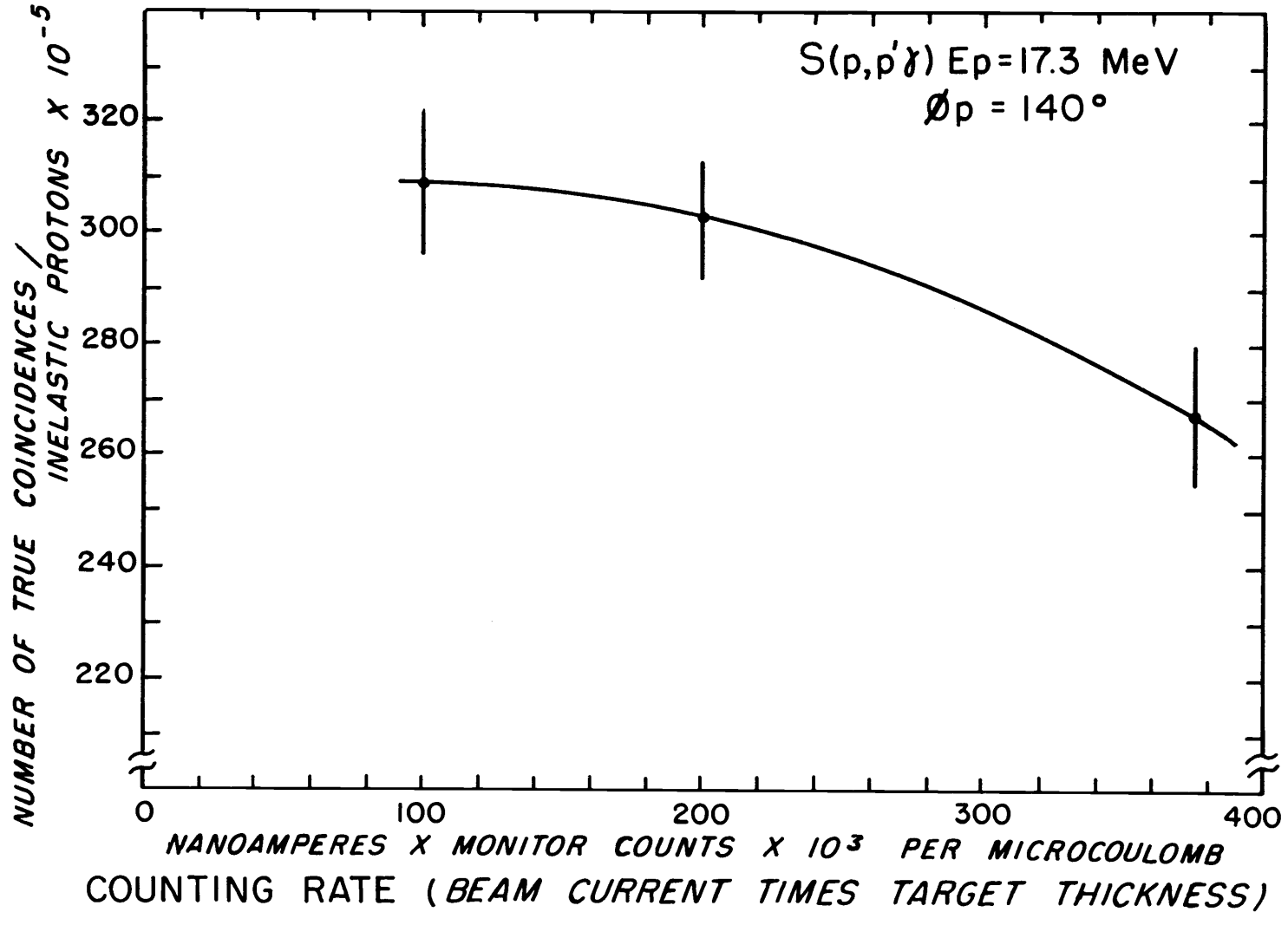

Figure 5-4. Coincidence counting loss vs. counting rate.

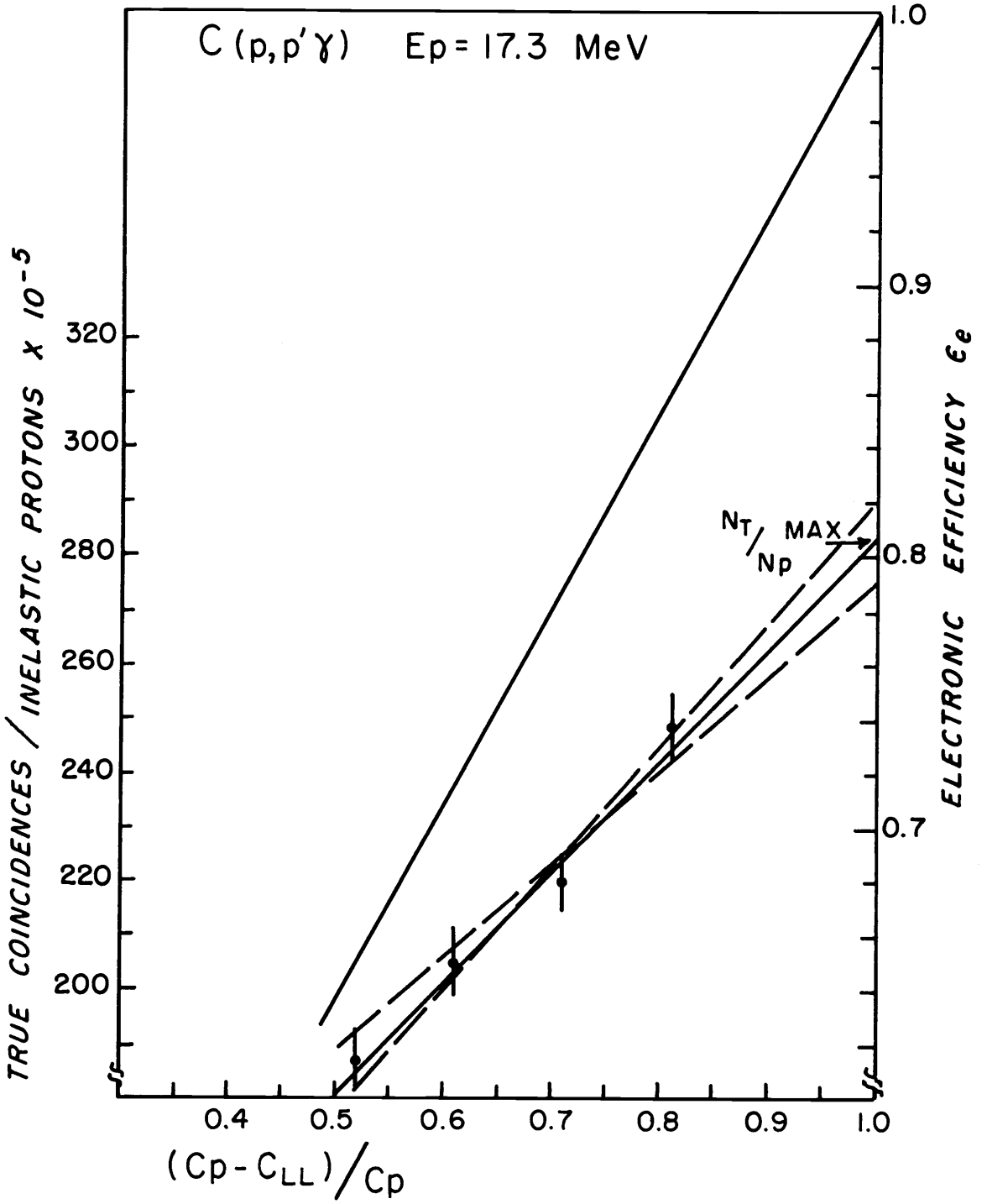

Figure 5-5a. Electronic detection efficiency vs. lower-level discriminator setting, for 4.43 MeV gamma-rays.

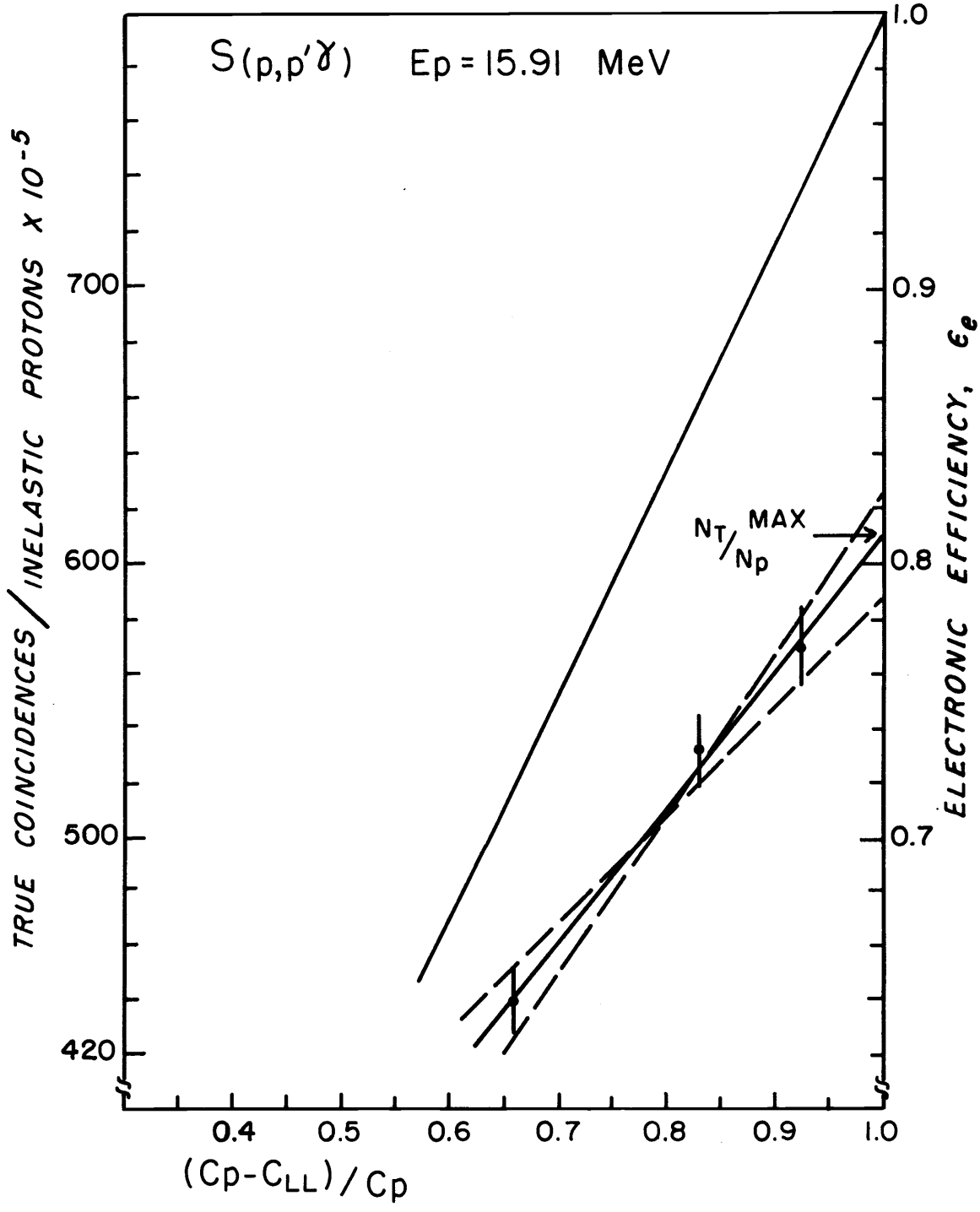

Figure 5-5b. Electronic detection efficiency vs. lower-level discriminator setting, for 2.24 MeV gamma-rays.

gamma-ray scintillation spectrometers), a good approximation for the maximum possible value of N_t/N_p is a straight-line extrapolation of data points to the value of N_t/N_p on the axis where $(C_p - C_{LL})C_p = 1$, hence to zero discriminator level.

In practice the value of $(C_p - C_{LL})/C_p$ is obtained by recording an ungated gamma spectrum briefly before each long coincidence collection, which enables a determination of $\frac{(N_t/N_p)}{(N_t/N_p)_{max}}$ to be made from the plots in Figures 5-5a and 5-5b. This ratio, referred to as the electronic detection efficiency, ϵ_e, is then used to correct the spin-flip probability measurement for the gamma-signal threshold detection efficiency. The statistical uncertainty in the values of N_t used in the data points contributes an error of about 3% to the extrapolation. The electronic detection efficiency is therefore uncertain by $\pm$ 3%.

It was observed that the photomultiplier power supply was not sufficiently stable to prevent a slow increase in gain, corresponding to 5 to 10 channels out of 250, in the course of a day's operation. This is evident in Figures 5-2 and 5-3, where the coincidence-gated spectra, taken after the short, ungated spectra, show a shift of 4 to 5 channels. This shift was most conspicuous during the early part of the day, but never completely ceased throughout the day, even when the equipment remained on continuously. The curves in Figures 5-5a and 5-5b were used, along with the measured value of $(C_p - C_{LL})/C_p$

to correct each run for the subsequent change in ϵ_e.

The combination of acceptance angle and intrinsic efficiency (absolute detection efficiency) of the NaI crystal was determined, as a function of gamma energy, by measuring the response of the detector to gamma sources of known energy and intensity placed in the mid-plane of the scattering chamber at the position usually occupied by the target.

Standard point sources ^{54}Mn (0.84 MeV), ^{22}Na (1.28 MeV), ^{60}Co (1.17, 1.33 MeV), and ^{88}Y (0.90, 1.84 MeV) were supplied by the International Atomic Energy Agency and calibrated prior to shipment. The subsequent decay in intensity of each source was computed from the known half-life. Figures 5-6a and 5-6b show the spectra obtained by placing samples of ^{88}Y and ^{60}Co in the chamber for a period of five minutes each. Dividing the measured counting rate by the source strength gives the absolute detection efficiency of the detector system for each gamma-ray energy. When two lines with an appreciable difference in energy are present, as in the case of ^{88}Y, then the spectra are unfolded, as indicated in Figure 5-6a, to give the counting rate for each gamma energy.

An additional calibration point was obtained at 2.75 MeV from the decay of ^{24}Na, produced by neutron irradiation of ^{23}Na, in the form of NaOH, at the Oregon State University TRIGA reactor.

The strength of this source was determined by a technique

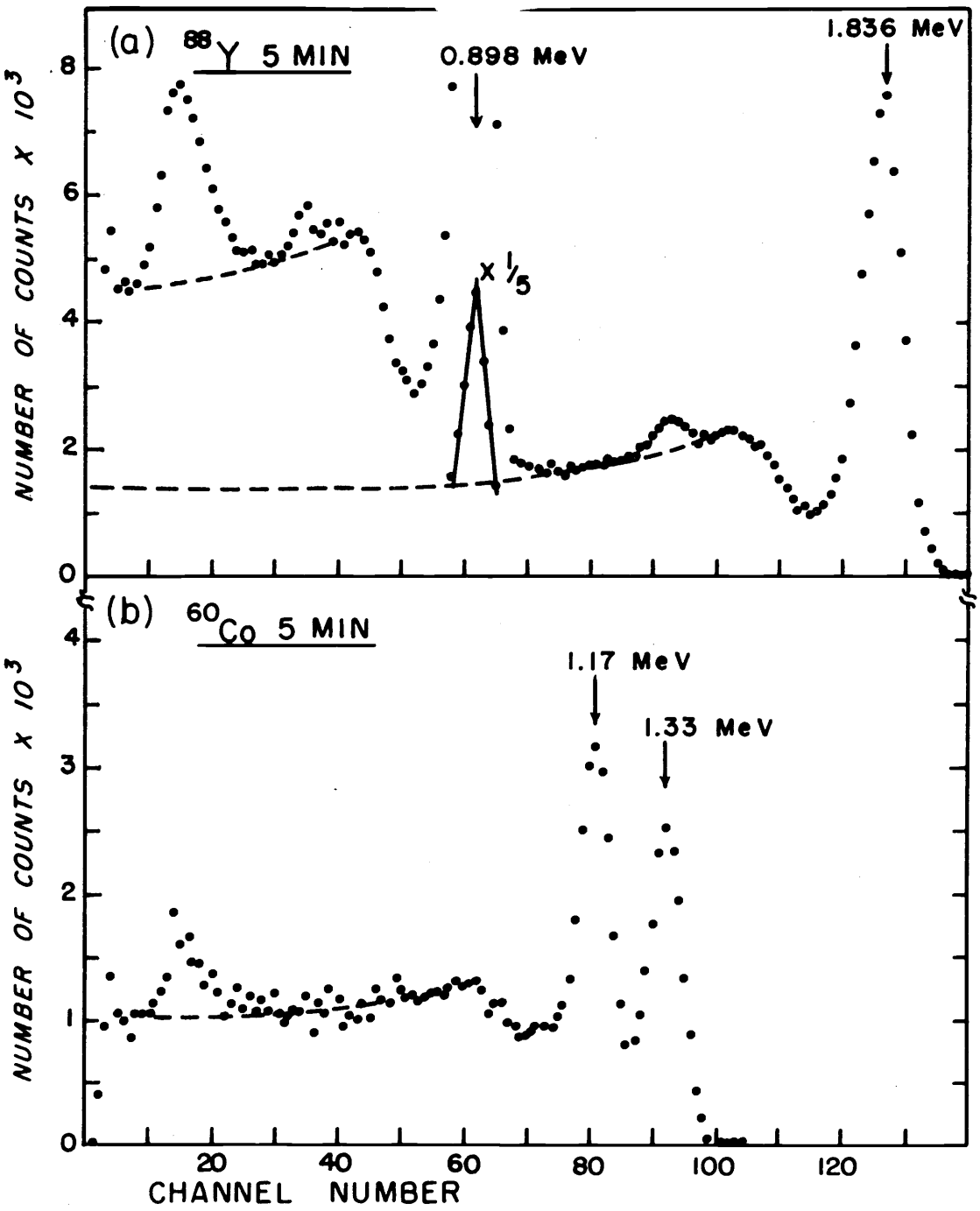

Figure 5-6. (a) Gamma spectrum from ^{88}Y.
(b) Gamma spectrum from ^{60}CO.

employing two NaI detectors in coincidence, since both a 2.75 MeV and a 1.37 MeV gamma-ray are emitted for 99.94% of the β^- decay of ^{24}Na. The following expressions show how this property may be used to determine the strength of the ^{24}Na sample:

Let ϵ = the detection efficiency, including electronics, of a 1.37 MeV gamma and ϵ' = the detection efficiency, including electronics of a 2.75 MeV gamma.

The number, N_1, of singles recorded by detector system one;

$$N_1 = S(\epsilon_1 + \epsilon'_1) , \tag{5-1}$$

where S is the source strength.

The number, N_2, of singles recorded by detector system two;

$$N_2 = S(\epsilon_2 + \epsilon'_2) . \tag{5-2}$$

The number of coincidences, C, between detector systems 1 and 2 is proportional to the probability that a 1.37 MeV gamma is being detected by system 1 while the corresponding 2.75 MeV gamma is being detected simultaneously by system 2, plus the reverse arrangement:

$$C = S\epsilon_2\epsilon'_1 + S\epsilon'_2\epsilon_1 = S(\epsilon_2\epsilon'_1 + \epsilon'_2\epsilon_1) \tag{5-3}$$

Since

$$N_1N_2 = S^2(\epsilon_1 + \epsilon'_1)(\epsilon_2 + \epsilon'_2) , \tag{5-4}$$

therefore

$$\frac{N_1 N_2}{C} = S\left(1 + \frac{\epsilon_1\epsilon_2 + \epsilon'_1\epsilon'_2}{\epsilon_1\epsilon'_2 + \epsilon'_1\epsilon_2}\right). \qquad (5\text{-}5)$$

This last expression is used to determine the source strength from the experimentally measured quantities. The term involving the detector efficiencies can be simplified by choosing the energy gains of the two systems to be equal, and by positioning the source such that the total count rates of the two systems are equal. If the detection efficiency vs. gamma energy does not vary between systems one and two, then on has $\epsilon_1 = \epsilon_2$ and $\epsilon'_1 = \epsilon'_2$. Hence,

$$N_1 N_2 / C = S\left[1 + \tfrac{1}{2}\left(\epsilon_1/\epsilon'_1 + \epsilon'_1/\epsilon_1\right)\right]. \qquad (5\text{-}6)$$

Thus, only the detection efficiency ratio of the two gamma-rays from the pulse-height spectrum of one of the detection systems need be determined in addition to N_1, N_2 and C in order to calculate S.

This method was able to reproduce the stated source strength (corrected for decay) of the ^{88}Y sample to 6% and that of the ^{60}Co sample to within $1\frac{1}{2}$%. One contribution to the uncertainty for measuring the source strength of the ^{88}Y sample results from the β-decay going only 92% to the upper level at 2.74 MeV, with 8% going directly to the 1.84 MeV level. Eight percent of the gamma emissions are thus only singles. Hence, a portion less than 8% (to be determined by the setting of the lower level discriminator) of the singles counts,

N_1 and N_2, does not contribute to the coincidences and are subtracted before calculating S.

The estimated uncertainty in the determination of the strength S of the ^{24}Na sample by this method is about 3% to 4%.

In Figure 5-7 a smooth curve has been drawn through the points representing the experimentally determined absolute detection efficiencies as a function of gamma energy. In addition several points have been included from the catalogue of R. L. Heath [25] and from the computer calculations of C. C. Grosjeans [26] for the absolute detection efficiency of a 3x3 NaI crystal 20 cm from the source. A difference of from 5% to 8% exists between the present and the earlier works. Of this, 2% to 4% may result from the fact that the distance from the source to the front of the crystal covering was determined to be 19.68 $\pm$ 0.16 cm in the present experiment. The additional discrepancy may be due to the presence of large amounts of lead and aluminum (see Figure 4-3), causing some scattering into the detector. The geometry of Heath's apparatus was more open. At gamma energies above 2.75 MeV the experimental curve was extrapolated parallel to the points from the earlier works.

An estimate of the uncertainty in the absolute detection efficiency of the present NaI detector is about 6%. Adding quadratically the uncertainty in the extrapolation of the electronic detection efficiency, ϵ_e, the over-all uncertainty in the efficiency of the gamma

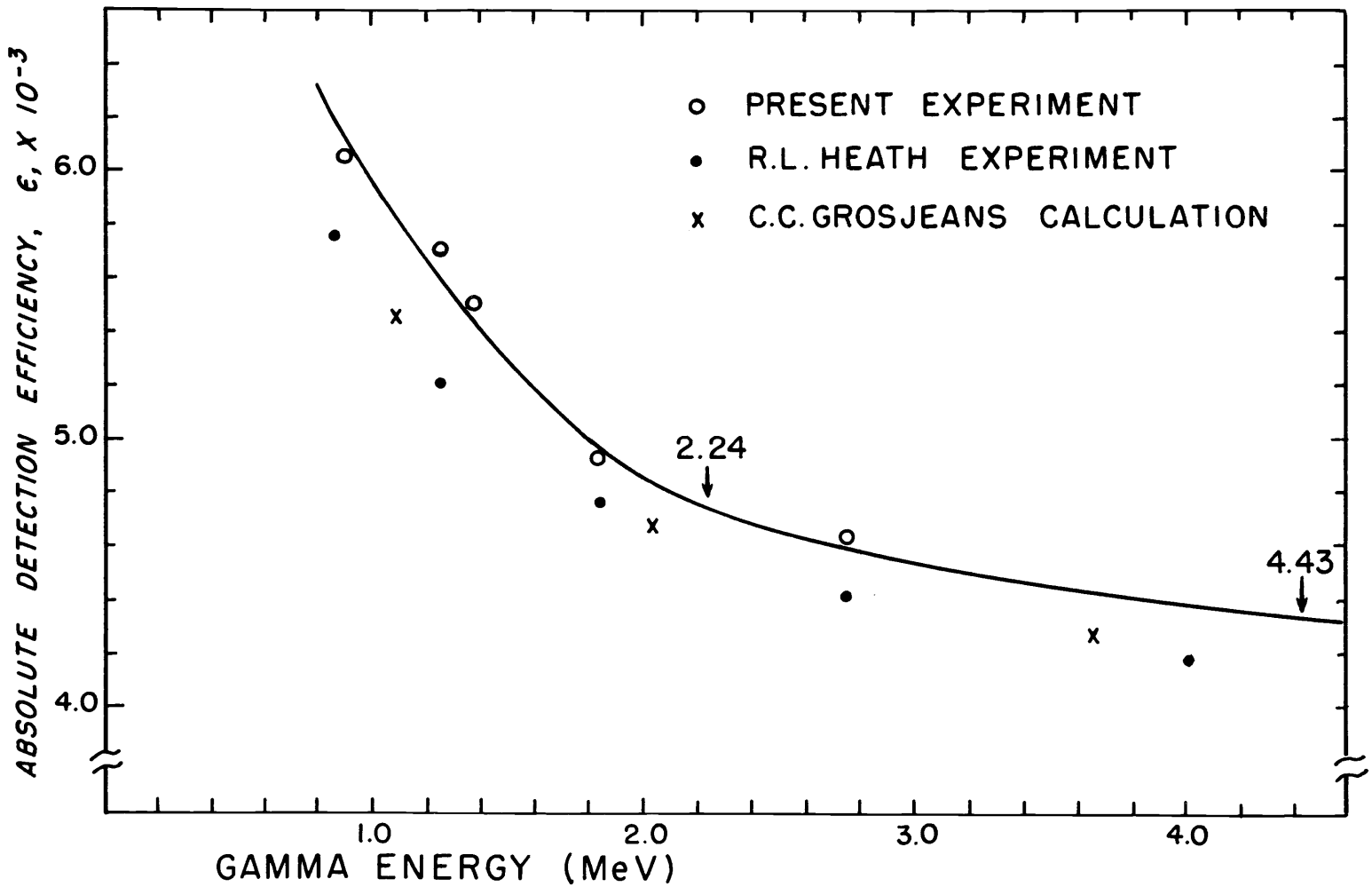

Figure 5-7. Absolute detection efficiency vs. gamma-ray energy for a 3"x3" NaI detector 7-7/8" from a point source.

detection system is about 7%.

Substate Contamination

The total probability $P(\phi_p)$ for the emission into the solid angle subtended by the detector of gammas from the transition 2^+ to 0^+, where the upper 2^+ level was populated by inelastic scattering of protons through angle ϕ_p, is given by (see Equation 2-9):

$$P_z(\phi_p) = M_1 S_1(\phi_p) + M_2 S_2(\phi_p) + M_0 S_0(\phi_o) , \qquad (5-7)$$

where for $\theta_0 = 10.4 \pm 0.4°$ (detector half-angle),

$$M_1 = 2\pi \int_0^{\theta_0} |X_2^1|^2 d\theta = 0.0197 \pm 0.0018 \qquad (5-8a)$$

$$M_2 = 2\pi \int_0^{\theta_0} |X_2^2|^2 d\theta = 0.00034 \pm 0.00003 \qquad (5-8b)$$

$$M_0 = 2\pi \int^{\theta_o} |X_2^0|^2 d\theta = 0.00102 \pm 0.00012 \qquad (5-8c)$$

The X_L^M are the normalized vector spherical harmonics, and $S_M(\phi_p)$ is the probability for populating the M-substate by inelastic proton scattering through angle ϕ_p. Further,

$$S_1(\phi) + S_2(\phi) + S_0(\phi) = 1 , \qquad (5-9)$$

which states that a gamma-ray is emitted for every proton inelastically scattered from the given level through angle ϕ .

The true number of proton-gamma coincidences at angle ϕ is:

$$N_t(\phi) = N_p(\phi)P_z(\phi)\epsilon_\gamma \quad , \tag{5-10}$$

where ϵ_γ is the scintillator detection efficiency times the electronic detection efficiency. The scintillator detection efficiency is the absolute detection efficiency, taken from the experimental curve in Figure 5-7, divided by the solid angle $\Delta\Omega$ subtended by the detector.

The solid angle calculated from the aperture size and position of the lead collimator was $4\pi \times 0.0078$ steradians, corresponding to a half-angle of 10.1°. However, from the efficiency measurements, the solid angle was computed to be $4\pi \times 0.0088$ steradians, corresponding to a half-angle of 10.8°. A compromise value of the aperture half-angle of 10.4°, corresponding to a solid angle of $4\pi \times 0.0082$ steradians was used in the limits of integration for the calculation of M-substate contributions and as the value for $\Delta\Omega$ in the expression for ϵ_γ. Although the calibration gamma sources may be assumed to radiate isotropically, while the M-states of sulfur may not, this compromise value for the detector acceptance angle will cancel, to first order, the uncertainty in the calculation for $S(\phi)$ due to the disagreement in the two methods for determining $\Delta\Omega$. A slight increase in the uncertainty of the $M = 0, \pm 2$ substate contributions

does occur if the unaccountable increase in detector efficiency is due to scattering from the chamber walls and shielding.

In order to compute $S_1(\phi)$, the spin-flip probability, the quantity $N_z(\phi)$ is now defined as:

$$N_z(\phi) = P_z(\phi)/M_1 = S_1(\phi) + S_0(\phi)M_0/M_1 + S_2(\phi)M_2/M_1 \quad (5-11)$$

or

$$N_z(\phi) = N_t(\phi)\Big/N_p(\phi)\epsilon_\gamma M_1 . \quad (5-12)$$

The values of S_0 and S_2 cannot be determined from the one angular correlation measurement, and are approximated by letting $S_0 = S_2$.

Since $S_1 + S_2 + S_0 = 1$, and substituting the above approximation, one has for N_z:

$$N_z = S_1(\phi) + (M_0 + M_2)[1 - S_1(\phi)]/2M_1 . \quad (5-13)$$

Inserting the values of the integrals, M:

$$N_z(\phi) = S_1(\phi)(1-0.034) + 0.034 \quad (5-14)$$

$$S_1(\phi) = 1.035N_z(\phi) - 0.035 . \quad (5-15)$$

N_z is calculated from the measured quantities in Equation (5-12) above.

The lack of knowledge of S_0 and S_2 introduces an uncertainty into the determination of S_1, the limits of which are set by selecting the extreme values for S_0 and S_2.

Upper limit: $S_0 = 0$, $S_2 = 1-S_1$.

Hence,

$$N_z = S_1 + (1-S_1)M_2/M_1 , \tag{5-16}$$

giving

$$S_1(\max) = 1.018N_z - 0.018 . \tag{5-17}$$

Lower limit: $S_2 = 0$, $S_0 = 1-S_1$,

hence,

$$N_z = S_1 + (1-S_1)M_0/M_1 , \tag{5-18}$$

giving

$$S_1(\min) = 1.053N_z - 0.053 . \tag{5-19}$$

An average value for the uncertainty in S_1 due to the lack of knowledge of S_0 and S_2 is then given by

$$\Delta S_1 = \pm \tfrac{1}{2}[S_1(\max) - S_1(\min)] = \pm 0.0175(1-N_z) . \tag{5-20}$$

At forward angles ΔS_1 may be nearly half the size of the calculated value for S_1 . This uncertainty has been added quadratically to the statistical uncertainty in the spin-flip measurements.

Results

Carbon

Figures 5-8b and 5-8c display the dependence on scattered proton

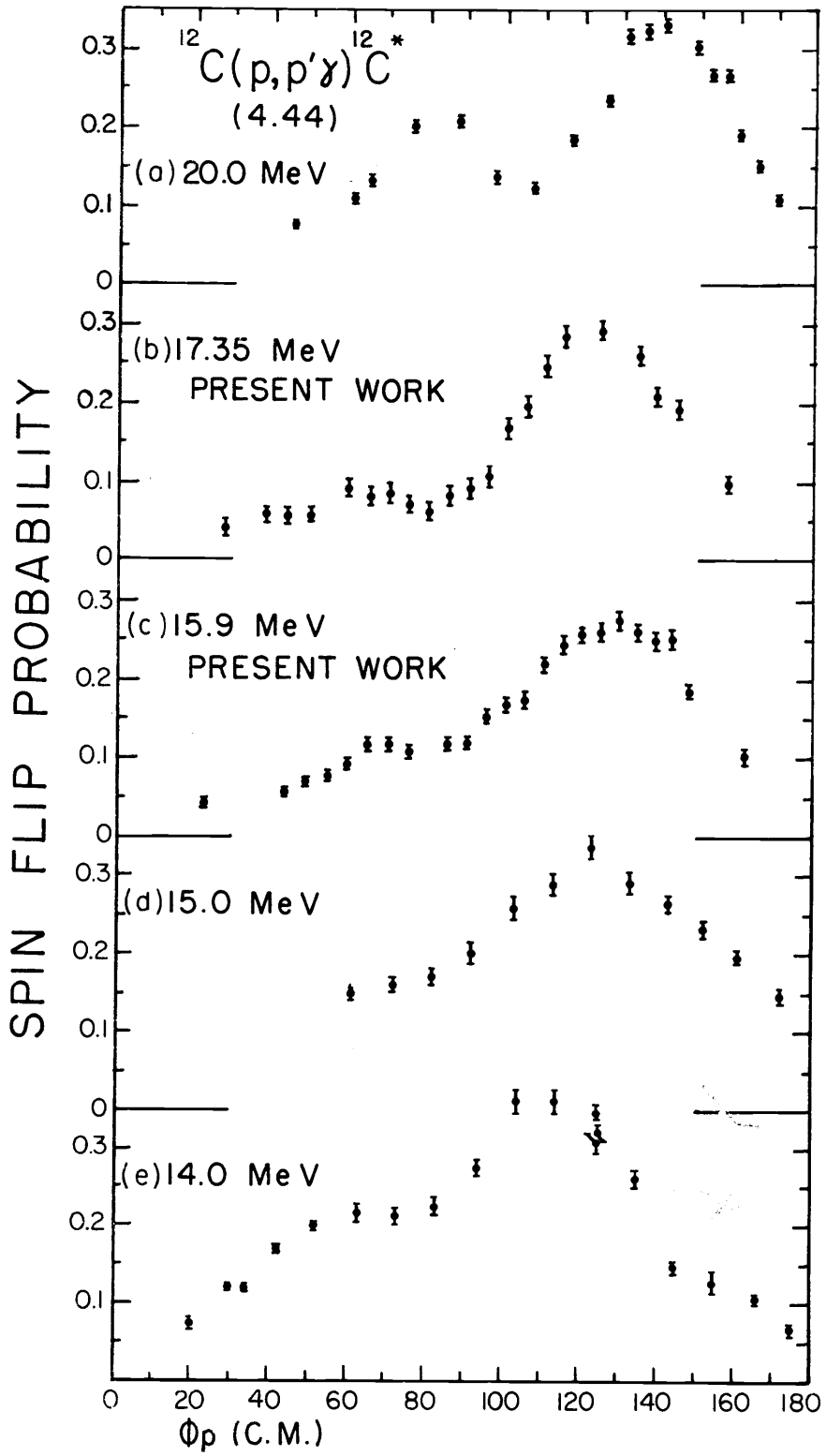

Figure 5-8a, b, c, d, e. Spin-flip probability in the reaction $^{12}C(p, p')^{12}C^*(4.43)$ at proton energies from 14 MeV to 20 MeV.

angle of the probability for proton spin flip during inelastic scattering from the first 2^+ state at 4.43 MeV in ^{12}C at incident proton energies of 15.93 MeV and 17.35 MeV, respectively. The gamma detector efficiency uncertainty places a 7% uncertainty in the absolute scale for S. Both figures show a small peak at about 70° and a maximum of about 30% at a backward angle of about 125°. The backward peak at 17.35 MeV is somewhat narrower and about 8% higher than the corresponding peak at 15.93 MeV, suggesting a slight dependence of $S(\phi)$ on the incident proton energy.

Included for comparison and a general check on the method, are Figures 5-8a, 5-8d and 5-8e, which display the results of proton spin-flip measurements to the same level at 20 MeV, 15 MeV and 14 MeV, respectively, by W. A. Kolasinsky et al. [20]. The forward peak is not evident at 15 MeV, but has become quite substantial at 20 MeV. Again, note that the back peak is narrower at 20 MeV than at 15 MeV.

Some differences do exist between the earlier data and the present work. Some prominent features are displayed in Table 5-1.

Table 5-1. Amplitude and position of peak spin-flip probability.

E_p (MeV)	Maximum Value	Angle of Maximum	
14	0.36 ± 0.034	110°	previous
15	0.34 ± 0.034	125°	"
15.93	0.275 ± 0.022	130°	present
17.35	0.293 ± 0.023	125°	"
20	$0.33 + 0.031$	140°	previous

The variation in the peak angle could be due to a dependence of $S(\phi)$ on the incident proton energy. The uncertainties associated with the spin-flip measurements very nearly account for the differences in the two sets of maximum values. The numerical value for the errors in the results by Kolasinsky was obtained by adding quadratically the uncertainty in the absolute gamma detection efficiency of $\pm$ 9% for $C(p, p'\gamma)$ [1, 5, p. 90] to the statistical uncertainty represented by the error bars in Figure 5-8. The error quoted in the present result is the quadratic sum of the uncertainty in the absolute gamma detection efficiency and the statistical uncertainty.

Some of the difference in the maximum values between the present work and the previous results may also be due to the way in which corrections for substate contamination were made. In the method employed by Kolasinsky [5, p. 89-92], the gamma-proton angular correlation function is expanded in terms of the gamma polar angle θ_γ and the integration is then performed over the solid angle (θ_0 = half-angle) subtended by the gamma detector. The results were carried out only to second order in θ_0, giving an expression for N_z:

$$N_z = (3/2)\theta_0^2 S_0 + [1-(5/4)\theta_0^2]S_1 + \tfrac{1}{2}\theta_0^2 S_2 . \qquad (5\text{-}21)$$

Assuming $S_0 = S_2$, then S_1 becomes:

$$S_1 = N_z - \theta_0^2[1-(9/4)N_z] \qquad (5\text{-}22)$$

As can be seen from this equation, $S_1 > N_z$ for $N_z > 4/9$. This result, possibly due to the truncation in the expansion in θ_0, leads to an over-estimation of the value of S_1. An exact expression would require $S_1 < N_z$ for $N_z < 1$.

In order to observe the difference in S_1 as calculated the two ways, let $\theta_0^2 = 0.033$ radians^2 (present aperture), then,

$$S_1 = 1.074N_z - 0.033 \quad \text{Kolasinsky Method}$$

$$S_1 = 1.035N_z - 0.035 \quad \text{Present Method},$$

which leads to a discrepancy $S_1 = 0.038N_z + 0.002$. For $N_z = 0.35$, the method by Kolasinski leads to a value of S_1 more than 4% higher than calculated by the present method.

It can be concluded that the shape and magnitude of the probability for spin flip of protons inelastically scattered from ^{12}C at 15.93 MeV and 17.35 MeV in the present work is in general agreement with results of previous measurements at 14 MeV, 15 MeV and 20 MeV incident proton energy. This agreement strengthens our confidence in results of measurements on sulfur obtained in the present work by the same method.

Sulfur

Figure 5-9 shows the probability as a function of proton scattering angle, for spin-flip of protons inelastically scattered from the

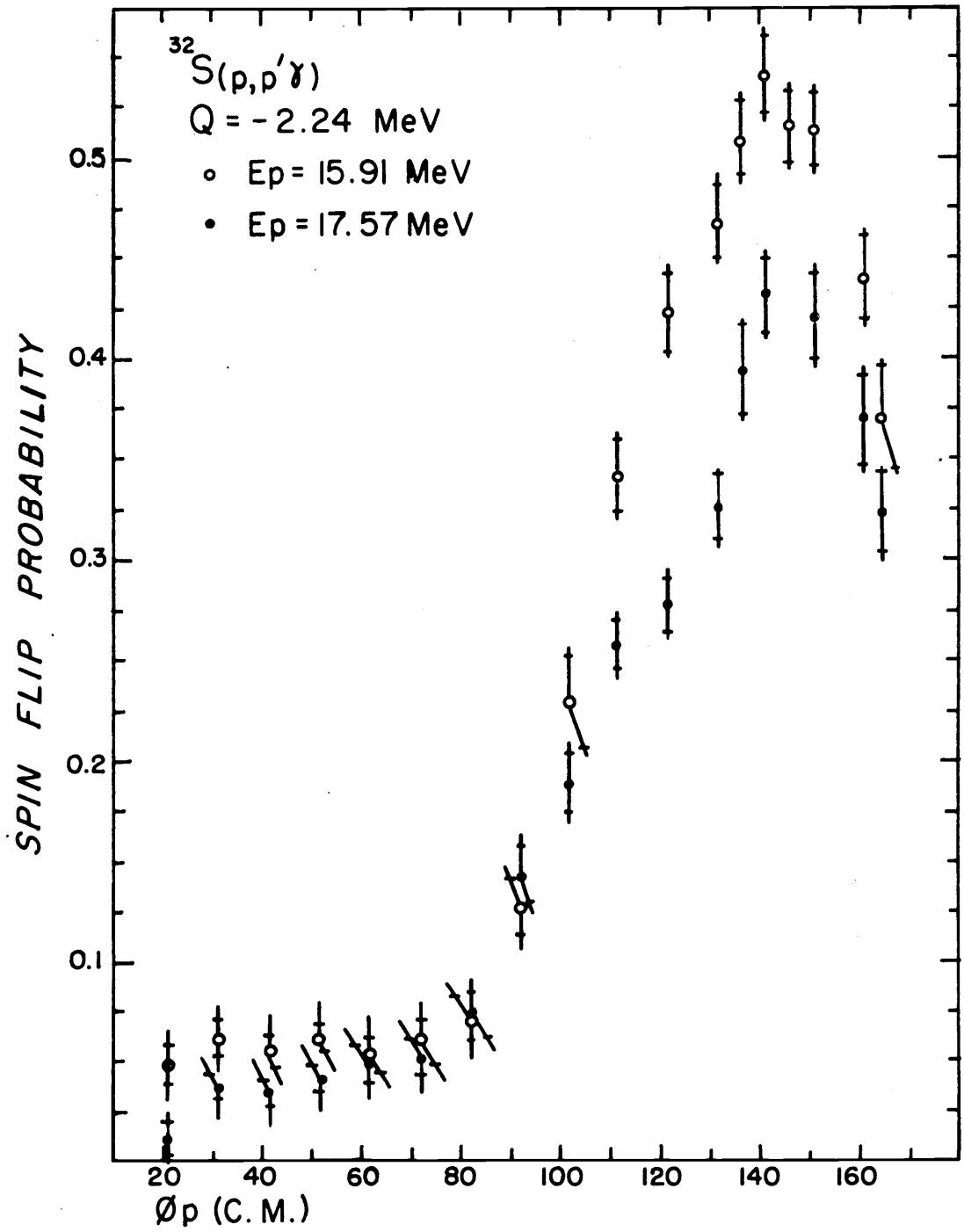

Figure 5-9. Spin-flip probability in the reaction $^{32}S(p, p')^{32}S^{*}(2.24)$ at proton energies of 15.91 MeV and 17.57 MeV.

2.24 MeV level in ^{32}S at incident proton energies of 15.91 MeV and 17.57 MeV. The small crosses on the vertical error bars indicate the limits of uncertainty due to statistical fluctuations, while the overall length of the error bars includes the M-substate mixing uncertainty.

The salient feature is the peak at 145° at both energies. At E_p = 15.91 MeV the maximum spin-flip probability is over 0.5, which is more than 20% higher than the maximum value at the higher proton energy. The difference is considerably more than could be expected from statistical fluctuation alone.

The behavior of $S(\phi)$ is devoid of any other structure except a slight fluctuation between 110° and 125°, which is better defined at 17.57 MeV than at 15.91 MeV.

Improved statistics and smaller proton and gamma acceptance angles would probably reveal this fluctuation more clearly, but each of these improvements would entail a considerable increase in running time. At the lower proton energy, however, the incident beam current could be doubled for the same target yield without introducing any appreciable counting losses in the gamma detection system. This would serve to reduce the increased data collection time required to diminish the uncertainty in the measured values of the spin-flip probabilities.

VI. COMPARISON BETWEEN THEORY AND EXPERIMENT AND CONCLUSIONS

A computer program has been developed [7, p. 143-196][27], for calculating proton spin-flip probabilities using the DWBA and based upon the optical model extension to collective excitations discussed in Chapter III. The optical potential employed in this program is of the form of Equation (3-4). This program was used in the present work to predict the inelastic proton spin-flip probability angular distributions for carbon and sulfur. Any value of the volume absorption parameter W, and imaginary spin-orbit strength W_{SO}, different from zero did not improve the spin-flip fits. Therefore, these parameters were subsequently set equal to zero in the calculations.

Sulfur

A spin-flip probability amplitude as large as the back-angle for protons on sulfur has not been reported for any other target nucleus. Considerable effort has been spent to fit the spin-flip data for sulfur at the higher proton energy (17.57 MeV) in this investigation.

The first attempt is shown in Figure 6-1. As mentioned in Chapter III, the quantity $\Delta = \beta_{SO}/\beta_0$ is a measure of the deformation of the spin-orbit interaction potential relative to the central potential deformation. This ratio is treated as an adjustable parameter in this program, with the view of improving the parametrization of the

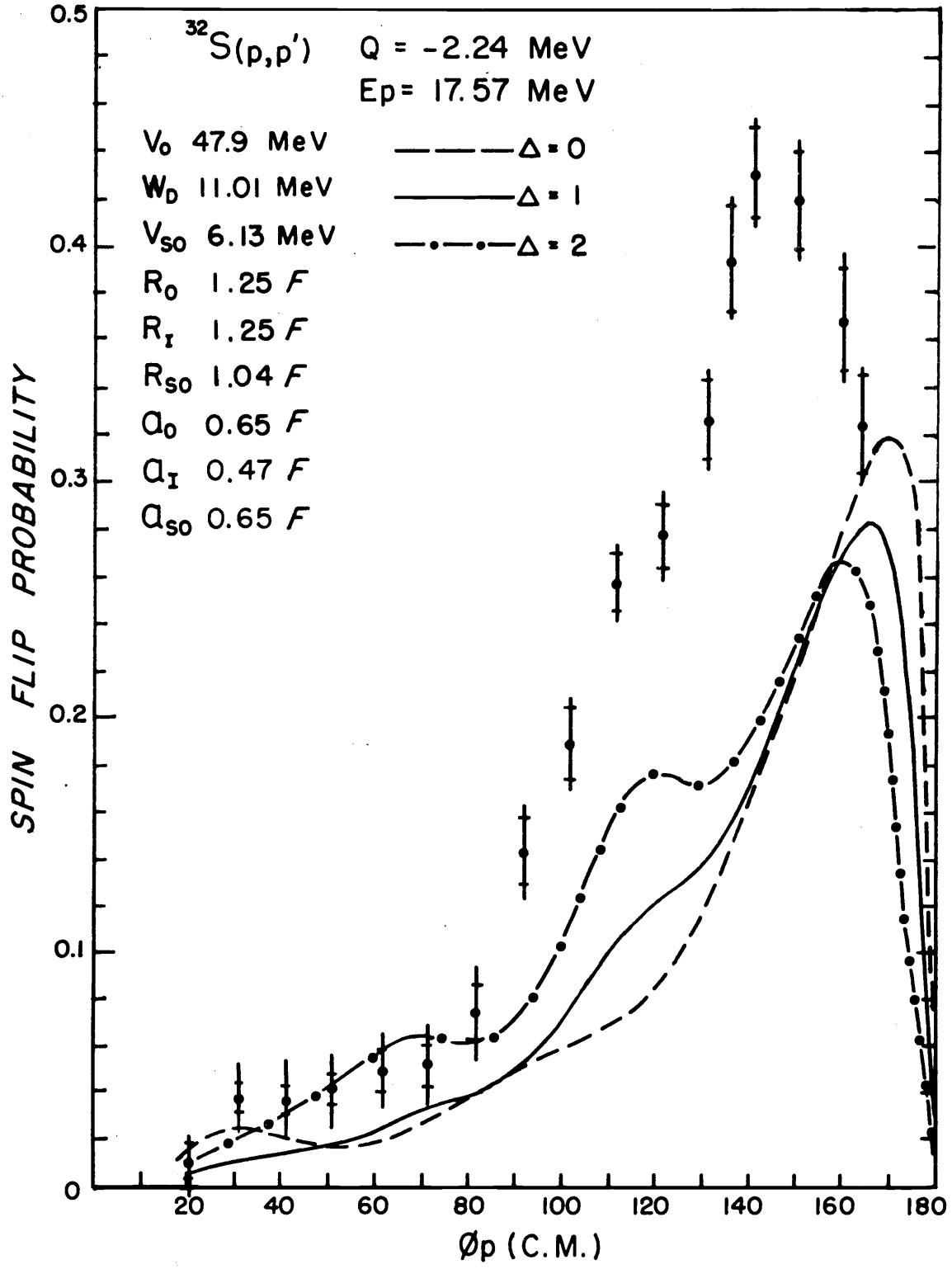

Figure 6-1. DWBA fit to the spin-flip probability in the reaction $^{32}S(p, p')^{32}S^*(2.24)$ for 17.57 MeV protons, using the set of O. M. parameters which best fit the elastic polarization.

inelastic spin-orbit interaction, just as the adjustment of the spin-orbit interaction radius R_{SO}, independent of the central radius R_0, has led to better fits to the elastic polarization [28].

The spin-dependent part of the interaction leading to the excitation of the collective state can be suppressed by stipulating no spin-orbit deformation (DSO) in the program. The result is the curve labelled $\Delta = 0$ in Figure 6-1. Note that the only appreciable effect is to eliminate the slight structure at about 120°, which appears in the curves for $\Delta = 1, 2$. The height and position of the prominent back-angle peak remain nearly the same with and without spin-flip included in the excitation process. The presence of substantial spin-flip probability in the absence of a deformed spin-orbit potential indicates [20, 29] that spin-flip occurs predominantly by way of the spin-orbit interaction in the elastic channels. It would seem to follow from this evidence that the same optical model parameters which best fit the elastic polarization should predict the proton spin-flip probability with about the same measure of success. These parameters have been determined [28] from fits to $\sigma_e(\phi)$ and $P_e(\phi)$ at $E_p = 17.8$ MeV. $P_e(\phi)$ is shown in Figure 6-2 along with the best fit. (The 230 keV projectile energy difference between experimental and theoretical determinations is considered negligible for our purposes.) These parameters were then used to construct the curves in Figure 6-1. The predicted spin-flip probability (including DSO) has the same general

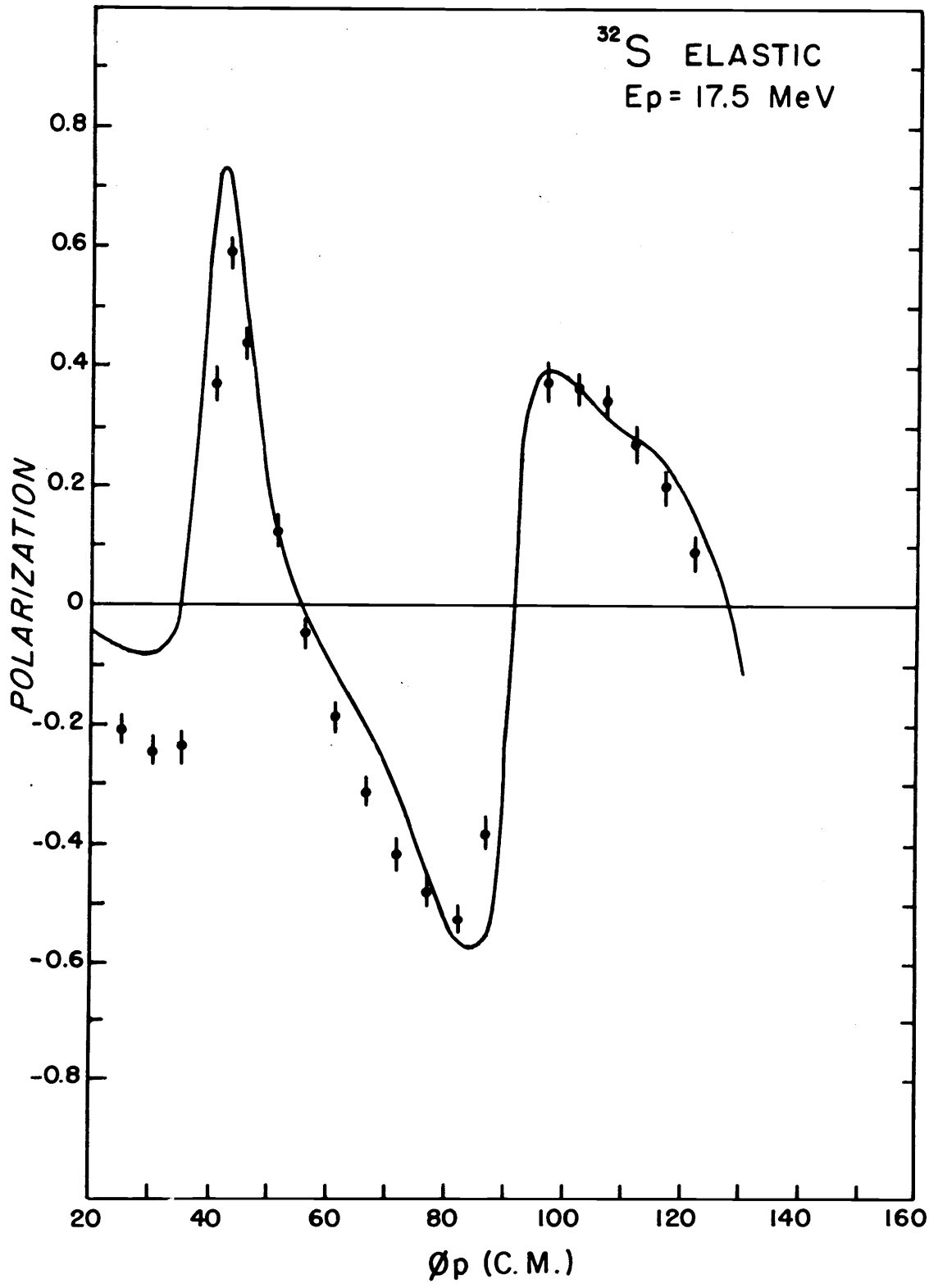

Figure 6-2. Best DWBA fit to the elastic polarization of 17.5 MeV protons on sulfur.

shape (including a hint of structure at 120°) as the measurements at 17.57 MeV, but the predicted backward peak is lower in magnitude by about 30% and is shifted backward about 15°. Moreover, this set of parameters results in a considerable underestimation of the inelastic scattering of 17.57 MeV protons from the 2^+ state at 2.24 MeV (Figure 6-3). A substantial, but by no means impressive improvement in the spin-flip fit is gained only by adjusting the spin-dependent interaction parameters (Figure 6-4), mainly by increasing V_{SO} from 6.13 MeV to 10 MeV. This results in a poorer fit to the polarization data (Figure 6-5). There is a slight increase in the inelastic scattering cross section, shown in Figure 6-6, produced apparently by the increase in V_{SO}. It is worth noting that the calculations for both $S(\phi)$ and the inelastic scattering cross section depend on the value of Δ, but those for $P_e(\phi)$ do not.

A different set of optical model parameters was obtained [16] from DWBA fits to the cross section measurements for 17.57 MeV proton elastic scattering and inelastic scattering to the 2^+ state. Using the present program, the fits to the inelastic scattering data are shown in Figure 6-7. It is significant that the value of the quadrupole deformation parameter, β_2, for the 2^+ level in ^{32}S, extracted from DWBA fits to the proton inelastic scattering is 30% larger than has been recently obtained both from other nuclear scattering experiments and from electromagnetic interactions (Table 3-1).

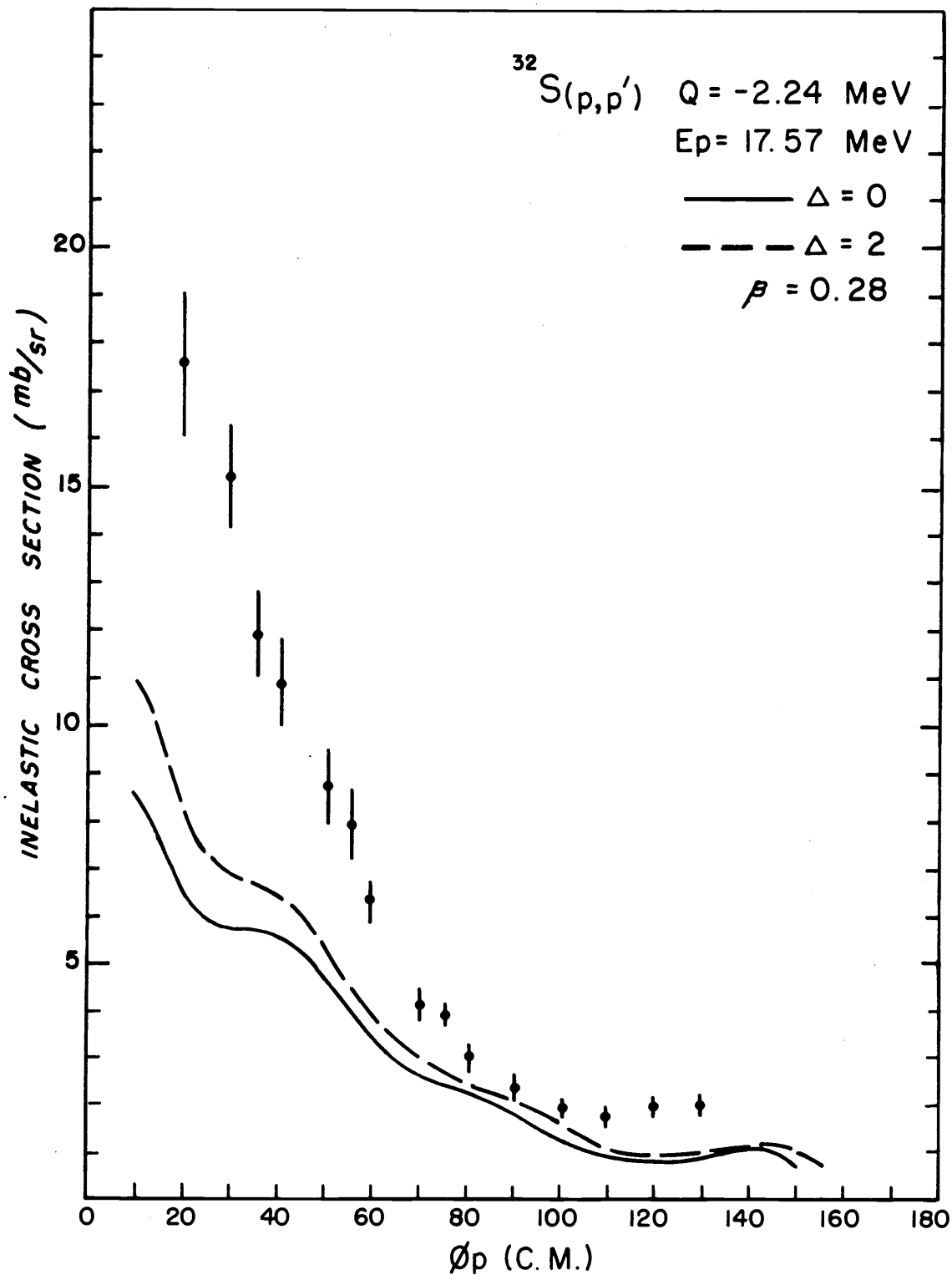

Figure 6-3. DWBA fit to the inelastic scattering of 17.57 MeV protons from the 2.24 MeV level in ^{32}S, using the set of O. M. parameters which best fit the elastic polarization.

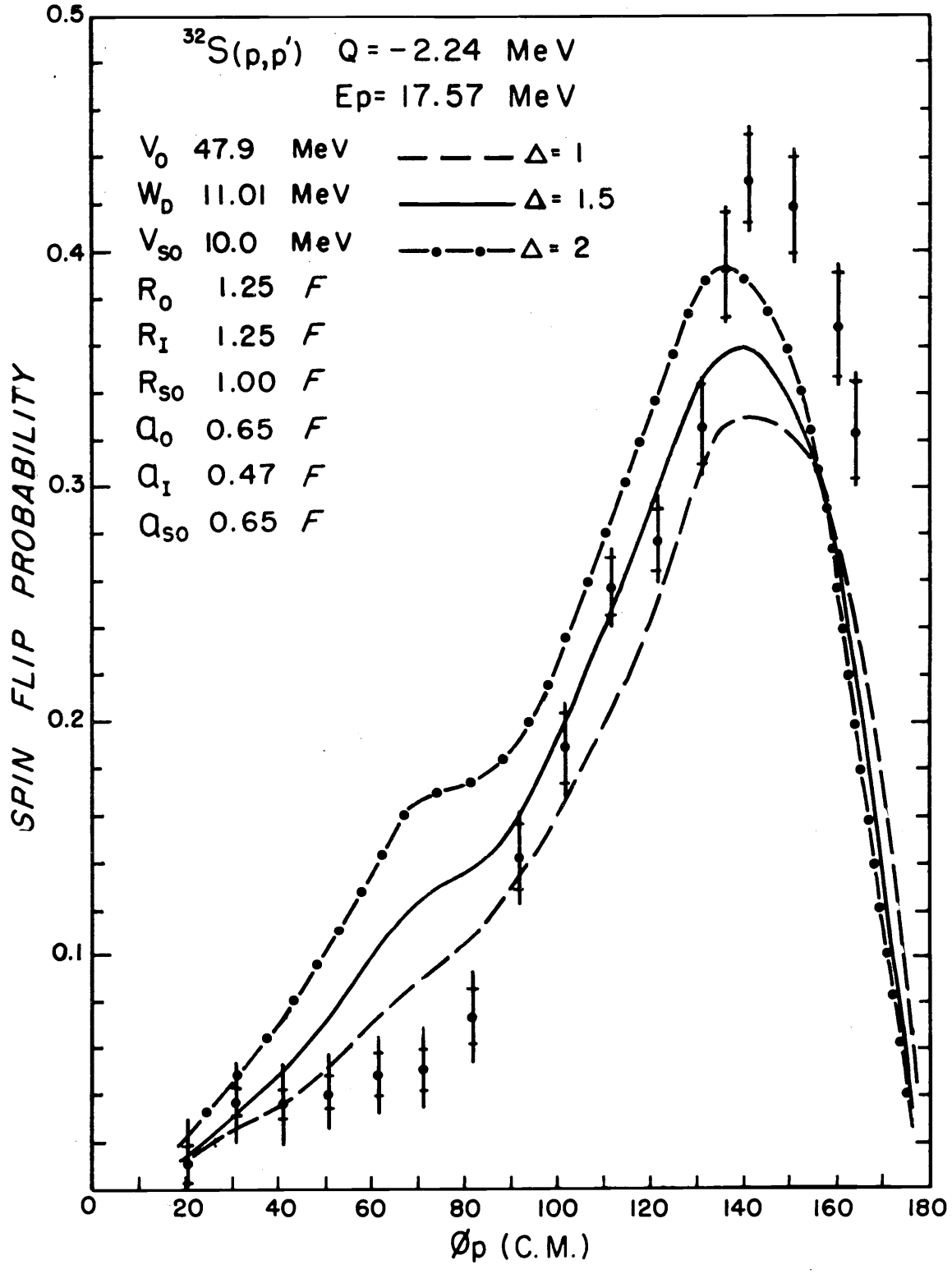

Figure 6-4. DWBA fit to the spin-flip probability in the reaction $^{32}S(p, p')^{32}S^*(2.24)$ for 17.57 MeV protons, after adjusting the spin-dependent O. M. parameters in the set which best fit the elastic polarization.

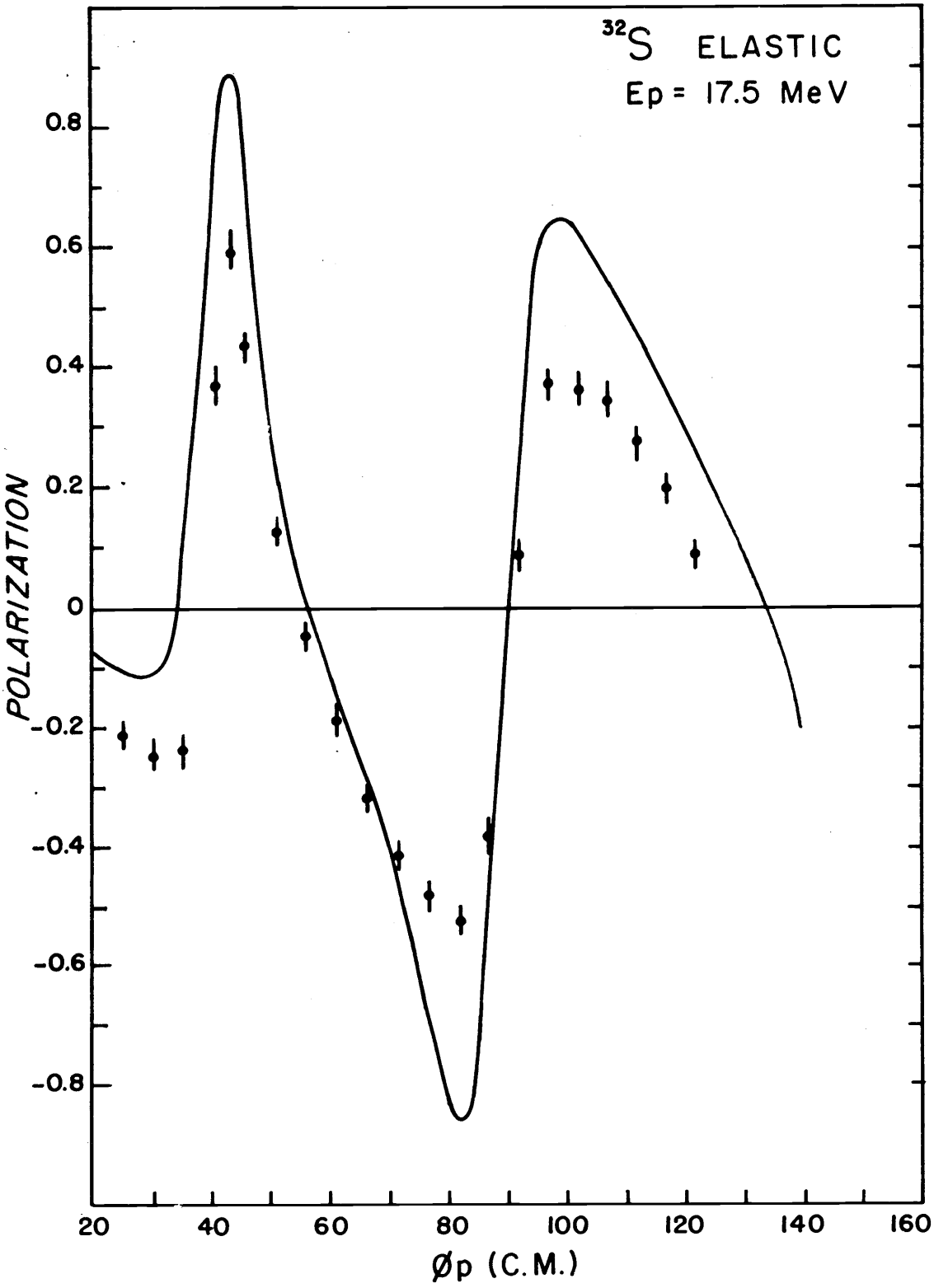

Figure 6-5. DWBA fit to the elastic polarization of 17.57 MeV protons on sulfur, using the set of O. M. parameters given in Figure 6-4.

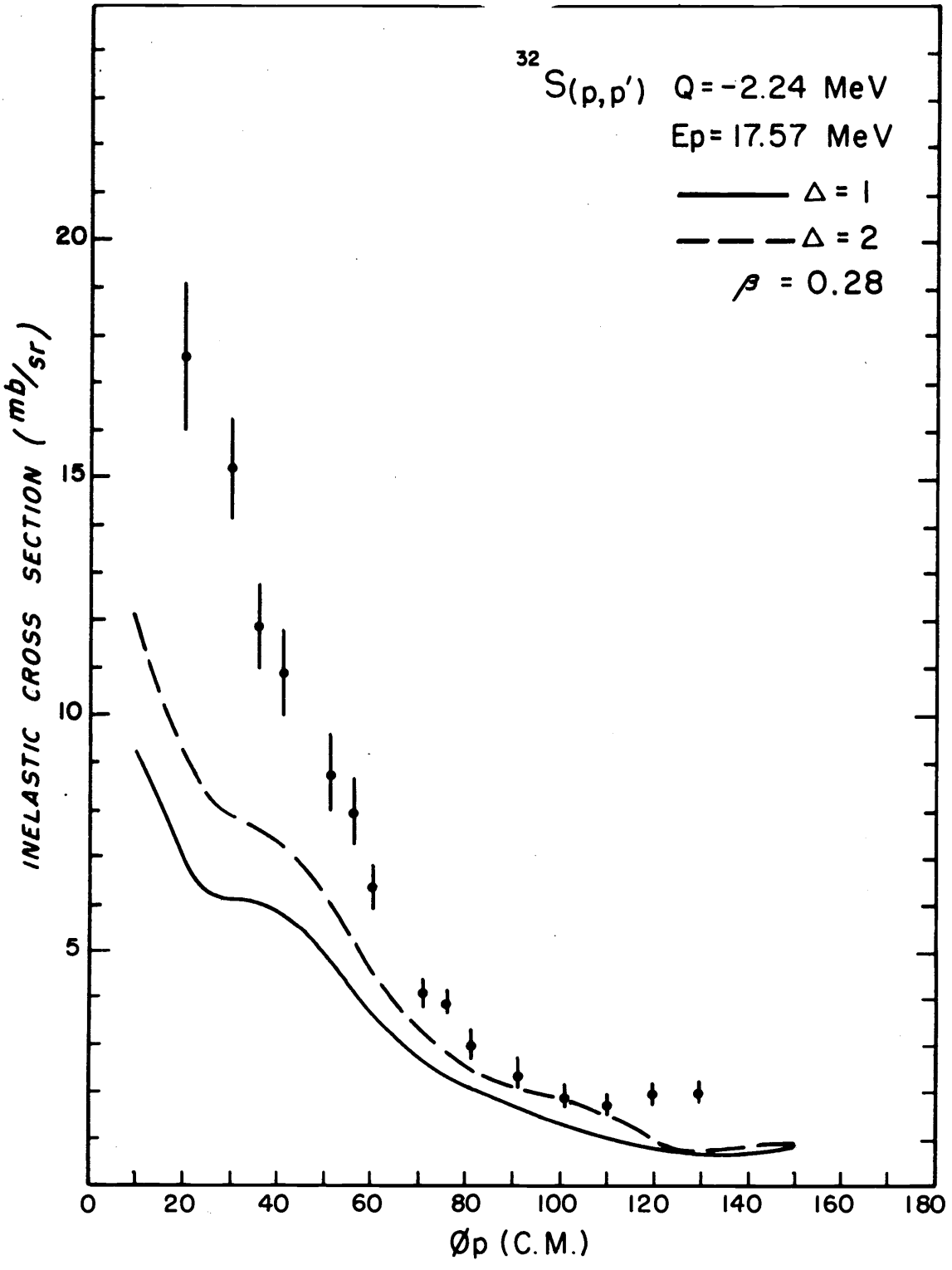

Figure 6-6. DWBA fit to the inelastic scattering of 17.57 MeV level in ^{32}S, using the set of O. M. parameters given in Figure 6-4.

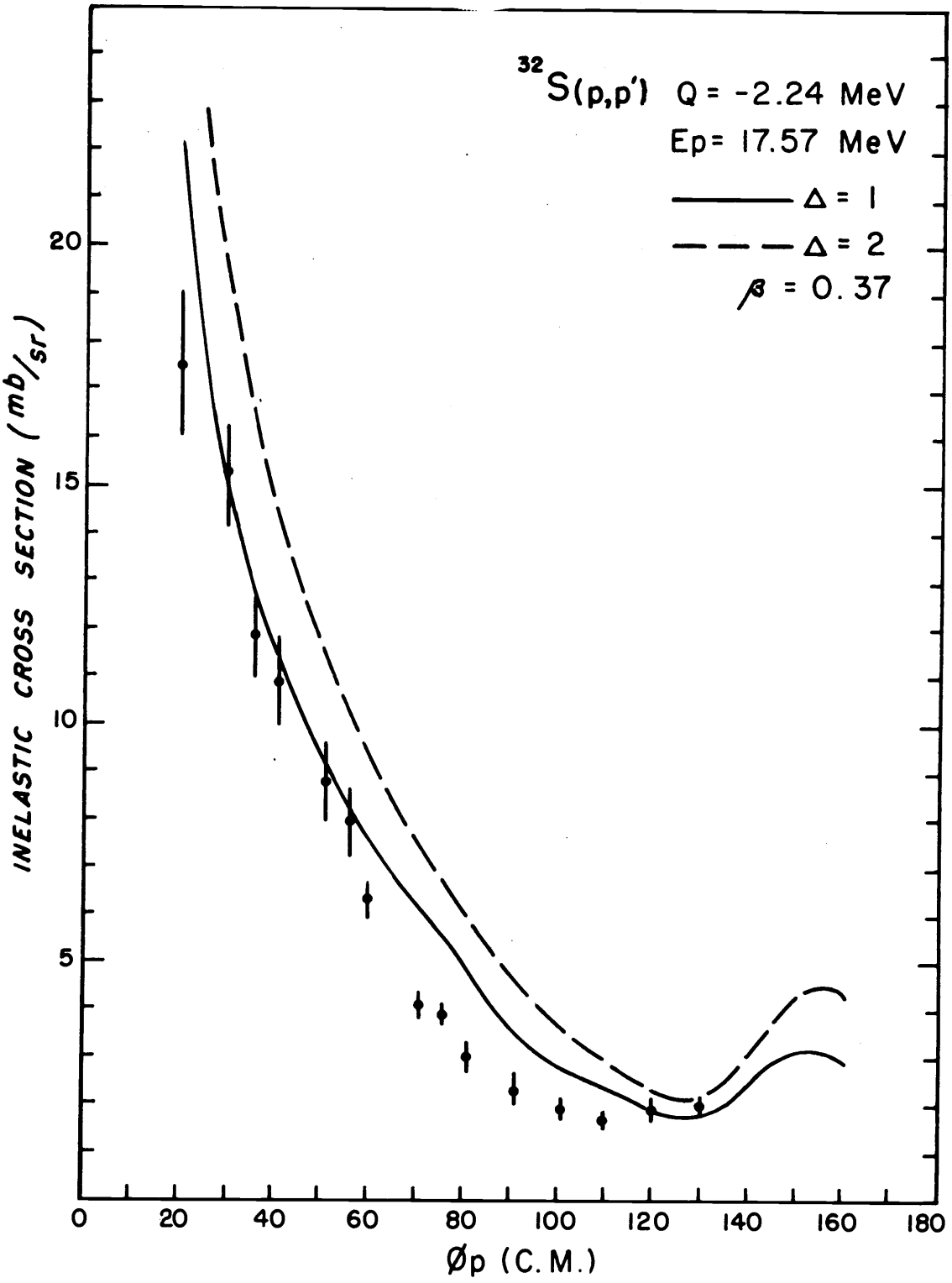

Figure 6-7. DWBA calculation of the inelastic scattering of 17.57 MeV protons from the 2.24 MeV level in ^{32}S, using the present program (full Thomas spin-orbit term) and the O. M. parameters obtained by Crawley and Garvey [16] (Oak Ridge spin-orbit term).

The spin-flip fits in Figure 6-8 show some improvement over those in Figure 6-1, due apparently to the increase in both V_{SO} and R_{SO}. This increase has, however, again resulted in a poorer fit to the elastic polarization (Figure 6-9).

Variation of the remaining optical model parameters had some effect on the spin-flip predictions, but they could not be simultaneously optimized without a seach program.

Instead, it was decided to obtain a more generalized set. Bechetti and Greenlees [30] have studied the variation of the optical model parameters as a function of atomic number A and projectile energy E by fitting to $\sigma_e(\phi_p)$, $P_e(\phi_p)$ and σ_R over a range of incident proton energies from 10 MeV to 50 MeV and a range of A from 40 to 90. Several sets of parameters were developed, having about the same goodness of fit but with a different functional dependence of one or more of the parameters on E and A.

For nuclei with $A < 40$, adjustments other than the forms of parametrization found for the heavier nuclei were required to fit the data. In particular, a substantial increase in R_I was required. Also, due to the decrease in the number of non-elastic channels in lighter nuclei, the radial form of the imaginary potential may not be appropriate. Those sets were selected from the tables of Bechetti and Greenlees which were considered to affect the spin-flip calculations, yet still give good fits to the polarization. The fits to $P_e(\phi)$

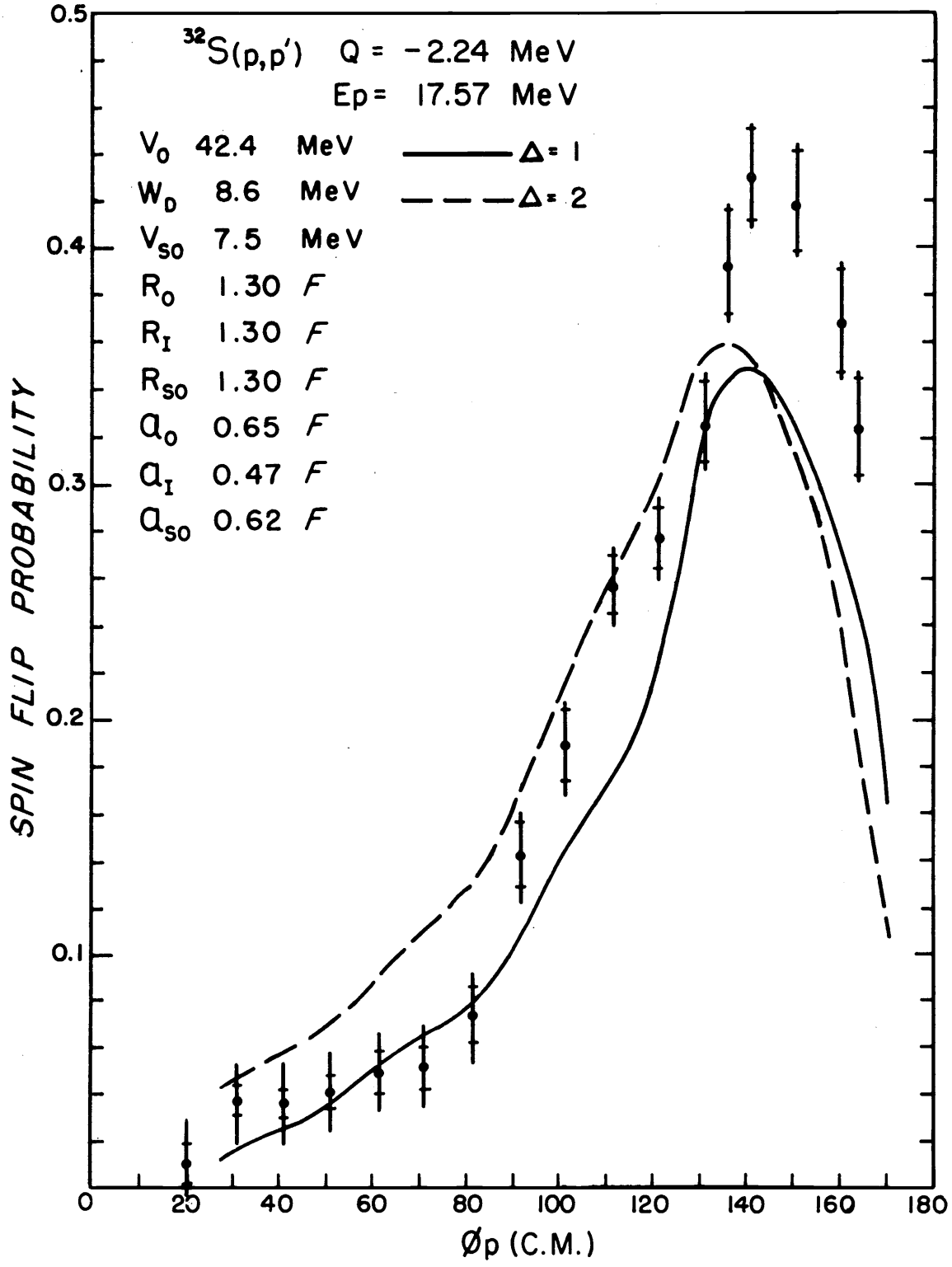

Figure 6-8. DWBA fit to the spin-flip probability in the reaction $^{32}S(p, p')^{32}S^*(2.24)$ for 17.57 MeV protons using the reaction which best fit the inelastic proton scattering cross section.

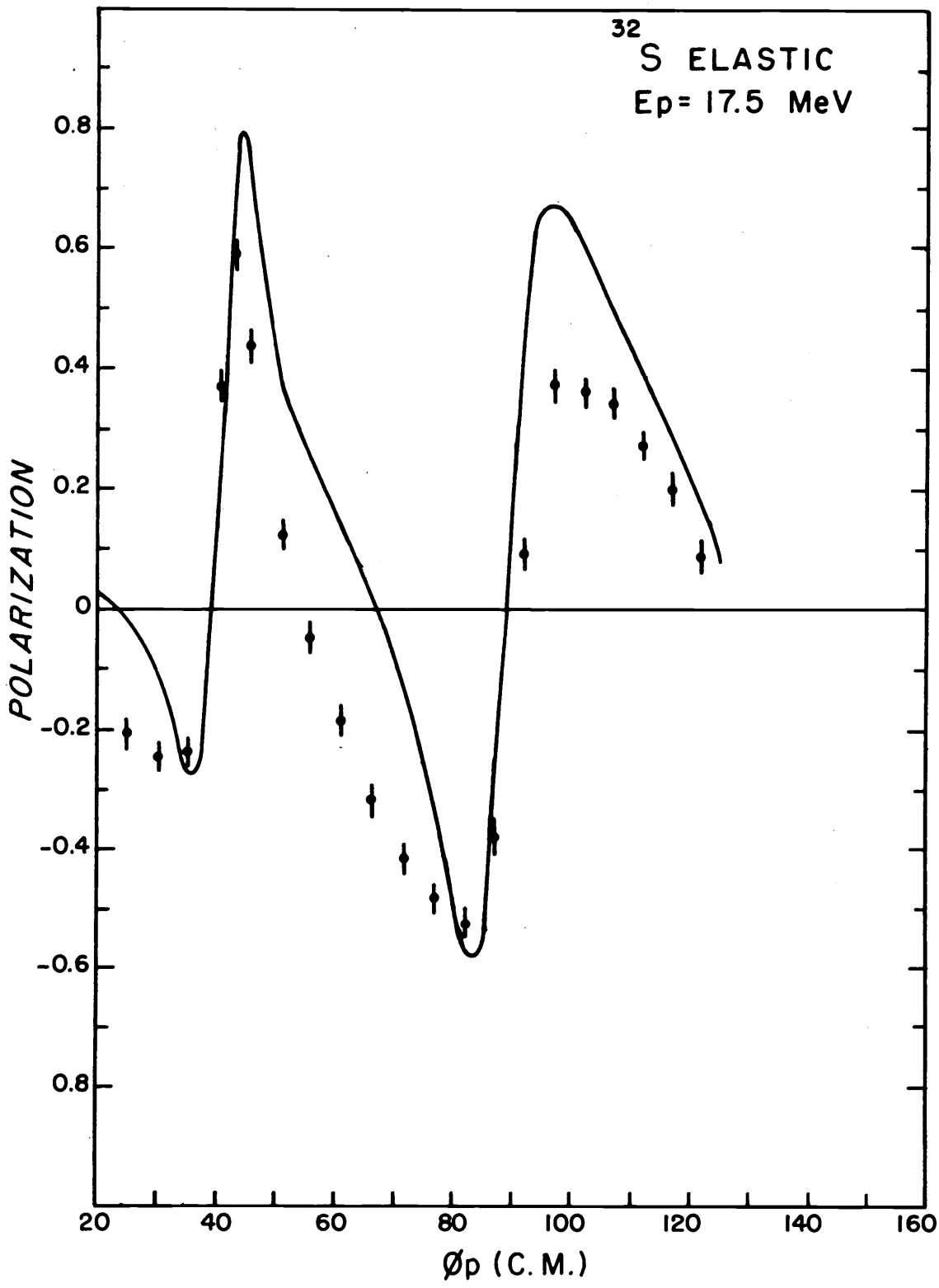

Figure 6-9. DWBA prediction for the elastic polarization of 17.57 MeV protons of sulfur using the set of O. M. parameters given in Figure 6-8.

and $S(\phi)$, using the most promising set are shown in Figure 6-10 and 6-11, respectively. Again, the magnitude of the predicted spin-flip probability is too low.

In addition, further variations were tried in the imaginary parameters, W_D, R_I and a_I. The effect of these parameters on the shape and amplitude of $S(\phi)$ was noticable, but too limited to substantially improve the fit to the data.

The over-all best fit, in terms of position and amplitude of the main peak of the proton spin-flip probability, is given by the solid line in Figure 6-12. It is found that, again, a change in the spin-orbit parameters, V_{SO} and R_{SO}, must be made in order to fit the amplitude and position of $S(\phi)$. However, some progress has been made by this parameter search in the sense that a lower value of V_{SO} was required to fit the spin-flip data than with the set of parameters in Figure 6-4.

Although the predicted inelastic scattering cross section in Figure 6-13 has increased slightly over that in Figure 6-6, it still underestimates the experimental results by nearly a factor of two except at back angles.

Figure 6-14 shows the effect of the change in V_{SO} and R_{SO} on the fit to the elastic polarization. Note the increased amplitude of the back angle peak with increased V_{SO}.

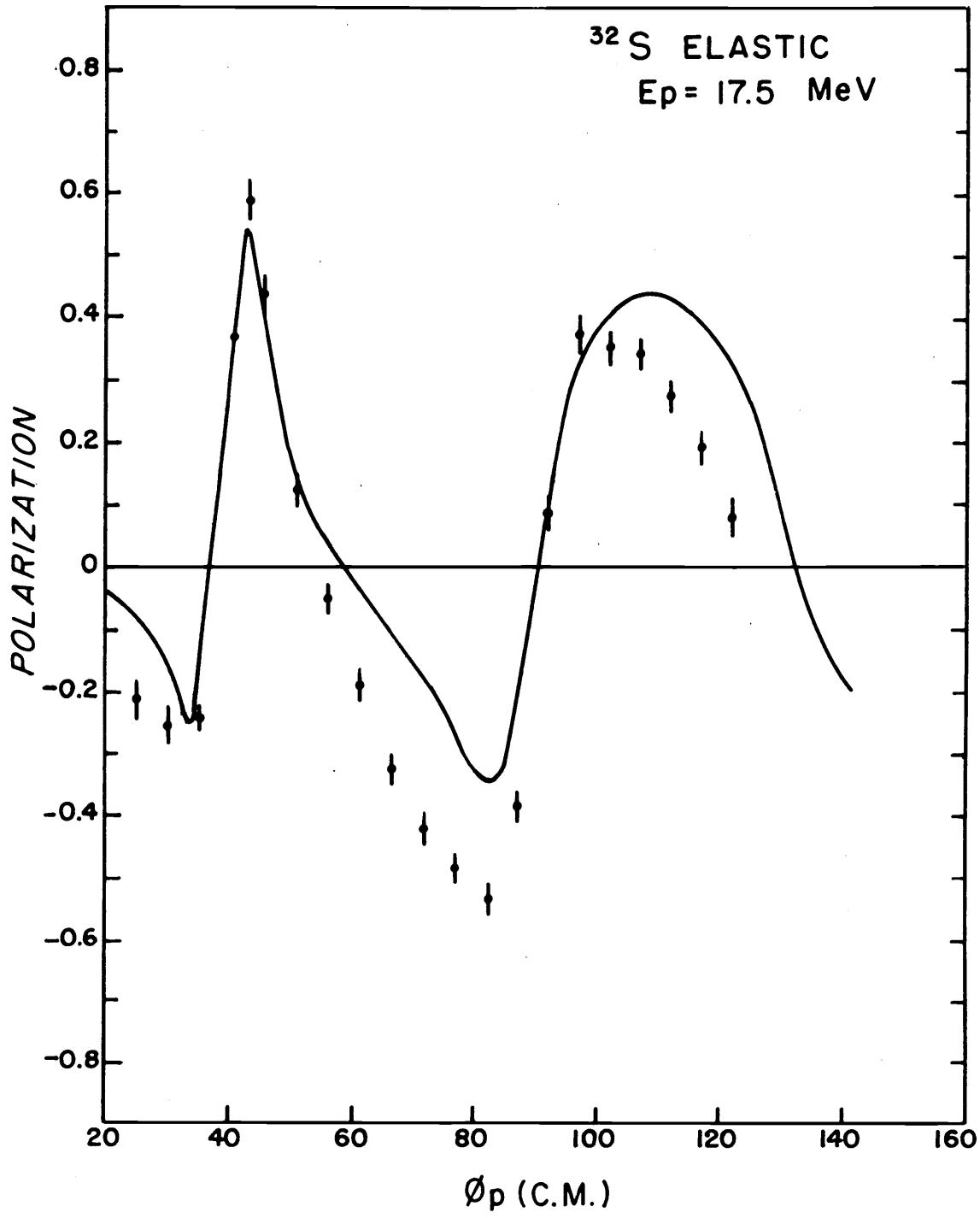

Figure 6-10. DWBA prediction for the elastic polarization of 17.57 MeV protons on sulfur, using the best set of O. M. parameters from Bechetti and Greenlees [30].

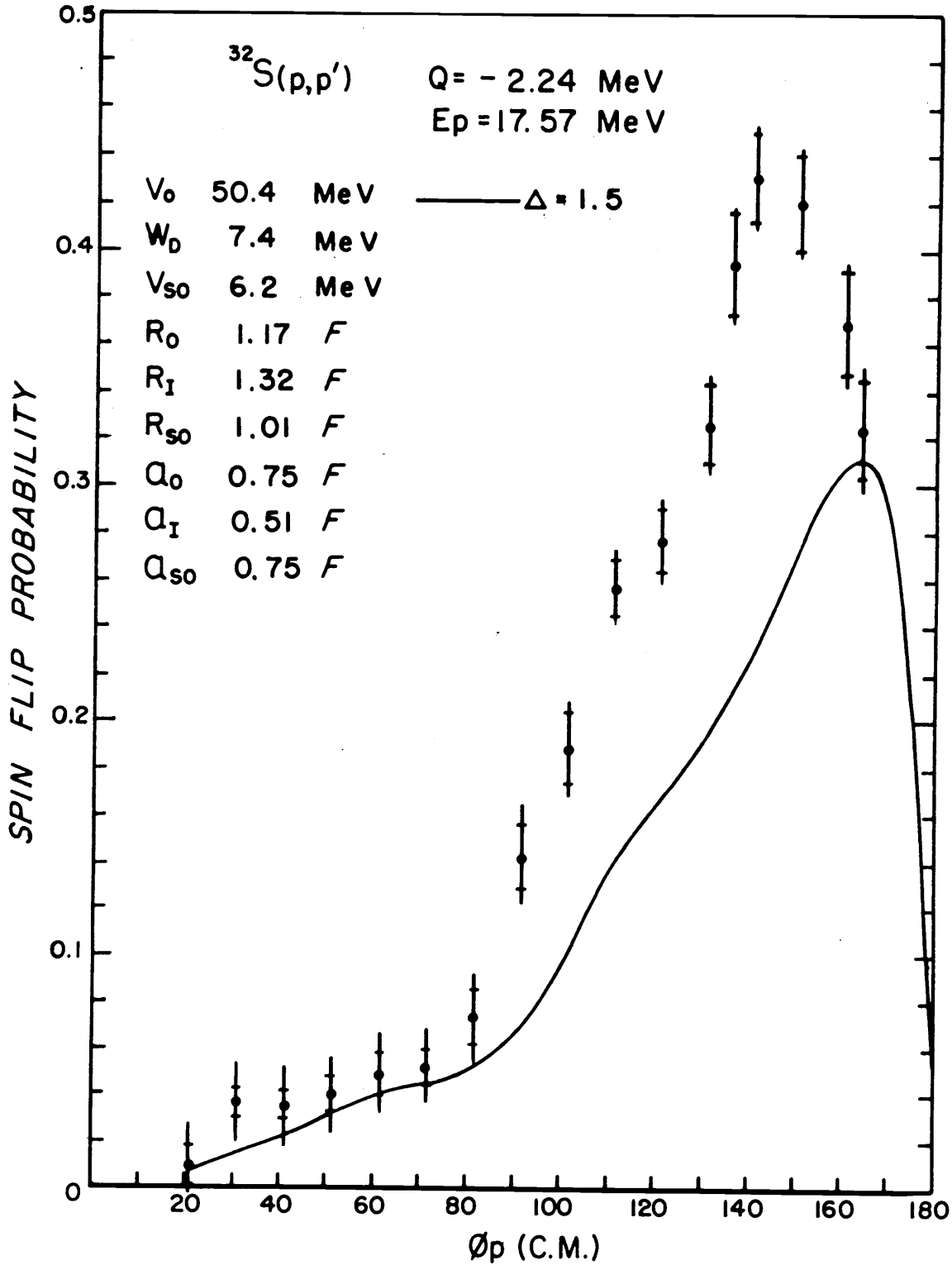

Figure 6-11. DWBA prediction for the spin-flip probability in the reaction $^{32}S(p,p')$ $^{32}S^*(2.24)$ for 17.57 MeV protons, using the best set of O.M. parameters from Bechetti and Greenlees [30].

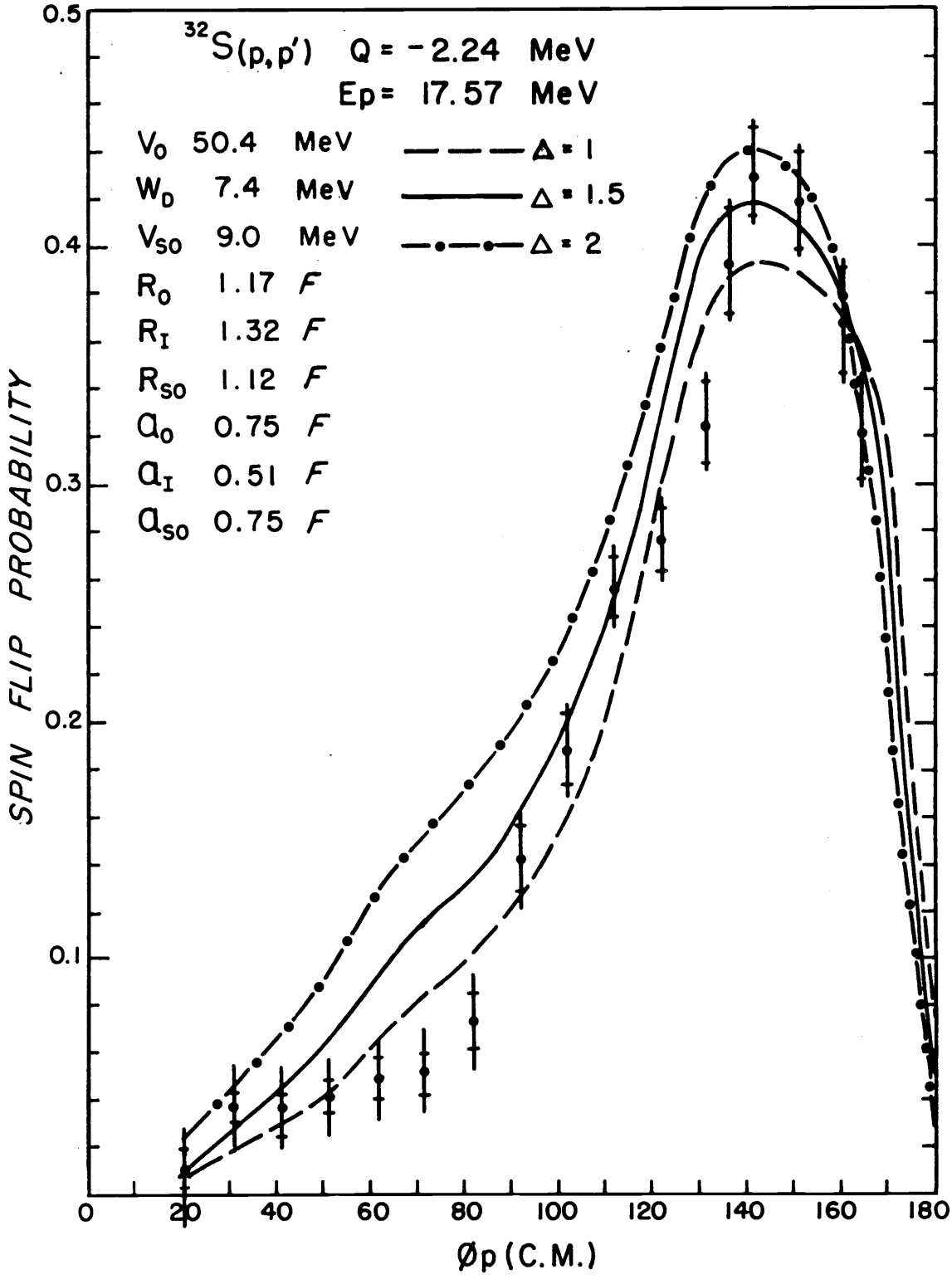

Figure 6-12. DWBA best fit to the spin-flip probability in the reaction $^{32}S(p, p')^{32}S^*(2.24)$ for 17.57 MeV protons.

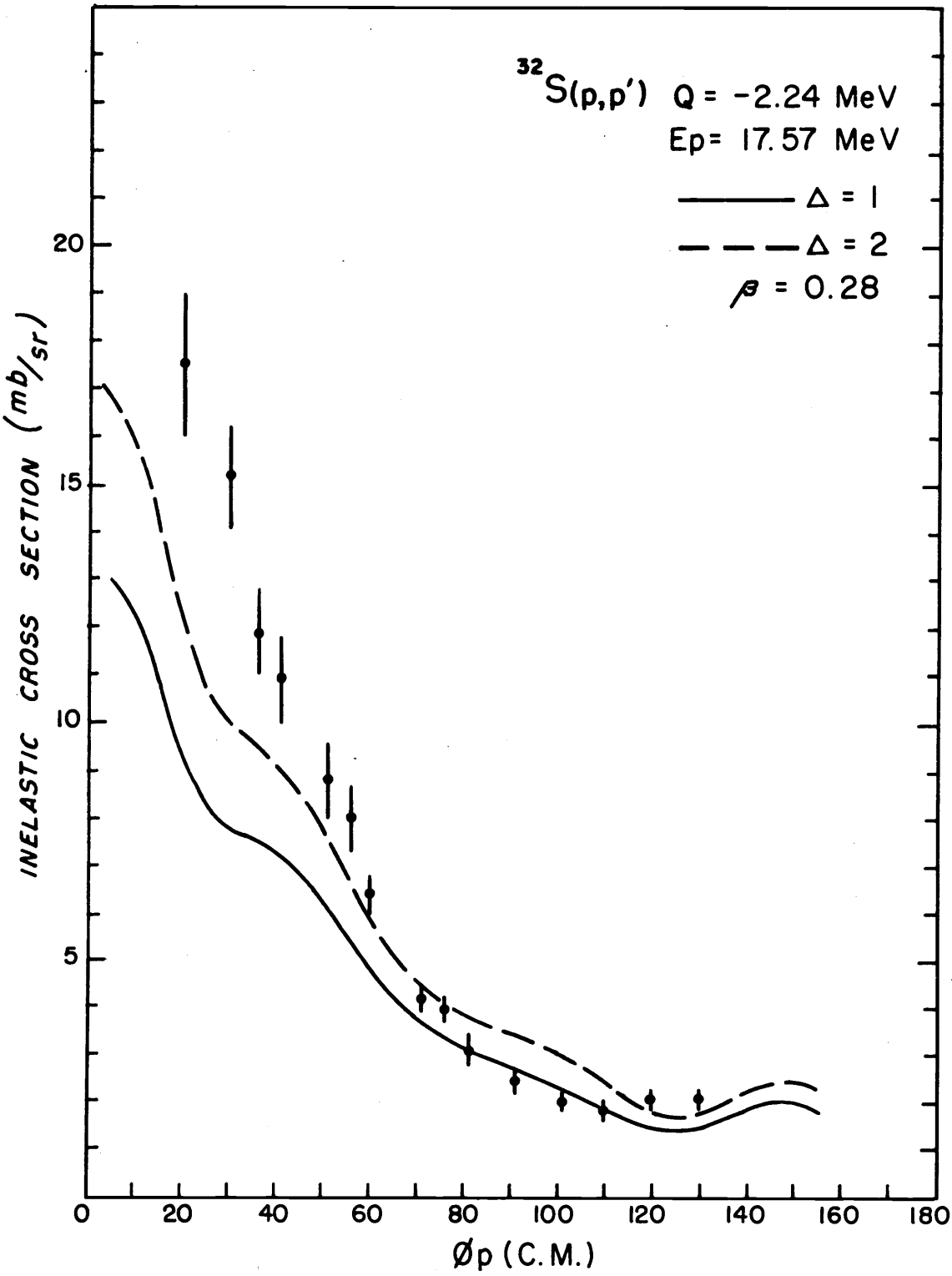

Figure 6-13. DWBA prediction for the inelastic scattering of 17.57 MeV protons from the 2.24 MeV state in sulfur, using the set of O. M. parameters given in Figure 6-12.

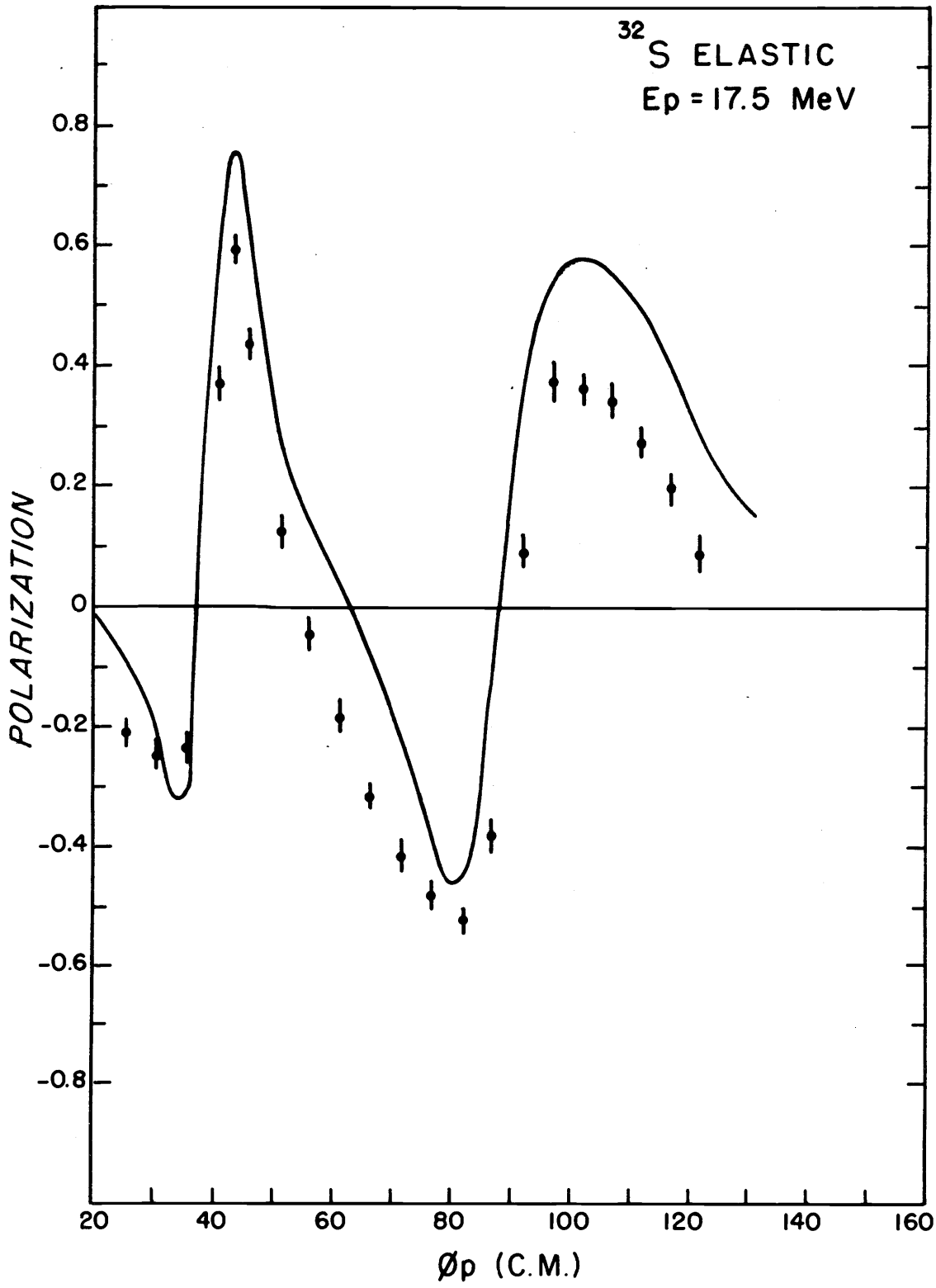

Figure 6-14. DWBA prediction for the elastic polarization of 17.57 MeV protons on sulfur, using the set of O. M. parameters given in Figure 6-12.

The two sets of optical model parameters giving the best fit to either the measured spin-flip probability or the elastic polarization are shown in Table 6-1. Different values of V_{SO} and R_{SO} are required to fit each set, in spite of attempts to vary only the values of the central parameters.

Table 6-1. Optical model parameters from DWBA best fit to either elastic polarization or inelastic spin-flip probability of 17.57 MeV protons on sulfur.

	$P_e(\phi)$	$S(\phi)$
V_0 (MeV)	47.9	50.4
W_D "	11.01	7.4
V_{SO} "	6.13	9.0
R_0 (F)	1.25	1.17
R_I "	1.25	1.32
R_{SO} "	1.04	1.12
a_0 "	0.65	0.75
a_I "	0.47	0.51
a_{SO} "	0.65	0.75

The fits to the spin-flip data for protons on sulfur at E_p = 15.91 MeV is shown on Figure 6-15. The optical model parameters (adjusted for the different proton energy) are obtained from the set giving the best fit to the spin-flip data at the higher proton energy

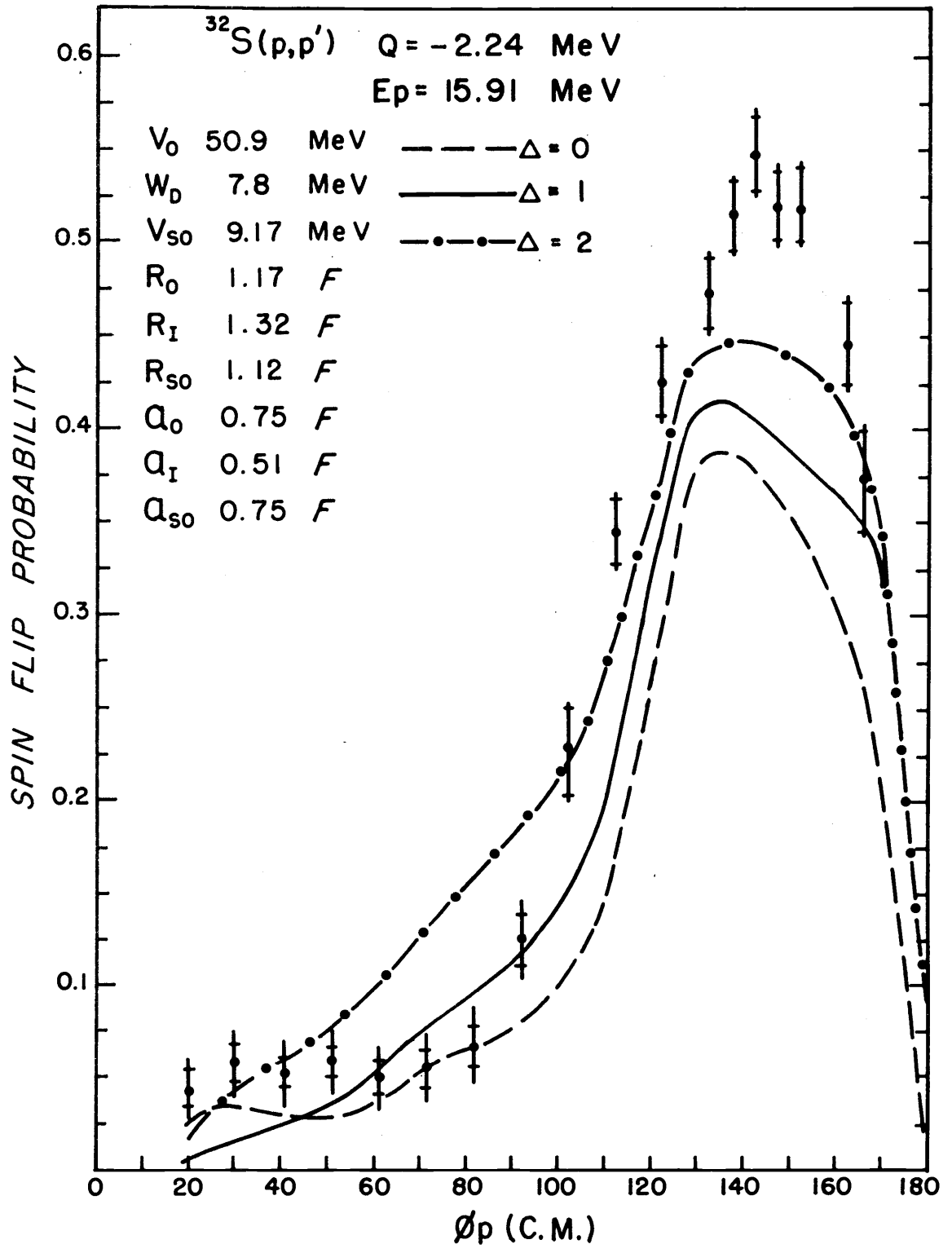

Figure 6-15. DWBA prediction for the spin-flip probability in the reaction $^{32}S(p, p')^{32}S^*(2.24)$ for 15.91 MeV protons, using the set of O. M. parameters given in Figure 6-12, but adjusted for the lower proton energy.

(Figure 6-12). The predicted spin-flip probability did not change appreciably with the change in energy, while the measured probability increased 20% at back angles.

Carbon

The predicted fits to the spin-flip probability for 15.93 MeV and 17.35 MeV protons inelastically scattered to the first 2^+ state of ^{12}C are shown in Figures 6-16 and 6-17, respectively. The optical model parameters were obtained [31] from fits to the elastic scattering and polarization. The predictions are in better agreement with the spin-flip data than was found for the case of protons on sulfur. However, the fits, notably at 17.35 MeV, are not quite as good as those obtained by other investigators [3] at 26.2 MeV. The small forward peak at about 70° is not reproduced at either energy by the calculation.

Conclusion

Although a collective DWBA calculation has been somewhat successful in predicting the general features of inelastic proton spin-flip for many nuclei [2, 3, 7, 20], this approach fails notably to account for the amplitude of the back-angle peak resulting from protons incident on sulfur in the region of proton energies between 15 MeV and 18 MeV. The uncommonly large amplitude of this peak can be fitted by the DWBA method only with values of the spin-dependent

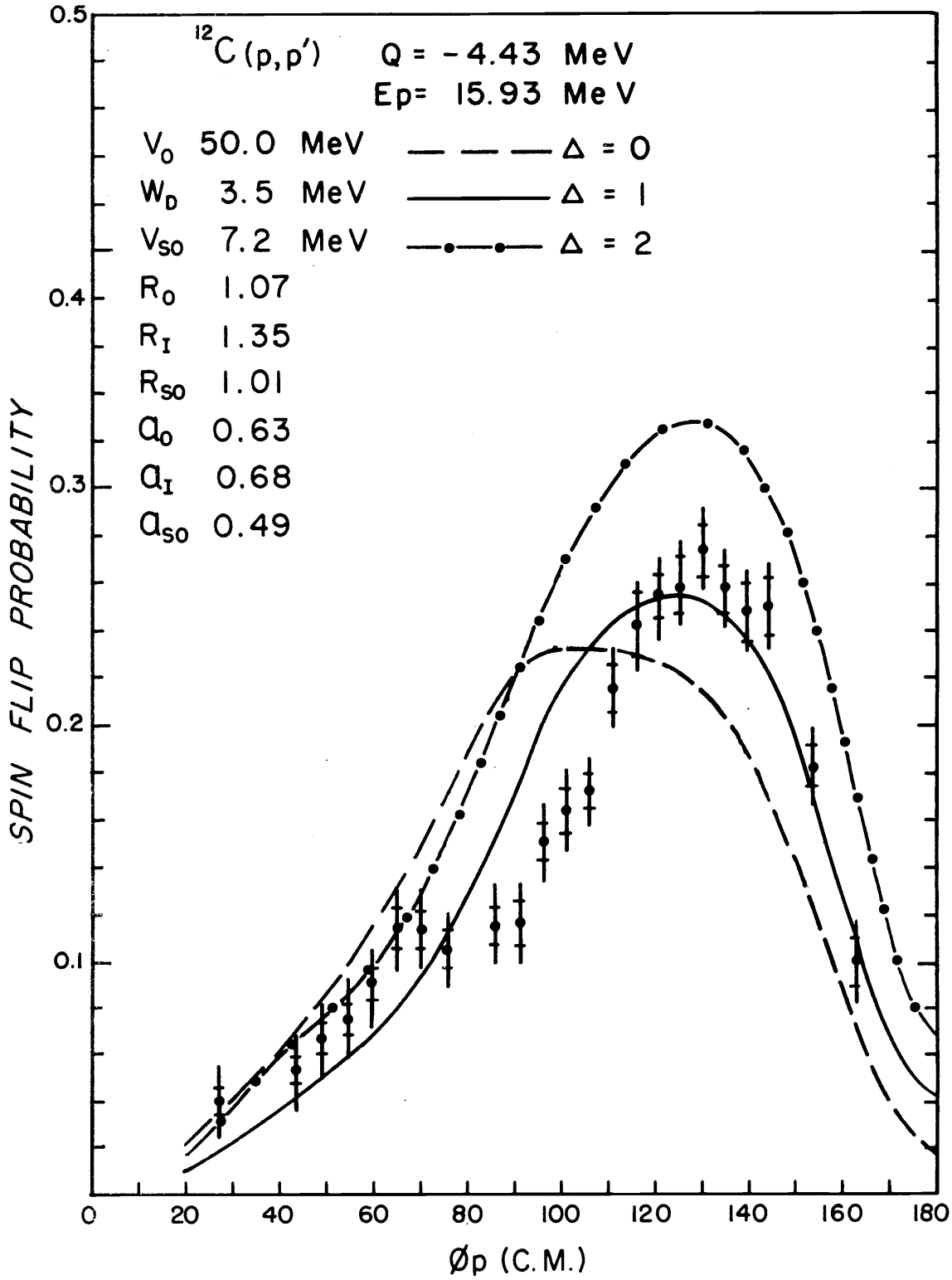

Figure 6-16. DWBA prediction for the spin-flip probability in the reaction $^{12}C(p, p')^{12}C^*(4.43)$ for 15.93 MeV protons, using the set of O. M. parameters from the best fit to the elastic scattering and polarization.

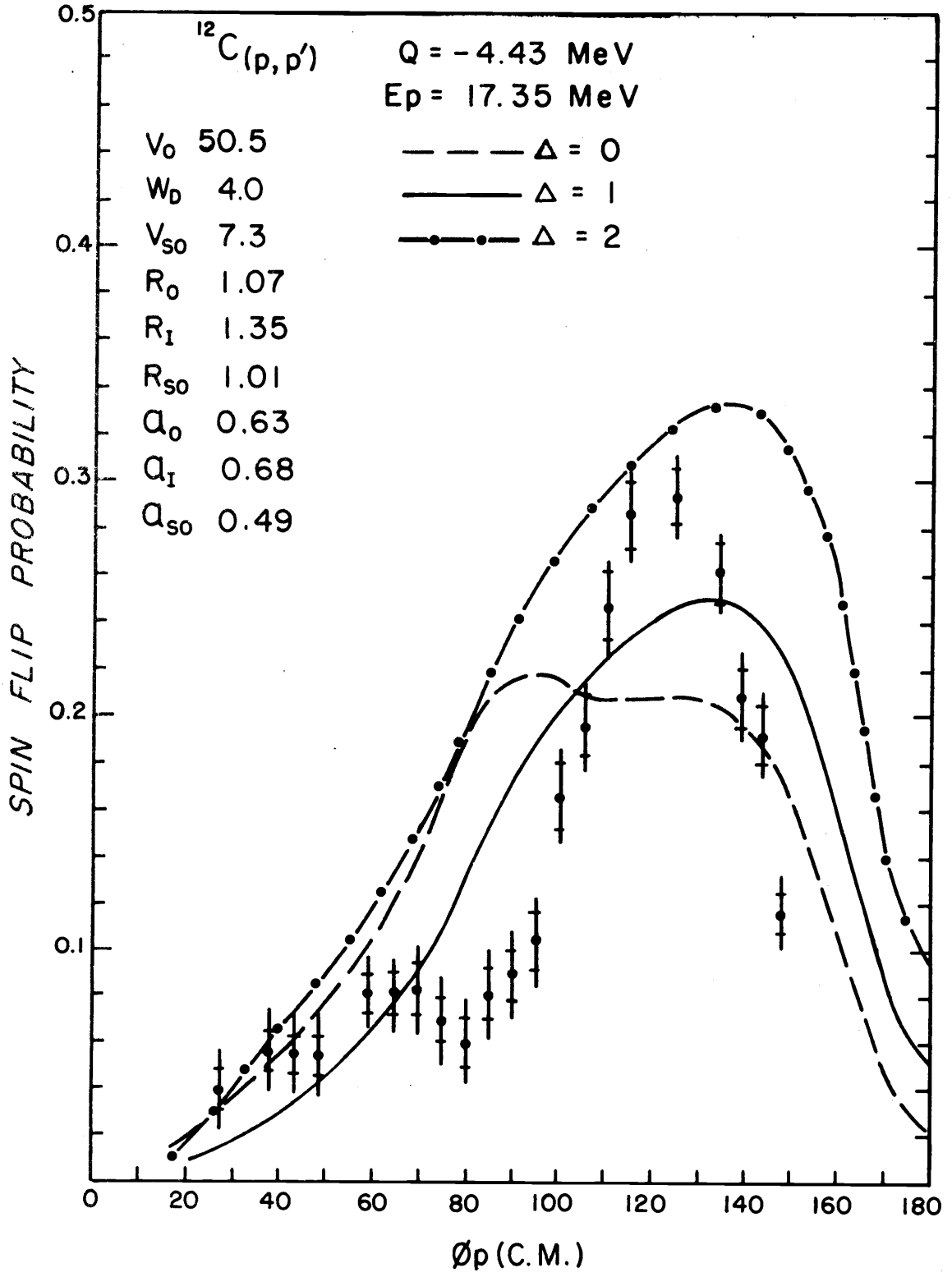

Figure 6-17. DWBA prediction for the spin-flip probability in the reaction $^{12}C(p,p')^{12}C^*(4.43)$ for 17.35 MeV protons, using the set of O. M. parameters from the best fit to the elastic scattering and polarization.

optical model parameters which are inconsistent with values determined from fits to the elastic polarization.

The increase of 20% in the peak amplitude of $S(\phi)$ as E_p is changed from 17.57 MeV to 15.91 MeV is not consistent with the slow dependence of the interaction of the projectile kinetic energy as seen in the direct interaction picture.

Since the DWBA collective model predicts that very little of the spin flip occurs during the excitation process, it may be that the missing amplitude is due to spin flip during the excitation by a process not present in the collective model.

In addition, DWBA analysis of the inelastic proton scattering requires a value of 0.37 for the quadrupole deformation parameter β_2 for the 2^+ level, while a measure of this parameter from other experiments involving either electromagnetic interactions or other nuclear interactions are more in agreement on a value of 0.28 (refer to Table 3-1).

Measurements have been recently made [32] of the inelastic deuteron half-spin-flip probability on the even nuclei: ^{24,26}Mg, ^{32}S, ^{48,50}Ti and ^{58,60}Ni at E_d = 11.8 MeV. The resulting angular distribution of half-spin-flip probability on ^{32}S is similar to those measured for the other nuclei; being small at forward angles and peaking up to about 0.30 at an angle of about 150°. A DWBA analysis performed by the same authors generally reproduced these features.

Thus, the presently measured inelastic proton spin-flip behavior on sulfur is a notable exception to a process apparently well-understood, at least in its main features.

A measure of the inelastic polarization of protons on sulfur in this same proton energy region might help clarify the picture.

Summary

The spin-flip probability of protons inelastically scattered to the first 2^+ excited states of ^{12}C and ^{32}S has been measured at proton energies of 15.93 MeV and 17.35 MeV for carbon and at 15.91 MeV and 17.57 MeV for sulfur.

The results of the measurements on carbon are in good agreement with earlier work [20].

The measurement of the inelastic proton spin-flip probability on sulfur is higher than that reported for any other nucleus, exceeding a peak value of 0.5 at $\phi_p = 145°$ at the lower proton energy.

A collective DWBA analysis of the spin-flip probability, employing the full Thomas spin-orbit interaction, was carried out. The amplitude and position of the main experimental peak was reproduced in the case of protons on carbon, but the observed forward structure was not predicted.

Attempts to fit the spin-flip probability of protons on sulfur at $E_p = 17.57$ MeV required a substantial increase in the spin-orbit

strength V_{SO} from the value found to best fit the elastic polarization data. Efforts to fit the even larger value of the spin-flip probability observed at $E_p = 15.91$ MeV were even less successful since the DWBA analysis does not predict much variation of $S(\phi)$ with incident proton energy.

BIBLIOGRAPHY

1. Schmidt, F. H. et al. Proton spin flip and substate excitation in inelastic scattering. Nuclear Physics 52:353-380. 1964.

2. Hendrie, D. L. et al. Spin flip in the inelastic scattering of 19.6 MeV protons from ^{54}Fe and ^{56}Fe. Physical Review 186: 1188-1199. 1969.

3. Kolata, J. J. and A. Galonsky. Proton spin flip in the reaction ^{12}C(p, p')^{12}C*(4.43 MeV). Physical Review 182:1073-1082. 1969.

4. Bohr, Aage. Relation between intrinsic parities and polarizations in collision and decay processes. Nuclear Physics 10: 486-491. 1959.

5. Kolasinski, W. A. Studies of proton spin flip in inelastic scattering from carbon and nickel isotopes. Doctoral dissertation. Seattle, University of Washington. 1967. 96 pages.

6. Sherif, Helmy and J. S. Blair. Inelastic proton scattering and the deformed spin-dependent optical model. Physics Letters 26A:489-492. 1968.

7. Sherif, Helmy. Spin-dependent effects in proton inelastic scattering. Doctoral dissertation. Seattle, University of Washington, 1968. 196 pages.

8. Fricke, M. P., E. E. Gross and A. Zucher. Inelastic scattering of 40 MeV polarized protons. Physical Review 163:1153-1169. 1967.

9. Ginaven, R. O. et al. Spin-flip in the inelastic scattering of 30- and 40-MeV protons by ^{28}Si. Physical Review Letters 21:552-554. 1967.

10. Eenmaa, J., F. H. Schmidt and J. R. Tesmer. Proton spin flip in the reaction ^{58}Ni(p, p'γ)^{58}Ni*(1.45 MeV) at 20 MeV. Physics Letters 28B:321-323. 1968.

11. Blair, J. S. Inelastic excitation of collective modes. In: Proceedings of the Padua conference on direct interactions and nuclear reaction mechanisms, 1962, ed. by E. Clementel and C. Villi. London, Gordon and Breach, 1963. p. 669-694.

12. Austern, N. Optical model wave functions for strongly absorbed nuclei. Annals of Physics 15:299-313. 1961.

13. Gregoire, G. and P. C. Macq. Niveaux collectifs dans le ^{32}S. Nuclear Physics A99:481-486. 1967.

14. Budzinowsky, A., A. D. Hill and P. E. Hodgson. The elastic and inelastic scattering of 25 MeV alpha particles by ^{31}P, ^{32}S and ^{40}Ca. Nuclear Physics A117:509-532. 1968.

15. Clarke, R. L. and W. G. Gross. Elastic and inelastic scattering of 14.1 MeV neutrons from C, Mg, Si and S. Nuclear Physics 53:177-203. 1964.

16. Crawley, G. M. and G. T. Garvey. Inelastic scattering in the 2s-1d shell. I. Even nuclei. Physical Review 160:981-996. 1967.

17. Lombard, R., P. Kossanyi-Demay and G. R. Bishop. The scattering of high-energy electrons by ^{32}S. Nuclear Physics 59:398-416. 1964.

18. Malaker, D. L., L. Schaller and W. C. Miller. Nuclear resonance flourescence from the 2.24 MeV state of ^{32}S. Bulletin of the American Physical Society 9:9. 1964.

19. Nakai, K. et al. Quadrupole moments of first excited states in ^{28}Si, ^{32}S and ^{40}Ar. Physical Review Letters 24:903-906. 1970.

20. Kolasinski, W. A. et al. Spin flip in inelastic scattering of protons. Physical Review 180:1006-1014. 1969.

21. McDaniel, F. D. and K. A. Amos. Professors, University of Georgia Physics Department. Private communication, Jan. 23, 1971. Proton spin flip in the microscopic distorted wave approximation. To be published in Nuclear Physics.

22. Pierce, W. L. and J. C. Hicks. Improved NMR probe for magnetic field measurements. Review of Scientific Instruments 36:202-203. 1965.

23. Bardin, B. M. and M. E. Rickey. Kinematic method for determination of accelerator beam energies. Review of Scientific Instruments 35:902-903. 1964.

24. Smythe, Rodman. Relativisitic equations and tables for ion energy determination by the crossover technique. Review of Scientific Instruments 35:1197-1200. 1964.

25. Heath, R. L. Scintillation spectrometry and gamma-ray spectrum catalog. 2nd ed. A. E. C. research and development report, physics. T. I. D. -4500 (31st ed.) August, 1964. 2 vols. 480 pages.

26. Grosjeans, C. C. and Walter Bossaert. Table of absolute detection efficiencies of cylindrical scintillation gamma-ray detectors. Ghent, Belgium, Computing Laboratory of the University of Ghent. 1965. 512 pages.

27. Sherif, Helmy. Spin-dependent effects in proton inelastic scattering. Nuclear Physics A131:532-550. 1969.

28. Baugh, D. J., J. A. R. Griffith and S. Roman. Polarization of 17.8 MeV protons elastically scattered by nuclei. Nuclear Physics 83:481-492. 1966.

29. Rybicki, F., T. Tamura and G. R. Satchler. Particle-gamma angular correlations following nuclear reactions. Nuclear Physics A146: 659-676. 1970.

30. Bechetti, F. D. and F. G. Greenlees. Nucleon-nucleus optical model parameters, $A > 40$, $E < 50$ MeV. Physical Review 182:1190-1209. 1969.

31. Watson, B. A., P. P. Singh and R. E. Segel. Optical-model analysis of nucleon scattering from 1-p shell nuclei between 10 and 50 MeV. Physical Review 182:977-989. 1969.

32. Hippelein, H. H. et al. Deuteron spin-flip in inelastic scattering. Nuclear Physics A142:369-384. 1970.